

SPATIOTEMPORAL CHAOS IN THE NONLINEAR THREE WAVE INTERACTION

by

CARSON C. CHOW

B.A.Sc., University of Toronto (1985)

SUBMITTED TO THE DEPARTMENT OF PHYSICS
IN PARTIAL FULFILLMENT OF THE REQUIREMENTS FOR
THE DEGREE OF

DOCTOR OF PHILOSOPHY IN PHYSICS


at the

MASSACHUSETTS INSTITUTE OF TECHNOLOGY

December 1991

© Carson C. Chow, MCMXCI. All rights reserved.


The author hereby grants to MIT permission to reproduce and
to distribute copies of this thesis document in whole or in part.

Author  Signature redacted

..... Department of Physics
December 17, 1991

Certified by  Signature redacted

.....
Abraham Bers
Professor, Department of Electrical Engineering
Thesis Supervisor

Accepted by  Signature redacted

..... George F. Koster
Chairman, Departmental Committee on Graduate Students

MASSACHUSETTS INSTITUTE
OF TECHNOLOGY

FEB 11 1992

LIBRARIES

ARCHIVES

Spatiotemporal Chaos in the Nonlinear Three Wave Interaction

by

Carson C. Chow

Submitted to the Department of Physics
on December 17, 1991, in partial fulfillment of the
requirements for the degree of
Doctor of Philosophy in Physics

Abstract

The nonlinear three wave interaction (3WI) is used as a paradigm for spatiotemporal chaos (STC), which refers to the chaotic evolution of coherent structures. The 3WI describes many phenomena in plasma physics, nonlinear optics and hydrodynamics. The conservative form is integrable by inverse scattering transforms (IST). Two non-integrable models that exhibit STC and one model that exhibits low dimensional chaos are studied.

The first model involves the saturation of a linearly unstable high-frequency wave by coupling to two damped daughter waves. The unstable wave has the middle group velocity of the three waves. The integrable form of the equations has soliton solutions. The system is numerically simulated and STC is observed. The correlation function is measured and spatial and temporal scales are observed. These scales and the energy saturation conditions were estimated with linear analysis and by perturbation expansions of the IST soliton solutions.

The second model is the same as the first except the unstable wave has the highest group velocity. The IST solutions for the integrable form do not involve solitons. The nonlinear interactions are radiation dominated. STC is observed in numerical simulations with characteristic length and time scales. Estimates for these scales and the saturated energy based on linear analysis and the IST solutions are again made.

The final system models Stimulated Brillouin Scattering in a finite medium. With temporal dephasing bifurcations from a fixed state to periodicity, quasi-periodicity and chaos occur in the controlling parameter space. This model does not exhibit STC as defined above. The differences between low dimensional chaos, spatiotemporal chaos and fully developed turbulence are discussed.

Thesis Supervisor: Abraham Bers

Title: Professor, Department of Electrical Engineering

Acknowledgments

My time at M.I.T. has been eventful and I leave here with many fond memories. I'll always miss this old place. Contrary to what its forbidding and intimidating reputation and architecture may suggest, I have found it to be quite warm and accommodating.

I express great gratitude to my advisor and mentor Professor Abraham Bers. He has been invaluable in guiding my research and career. His enthusiasm, experience, knowledge, and insight are forever inspiring. He always had the time and interest to discuss any problems I may have had. I thank Dr. Abhay Ram, for all of his technical advice of course, but more for his warmth and friendship and the many colourful discussions we've had. He and his wife Prabha have been great friends. I thank Dr. Vladimir Fuchs for his kindness and encouragement. I came to this group six months after my friend and officemate Ken Kupfer came and I leave six months after his departure. Through those years we've had many engaging discussions on physics and life. I must thank Laura Doughty for all of her support and for always having the answers I needed. Who knows where we'd all be without her. I wish to thank the members of my thesis committee, Professor M. Baranger and Professor G. Bekefi, for many valuable comments.

I've been very fortunate to have made the friends I've made here. I would have been infinitely poorer without the friendship of Kin Cheung, Steve Fromm, Jim Gelb, Terry Hwa, and Tom Luke – the original members of 'Somerville Tech'. Special thanks to Tom Luke for always making things happen and to Kin Cheung for rescuing me the time I got stranded. I owe a great deal to my roommate of two years, Terry Hwa, from whom I've learned a great deal about 'life, the universe and everything'. I also wish to thank Alastair Rucklidge, Will Evans, Gerald 'Gib' Gibson, Mike Yoo, Joe Kung, Albert Young, Tony Yen, and Z.R. Wang for making life more enjoyable.

I must thank my Auntie Verna for introducing me to my close friend Zara Weng. She and Karen Fu have been steadfast friends throughout my stay here. During this time I've made many friends at Wellesley. In particular, I am grateful to Judy Tsao for her thoughtfulness and generosity, to Laura Song for always having a smile when

I visited, and to Monica Sieh for helping me through the rough times. I especially thank my dear friend Maine Huang for all that she has given me.

I thank my wonderful host family, the Forbes, who have always made me feel at home and feel like part of the family. And finally I wish to thank my own family – my sister, my Mom, and my Dad, who have been all that a sister, a Mom, and a Dad could be.

Contents

1	Introduction	7
1.1	General Remarks	7
1.2	Spatiotemporal Chaos	11
1.3	Outline	14
2	The Nonlinear Three Wave Interaction	16
2.1	Derivation of the 3WI	17
2.2	Time Only Evolution and Chaos	21
2.3	Spacetime Parametric Interaction	24
2.4	The Inverse Scattering Transform Solution	25
2.4.1	The Soliton Decay Interaction	27
2.4.2	The Stimulated Backscatter Interaction	31
3	The Nonintegrable Soliton Decay Interaction	36
3.1	The Model	36
3.2	The Nearly Integrable Regime	38
3.2.1	Simulation Results	38
3.2.2	Qualitative Description of the Dynamics	44
3.2.3	Conservation Equations	48
3.2.4	Short Time Behaviour	50
3.2.5	Multiple Scale Analysis	51
3.2.6	Scattering Space Perturbation Theory	60
3.2.7	Long Time Behaviour and STC	68

3.2.8	Discussion	70
3.3	Other Parameter Regimes	71
3.3.1	The Strong Growth Regime	72
3.3.2	The Strongly Diffusive Regime	77
3.4	Conclusions	83
4	Langmuir Decay Instability	86
4.1	The Model	86
4.2	Simulation Results	87
4.3	Analysis and Discussion	96
4.4	Saturation of SRS in Laser Plasma Interactions	101
4.5	Conclusions	103
5	Stimulated Brillouin Scattering in a Finite Medium	105
5.1	The Model	105
5.2	The Dynamics	108
5.2.1	The Fixed State	108
5.2.2	Periodic Orbits	113
5.2.3	Quasi-periodicity and Chaos	115
5.3	Conclusions	125
6	Conclusions	133
A	The Zakharov-Manakov Scattering Problem	136
B	The Zakharov-Shabat Scattering Problem	141
C	Numerical Methods	144
	Bibliography	146

Chapter 1

Introduction

1.1 General Remarks

Nature abounds with complex phenomena where coherent ordered behaviour coexists with turbulent chaotic behaviour. One striking example is the Great Red Spot of Jupiter which is a coherent structure that has persisted for several centuries within a raging, turbulent Jovian storm. The Red Spot is a gargantuan version of vortices in complicated flows that occur on a more human scale as in tornados or eddies in white water rapids. Coherent structures within disorder are not limited to vortices. Moving fronts in propagating flames or chemical reactions, and interacting fluid convection rolls, are other examples of coherent structures either embedded within chaos or interacting chaotically (Campbell, 1987). A great effort has been made to understand such systems. This dissertation is part of that effort.

Very often diverse phenomena exhibit similar ‘universal’ nonlinear characteristics. Certain paradigmatic equations appear over and over again in descriptions of particular nonlinear phenomena. The nonlinear Schrödinger (NLS) equation, Korteweg-deVries (KdV) equation, Ginzburg-Landau (GL) equations are examples of ubiquitous nonlinear partial differential equations (PDE) that apply to many different contexts. The nonlinear three wave interaction (3WI) is another of this family. Some of the many applications of the 3WI are discussed in Chapter 2. Understanding the behaviour of these paradigmatic nonlinear equations goes a long way towards under-

standing nonlinear phenomena in general. The unity of phenomena stretches across many fields including physics, chemistry, biology and economics. This universality and the developments in computer simulations, dynamical chaos and soliton theory have spurred the field of nonlinear science (Campbell, 1987).

Dynamical chaos refers to the aperiodic, irregular, unpredictable behaviour that occurs in low dimensional deterministic dynamical systems (see Bergé, Pomeau and Vidal, 1984; Campbell, 1987). Although there are some more precise definitions of chaos (see Guckenheimer and Holmes, 1986; Devaney, 1989), one signature of chaos is a broad band power spectrum. The ground work for chaos had been laid out by Henri Poincaré (see Poincaré, 1952) a century ago. After Poincaré, mathematicians and physicists on both sides of the Atlantic concentrated mostly on Hamiltonian dynamics and ergodicity theory. Many very important results on dynamics and chaos (intrinsic stochasticity as it was then called) were produced. The contributions are too numerous to list but Arnol'd and Avez (1968) and Lichtenberg and Lieberman (1992) provide comprehensive reviews. However, it was a great shock when Lorenz (1963) showed that a simple dynamical system is completely unpredictable. This and the advent of computer simulations were the seeds that set off the avalanche of work on dynamics and chaos in dissipative systems. The study of fractals took on a new meaning as well after it was found that the attracting sets of chaotic orbits, the so-called strange attractors, were fractal-like. (Mandelbrot, 1975; see also Campbell, 1987). Chaos has been studied intensively and many excellent monographs exist (Schuster, 1984; Zaslavsky, 1985; Bergé, Pomeau and Vidal, 1986; Guckenheimer and Holmes, 1986; Devaney, 1989).

The equations of motion for fluid flow, the Navier-Stokes equation, have been known for over a hundred years. In the intervening years many have tackled the problem of fully developed turbulence (see Landau and Lifshitz, 1980; Herring and Kraichnan, 1972; Tennekes and Lumley, 1972; Sirovich, 1989). Yet success has been fairly limited and a complete theory is yet to be found. However given that many degrees of freedom are involved it was not so surprising that turbulent behaviour could arise. That the problem was so difficult to tackle may be the greater surprise.

However, chaos shows that unpredictability can arise from as few as three degrees of freedom or dimensions. George Gamow's book *One, Two, Three, Infinity* was so inspiring to me as a child and is serendipitously prophetic. Within chaotic dynamics three is a magic number. A three dimensional flow, and not an infinite number, is all that is required for unpredictability and chaos. Landau (1944) proposed that the broad band behaviour observed in turbulence arose from an infinite sequence of bifurcations. In contrast Ruelle and Takens (1971) showed that aperiodic behaviour could arise after three bifurcations. Li and Yorke (1975), found that 'period three implies chaos'. This was actually a rediscovery of Šarkovskii's (1964) theorem which laid out the sequence in which periodic orbits would appear; if period three existed then so would all the periods. In this abstract sense three implies infinity.

However, is three as complicated as infinity or rather is infinity as complicated as three? It all depends on what questions are asked. While the solution of three mutually gravitating bodies is intractable, the equilibrium state of a gas of 10^{26} molecules, each bouncing around in a fashion fathomable only to Maxwell's daemon, can be understood in an average sense in terms of average statistical quantities such as temperature and pressure. Even if one were able to obtain the trajectories of each particle it would be of little use. Collective effects such as sound waves would be completely overlooked if one only had the microscopic orbits.

A statistical formulation for fully developed turbulence has been attempted with some success (Herring and Kraichnan, 1972; Kraichnan and Chen, 1989). However it still has difficulties dealing with coherent structures that exist at many length scales and are located intermittently in space. At first it was thought that dynamical chaos would provide a framework to comprehending turbulence, but the attractor in fully developed turbulence has many dimensions and the characteristic time scales of turbulence are much shorter than the attractor cycling time (Kraichnan and Chen, 1989). However, chaos did open new doors and gave a new perspective on nonlinear dynamics in general. Surely if three dimensions are all that is required for unpredictability, then there must be a variety of interesting behaviour between chaos and fully developed turbulence. What happens when more dimensions are added to a

chaotic (low dimensional) system? The 3WI in spacetime will be used to address this issue.

While nonlinearity can induce chaotic and irregular behaviour it can also produce order and coherence. The discovery of solitons by Zabusky and Kruskal (1965) was as great a surprise as the discovery of chaos. Here were nonlinear structures that preserved their form even after collisions! There is a whole history of solitons dating back to J. Scott Russell's (1838) observation of a solitary wave in a narrow barge channel, but it was Zabusky and Kruskal (1965) who discovered the collisional properties and coined the term soliton. It was later realized that the PDE's that had solitons were integrable by inverse scattering transforms (IST). Integrable PDE's are a very special class, to which the 3WI along with the NLS, KdV and sine Gordon (SG) equations belong. A precise definition of integrability still does not exist (Kruskal, 1991). There is no sure-fire way to tell whether an equation is integrable or not. The question of what happens when an integrable PDE is perturbed remains. Chaotic behaviour is one possibility.

Some of the issues alluded to above will be probed by considering the 3WI. The 3WI is discussed in depth in chapter 2. In short, it can occur whenever three waves satisfy a frequency and wave vector resonance condition. The 3WI are the slowly varying amplitude equations that describe the lowest order nonlinear interaction of these waves. In its conservative form it is integrable by IST. In one spatial dimension the group velocities determine the structure of the solutions. As will be discussed in Chapter 2, there are two cases important cases. One case has soliton solutions, the other does not. Nonintegrable versions of these two cases are studied in Chapters 3 and 4. In each case an unstable high-frequency wave saturates nonlinearly to two damped daughter waves. These models apply to various physical situations which will be discussed. A spatially uniform version of this situation exhibits low dimensional chaos. The 3WI is an ideal system to study both a perturbed integrable PDE and a spatially extended chaotic ODE simultaneously.

The results are intriguing. The saturated state involves the chaotic evolution of coherent structures. This type of behaviour has recently been dubbed spatiotemporal

chaos (STC) (Hohenberg and Shraiman, 1989). A more thorough discussion of STC is given in Section 1.2. It involves the coexistence of coherence and chaos, yet unlike fully developed turbulence there is a separation of scales that perhaps allows a statistical description. Through numerical simulations and analysis an attempt is made to comprehend the dynamics and manifested STC. This dissertation, however opens many more doors than it closes. Much remains to be learned about nonintegrable systems, coherence and chaos. STC is not the only possibility of the perturbed 3WI. In Chapter 5. a spatially extended model that exhibits low dimensional chaos is studied and the contrast to STC is very evident. Section 1.2 will address the differences between chaos, STC and fully developed turbulence.

1.2 Spatiotemporal Chaos

The term spatiotemporal chaos (STC) has acquired a more specific meaning than simply chaos in space and time. Although there is no official definition, there has been a recent trend to use STC to refer to the chaotic behavior of coherent structures or patterns (Hohenberg and Shraiman, 1989). This is the usage that is taken for this dissertation. This is in contrast to the more familiar low dimensional chaos and fully developed turbulence. Examples of STC include large aspect ratio Rayleigh-Bénard convection (Ahlers and Behringer, 1978; Bergé, 1979; Ciliberto and Caponeri, 1990), Faraday ripples (Ezerskiĭ *et al.*, 1986), propagation of flame fronts (Sivashinsky, 1983), nonlinear optics (Arecchi *et al.*, 1990), chemical reactions (Kuramoto and Tsuzuki, 1976; Vidal *et al.*, 1986) and in everyday phenomena like the patterns of sand moving under the action of the surf. The nonlinear 3WI is another paradigm for STC.

STC differs from low dimensional chaos in that it deals with many degrees of freedom. Thus the traditional methods of analysing chaos such as bifurcation routes, strange attractors, Poincaré surface of sections, and so forth are not as relevant. On the other hand it is far simpler than fully developed turbulence; the latter is usually associated with an inertial range, coherent structures of many sizes, intermittency in space and time, and vortices. It was the growth of chaos and a need for simple models

of turbulence that led to the insurgence of STC as a field of its own. A connection to nonequilibrium statistical mechanics and dynamical renormalization group have also led to the interest (Yakhot, 1983; Zaleski, 1989; Hohenberg and Shraiman, 1989).

The distinction between the different possible dynamics of a spatially extended system can be made on the basis of length scales. Following Hohenberg and Shraiman (1989), for any dynamical system there exist certain length scales. There is: (a) the excitation length l_E , the length scale at which energy is put into the system; (b) the dissipation length l_D , the scale at which energy is dissipated; (c) the system size L ; and (d) the coherence or correlation length ξ . The correlation length is usually defined in terms of a correlation function $S(r - r') = \langle (u(r, t) - \langle u \rangle)(u(r', t) - \langle u \rangle) \rangle$, where the angled brackets denote time averages, and $u(r, t)$ is some local variable (eg. field amplitude, temperature, velocity, etc.). In many cases the correlation function will have an exponential decay such as $S(r) \sim \exp(-r/\xi)$ as $x \rightarrow \infty$, which defines the correlation length.

Systems where energy is created and destroyed at the same length scale, $l_E \sim l_D \sim L$, only involve a small number of modes. The dynamics are thus low dimensional. The system is completely spatially correlated. On the other extreme, in fully developed turbulence energy is usually injected at some large scale and dissipated at a small length scale, $L > l_E \gg l_D$, and the so-called inertial range lies between the length scales. Also in fully developed turbulence, coherent structures exist at all scale lengths and the correlation length is not well defined. However for systems where energy is injected and dissipated at the same length scale and if these lengths are both smaller than the system size, $L > l_E \sim l_D$, then the dynamics will depend on the correlation length. If $\xi > L$ then again the system is spatially coherent and the dynamics will be low dimensional. For instance single cell Rayleigh-Bénard convection is a spatially extended system that has low dimensional dynamics. However if $\xi \ll L$ the dynamics are incoherent in space and this corresponds to the regime of STC. In STC there is no inertial range yet spatial degrees of freedom are very important. The clean separation of scales also allows a statistical description in that correlation functions are well defined.

Hohenberg and Shraiman (1989) postulated that although the dynamics of the local variables are likely complicated, simple statistical properties may exist for the long wavelength behaviour which depend on data from many correlation volumes. For example, consider the Fourier transformed variable

$$u(q, t) = \int u(x, t) e^{iqx} dx. \quad (1.1)$$

In Eq. (1.1) an implicit average over many correlation volumes is taken. If the correlation length is finite, the central limit theorem implies that the fluctuations $\Delta u(q, t) = u(q, t) - \langle u(q, t) \rangle$ are Gaussian. The long wavelength, low frequency properties of STC are then expected to be described by a probability functional

$$P\{\Delta u(q, \omega)\} \sim \exp(-D(q, \omega) |\Delta u(q, \omega)|^2), \quad (1.2)$$

where the Gaussian measure $D(q, \omega)$ is directly related to the dynamic structure factor by

$$C(q, \omega) \equiv \langle |\Delta u(q, \omega)|^2 \rangle = \frac{1}{2} D^{-1}(q, \omega). \quad (1.3)$$

The local variables $\Delta u(x, t)$ need not be Gaussian. The Fourier modes are Gaussian with corrections of order $(\xi/L)^d$. Dropping these non-Gaussian corrections loses some of the information about the local behaviour, and transforming Eq. (1.2) back into real space yields a coarse-grained distribution.

The Kuramoto-Sivashinsky (KS) equation describing propagating flame fronts and chemical reactions (Kuramoto and Tsuzuki, 1976; Sivashinsky, 1979) has been studied intensively as a paradigm for STC (Manneville, 1981; Pomeau, Pumir and Pelcé, 1984; Pumir, 1985; Chaté and Manneville, 1987; Hyman, Nicolaenko and Zaleski, 1986; Shraiman, 1986; Zaleski, 1989). The statistics of STC have been tested experimentally in fluid convection (Ciliberto and Caponeri, 1990) and in nonlinear optics (Arecchi *et al.*, 1990). Both cases show that the Fourier variables are Gaussian distributed while the local variables are not.

Other work on perturbed integrable equations include studies of the SG equation (see Bishop and Lomdahl, 1986), and the NLS equation (Moon and Goldman, 1984; Goldman, 1986). Soliton turbulence has been studied in models of nonintegrable NLS equations (Zakharov *et al.*, 1988; D'yachenko *et al.*, 1989).

Theoretical and numerical studies of spatial chaos, instabilities, and loss of symmetry have been made in complex Ginzburg-Landau type amplitude equations (Coullet and Iooss, 1990; Coullet, Elphick and Repaux, 1987; Goldstein *et al.*, 1991).

1.3 Outline

The thesis is structured as follows. Chapter 2 gives a review of the Nonlinear Three Wave Interaction (3WI). The physical applications are touched upon but not reviewed in depth because an excellent review already exists (Kaup, Reiman, and Bers, 1979). A derivation is provided that emphasizes the generality of the 3WI and its connections to other amplitude equations. This is followed by a review of solutions for time only amplitudes, linearized parametric instabilities and the inverse scattering transform solution (IST) of the conservative equations. The IST solutions for the conservative form of the equations studied in the chapter are described. Formal IST details are given in Appendices A and B.

The next two chapters deal with specific models of the 3WI that exhibit STC. In Chapter 3, the Soliton Decay Interaction (SDI) is considered. Numerical simulations and analysis are combined to understand the manifested STC. The details of the numerical method is given in Appendix C. Linear analyses and a perturbation calculation around the IST solutions are given to explain some of the numerical results. Chapter 4 considers another model – Langmuir Decay Instability (LDI). Numerical simulations and analyses are again used. Both LDI and SDI are applicable to any physical situation that satisfies the generic properties. A specific application of LDI to current laser-plasma experiments is given. The LDI and SDI differ only in the order of the group velocities of the three waves. The integrable form of the equations with IST solutions have very different properties and this carries over into the nonintegrable form.

Chapter 5 considers a model of Stimulated Brillouin Scattering (SBS) in a finite medium. In this case low dimensional chaos is exhibited in contrast to the other two models. A fixed state solution is derived and its stability is discussed. As the

relevant parameters are varied the fixed state makes transitions to a periodic orbit, quasi-periodicity and chaos. The bifurcation diagram is mapped out numerically.

Chapter 2

The Nonlinear Three Wave Interaction

The Nonlinear Three Wave Interaction (3WI) is an ubiquitous set of equations, arising in many different contexts as diverse as plasma instabilities, laser-plasma interactions, nonlinear optics, Rossby waves, buckling of cylindrical shells, water waves, etc. References for these applications and more are found in Kaup, Reiman and Bers (1979), which gives a comprehensive review of the history and the many physical applications of the 3WI. It belongs to the family of paradigmatic equations such as the Korteweg-deVries (KdV), and nonlinear Schrödinger (NLS) equations. These equations arise in many different contexts because they capture the lowest order nonlinear effects of some generic interaction and many physical phenomena reduce to these equations under appropriate asymptotic considerations. For instance, the KdV equation is applicable to wave-like flow with weak dispersion and weak nonlinearity, while the NLS describes situations where there is strong dispersion and weak nonlinearity due to self-modal interaction. The 3WI describes systems where three nondispersive waves in resonance couple quadratically in the fields. The quadratic nonlinearity is often the lowest order effect and occurs at a much faster time scale than dispersion or self-modal interactions. Hence, if three wave resonances are allowed the 3WI will be the dominant nonlinear effect. The 3WI, NLS, and KdV among a few others also share the special property that they are integrable by Inverse Scattering Transforms (IST)

and possess soliton solutions. Here the term 3WI refers to the simplest conservative integrable form of this nonlinear effect. Of course it will be a nonconservative, nonintegrable form of the 3WI which exhibits spatiotemporal chaos and is studied in this thesis.

In this chapter a fairly complete and general derivation of the 3WI is presented. This is followed by a review of previous work on the 3WI. The time only 3WI is discussed emphasizing the chaotic solution. There is a short discussion on the linearized parametric interactions in space time. A review of the IST solutions ends the chapter.

2.1 Derivation of the 3WI

The 3WI has been derived in many ways for various contexts (see Kaup *et al.*, 1979). The underlying unity in all of the derivations is the use of a slowly varying amplitude expansion where waves may interact nonlinearly. The following derivation of the 3WI due to Benney and Newell (1967), emphasizes the generality of the 3WI and demonstrates its connection to other amplitude equations such as the NLS and Four Wave Interaction.

Consider a set of N discrete waves in a weakly nonlinear, conservative, homogeneous medium

$$\omega_l = \omega_l(\mathbf{k}_l) \equiv -\omega_{-l}, \quad (2.1)$$

where $l = 1, 2, \dots, N$. In the absence of any interaction, the equations for the complex Fourier amplitudes of the waves $A(\mathbf{k}_l, t)$ are given by

$$\frac{dA_l}{dt} + i\omega_l A_l = 0, \quad (2.2)$$

where $A_l = A(\mathbf{k}_l, t) = A_{-l}^*$. The nonlinearity in the medium will couple the waves together. For a weak nonlinearity an expansion in the product of the amplitudes is possible and yields asymptotic nonlinear amplitude equations (Phillips, 1960; Benney, 1962)

$$\frac{dA_l}{dt} + i\omega_l A_l = i\epsilon \sum_{m,n} \alpha_{lmn} A_m^* A_n^* e^{-i(\mathbf{k}_l + \mathbf{k}_m + \mathbf{k}_n) \cdot \mathbf{x}}$$

$$\begin{aligned}
& + i\epsilon^2 \left[\sum_p \beta_{lp} A_l A_p A_p^* + \sum_{q,r,s} \gamma_{lqrs} A_q^* A_r^* A_s^* e^{-i(\mathbf{k}_l + \mathbf{k}_q + \mathbf{k}_r + \mathbf{k}_s) \cdot \mathbf{x}} \right] \\
& + O(\epsilon^3), \tag{2.3}
\end{aligned}$$

where ϵ is a small parameter. The coupling constants α_{lmn} , β_{lp} , γ_{lqrs} are real for a conservative medium; β_{lp} is the self-modal interaction strength. The presence of a rapidly varying phase implies that only the terms where the wave number resonance conditions $\mathbf{k}_l + \mathbf{k}_m + \mathbf{k}_n = 0$, $\mathbf{k}_l + \mathbf{k}_q + \mathbf{k}_r + \mathbf{k}_s = 0$ are satisfied will be dominant.

For the situation where the linear waves are not completely discrete but are slightly spread about the wave numbers \mathbf{k}_l one can consider slow space and time variations of the amplitude

$$A_l = A(\mathbf{k}_l, t, \mathbf{X}, T), \tag{2.4}$$

where $\mathbf{X} = \mu\mathbf{x}$, $T = \mu t$, are slow scales depending on a small parameter μ . A multiple scale expansion can be performed on the amplitude equation (2.3). The time and space derivatives become

$$d/dt \rightarrow \partial/\partial t + \mu\partial/\partial T, \quad \partial/\partial x_r \rightarrow \partial/\partial x_r + \mu\partial/\partial X_r. \tag{2.5}$$

The slow scales in Fourier space are determined by Taylor expanding the frequency yielding

$$\omega(\mathbf{k} + \mu\mathbf{K}) = \left[1 + \mu \sum_r K_r \frac{\partial}{\partial k_r} + \frac{\mu^2}{2} \sum_{r,s} K_r K_s \frac{\partial^2}{\partial k_r \partial k_s} + O(\mu^3) \right] \omega(\mathbf{k}), \tag{2.6}$$

where $K_r = -i\partial/\partial X_r$. The amplitude equation (2.3) becomes

$$\begin{aligned}
\mu^2 \left(\frac{\partial a_l}{\partial T} + \sum_r \frac{\partial \omega_l}{\partial k_{lr}} \frac{\partial a_l}{\partial X_r} \right) &= i \frac{\mu}{2} \sum_{r,s} \frac{\partial^2 \omega_l}{\partial k_{lr} \partial k_{ls}} \frac{\partial^2 a_l}{\partial X_r \partial X_s} + i\epsilon \sum_{m,n} \alpha_{lmn} a_m^* a_n^* \\
&+ i\epsilon^2 \sum_p \beta_{lp} a_l a_p a_p^* \\
&+ i\epsilon^2 \sum_{q,r,s} \gamma_{lqrs} a_q^* a_r^* a_s^* \\
&+ O(\epsilon^3, \epsilon\mu, \mu^3). \tag{2.7}
\end{aligned}$$

The coordinate index and wave index both appear in the subscript. The fast time scales were removed by substituting

$$A_l = a_l(\mathbf{k}_l, X, T) e^{-i\omega_l t} = a_l e^{-i\omega_l t}. \tag{2.8}$$

The coupling coefficients $\alpha_{lmn}, \gamma_{lqrs}$ are nonzero only when the three and four wave resonance conditions are satisfied

$$\omega_l + \omega_m + \omega_n = 0, \quad \mathbf{k}_l + \mathbf{k}_m + \mathbf{k}_n = 0, \quad (2.9)$$

$$\omega_l + \omega_q + \omega_r + \omega_s = 0, \quad \mathbf{k}_l + \mathbf{k}_q + \mathbf{k}_r + \mathbf{k}_s = 0. \quad (2.10)$$

Depending on the relative ordering of the small parameters μ and ϵ different equations can result. If $\mu \sim \epsilon$ then to leading order equation (2.7) yields the nonlinear 3WI

$$(\partial_T + \mathbf{v}_1 \cdot \nabla_{\mathbf{x}})a_1 = i\theta_1 a_2^* a_3^*, \quad (2.11)$$

$$(\partial_T + \mathbf{v}_2 \cdot \nabla_{\mathbf{x}})a_2 = i\theta_2 a_1^* a_3^*, \quad (2.12)$$

$$(\partial_T + \mathbf{v}_3 \cdot \nabla_{\mathbf{x}})a_3 = i\theta_3 a_1^* a_2^*, \quad (2.13)$$

where $\mathbf{v}_l \equiv \partial\omega_l/\partial\mathbf{k}_l$, and $\theta_l \equiv \alpha_{lmn}$. For conservative couplings, the coupling constants θ_l have the same magnitude, (Bers, 1975; Bers *et al.*, 1976).

In many physical situations resonant triads and quartets are excluded. Then the dispersion and self-modal interaction are relevant and the equation for a single mode is given by

$$\frac{\partial a_l}{\partial T} + \sum_r \frac{\partial\omega_l}{\partial k_{lr}} \frac{\partial a_l}{\partial X_r} = i\epsilon \left[\frac{1}{2} \sum_{r,s} \frac{\partial^2\omega_l}{\partial k_r \partial k_s} \frac{\partial^2 a_l}{\partial X_r \partial X_s} + \beta a_l^2 a_l^* \right]. \quad (2.14)$$

In one spatial dimension and on translating to the frame of the wave and rescaling the time via

$$\mathbf{X}' = \mathbf{X} - \mathbf{v}T, \quad T' = \epsilon T, \quad (2.15)$$

equation (2.14) becomes the familiar and celebrated nonlinear Schrödinger equation

$$\frac{\partial a_l}{\partial T'} = i \left[\kappa \frac{\partial^2 a_l}{\partial X'^2} + \beta a_l |a_l|^2 \right], \quad (2.16)$$

where $\kappa \equiv (1/2)(\partial^2\omega_l/\partial k_l^2)$.

Furthermore for the scaling $\epsilon \sim \mu^2$ and when resonant triads and self-modal interactions are excluded but resonant quartets are allowed the four wave interaction results. For instance in nonlinear optics, isotropic media that have a center of inversion exclude quadratic nonlinearities and so the 3WI cannot occur (Bloembergen,

1965; Akhmanov and Khokhlov, 1972). In this context of generalized amplitude expansions, the resonant 3WI is the lowest order effect and will dominate if triad resonances are present. This emphasizes the importance and ubiquity of the 3WI. For plasma interactions the 3WI ignores wave particle ‘quasilinear’ interactions whose lowest order effect is also second order in the field amplitudes. The 3WI is then the lowest order nonlinear interaction for waves that are nonresonant with the plasma particles.

The above discussion dealt with conservative media. In many instances this will not be the case. The linear waves may have weak growth or dissipation (Bers, 1975; Chow *et al.*, 1991a)

$$\omega_l = \omega(\mathbf{k}_l) + i\nu(\mathbf{k}_l). \quad (2.17)$$

The imaginary part of the frequency can also be Taylor expanded as in Eq. (2.6). In an isotropic medium, the rotational symmetry would eliminate the nonsymmetric derivatives and so one is left with

$$\nu(\mathbf{k} + \mu\mathbf{K}) = \left[1 + \frac{\mu^2}{2} \sum_r |K_r|^2 \frac{\partial^2}{\partial k_r^2} + O(\mu^4) \right] \nu(\mathbf{k}), \quad (2.18)$$

or more simply as

$$\nu_l \simeq \gamma_l + D_l \nabla_{\mathbf{X}}^2, \quad (2.19)$$

where $D_l \equiv (\mu^2/2) \nabla_{\mathbf{k}}^2 \nu_l(\mathbf{k})$, and γ_l represents the zeroth order term in the expansion (2.18). The triad resonance does not necessarily have to be exact. There may be situations where the interaction is slightly dephased with

$$\delta = \omega_1 + \omega_2 + \omega_3 \neq 0. \quad (2.20)$$

If these effects are included in the 3WI a nonconservative form emerges

$$\partial_T a_1 + \mathbf{v}_1 \cdot \nabla_{\mathbf{X}} a_1 + \gamma_1 a_1 + D_1 \nabla_{\mathbf{X}}^2 a_1 = i\theta_1 a_2^* a_3^* \exp(i\delta T), \quad (2.21)$$

$$\partial_T a_2 + \mathbf{v}_2 \cdot \nabla_{\mathbf{X}} a_2 + \gamma_2 a_2 + D_2 \nabla_{\mathbf{X}}^2 a_2 = i\theta_2 a_1^* a_3^* \exp(i\delta T), \quad (2.22)$$

$$\partial_T a_3 + \mathbf{v}_3 \cdot \nabla_{\mathbf{X}} a_3 + \gamma_3 a_3 + D_3 \nabla_{\mathbf{X}}^2 a_3 = i\theta_3 a_1^* a_2^* \exp(i\delta T), \quad (2.23)$$

This is the symmetric form of the nonconservative 3WI. The diffusion term is included in Eqs. (2.21)-(2.23) even though the dispersion and diffusion terms both come in at

$O(\mu^2)$. This is because it was found to be necessary for nonlinear saturation in the models studied in Chapters 2 and 3. Often it is more convenient to distinguish the high frequency wave from the two lower frequency waves. Let ω_1 be the high frequency wave, and reassign the indices $(1, 2, 3) \rightarrow (i, j, k)$. Take the complex conjugate of Eq. (2.21) and let $a_i \rightarrow a_i^*$. Make the reassignment $i\theta_l = p_l K^*$, where p_l gives the sign of the wave energies. The normalization is chosen such that $|a_l|^2$ corresponds to the wave action density. With these changes Eqs. (2.21)-(2.22) take the form

$$\partial_t a_i + \mathbf{v}_i \cdot \nabla a_i + \gamma_i a_i + D_i \nabla^2 a_i = -p_i K a_j a_k \exp(-i\delta t), \quad (2.24)$$

$$\partial_t a_j + \mathbf{v}_j \cdot \nabla a_j + \gamma_j a_j + D_j \nabla^2 a_j = p_j K^* a_i a_k^* \exp(i\delta t), \quad (2.25)$$

$$\partial_t a_k + \mathbf{v}_k \cdot \nabla a_k + \gamma_k a_k + D_k \nabla^2 a_k = p_k K^* a_i a_j^* \exp(i\delta t), \quad (2.26)$$

where x and t are the slow variables. The resonance conditions now have the form

$$\omega_j + \omega_k - \omega_i = \delta, \quad (2.27)$$

$$\mathbf{k}_j + \mathbf{k}_k - \mathbf{k}_i = 0. \quad (2.28)$$

Three different forms of Eqs. (2.24)-(2.26) modelling different situations are studied in this dissertation. Two exhibit spatiotemporal chaos and one exhibits low dimensional chaos.

2.2 Time Only Evolution and Chaos

For amplitudes that depend only on time, the 3WI Eqs. (2.24)-(2.26) reduce to a set of three ordinary differential equations (ODE)

$$\dot{a}_i = \gamma_i a_i - p_i K a_j a_k e^{-i\delta t}, \quad (2.29)$$

$$\dot{a}_j = -\gamma_j a_j + p_j K^* a_i a_k^* e^{i\delta t}, \quad (2.30)$$

$$\dot{a}_k = -\gamma_k a_k + p_k K^* a_i a_j^* e^{i\delta t}. \quad (2.31)$$

This form of the 3WI applies to discrete modes, spatially uniform amplitudes, traveling waves with equal group velocities or for one dimensional steady state. For positive energy waves ($p_i = p_j = p_k$), the conservative, resonant interactions ($\gamma_l = 0, \delta = 0$)

are easily solved in terms of Jacobi Elliptic functions (Bloembergen, 1965; Sagdeev and Galeev, 1969; Davidson, 1972). The solutions are oscillatory with a period

$$T \sim \frac{1}{K|a_i(0)|} \ln \frac{|a_i(0)|}{|a_j(0)|}. \quad (2.32)$$

When the high frequency wave has wave energy opposite in sign to the low frequency waves ($p_j = p_k = -p_i$) then there is an 'explosive' instability, (i.e. where the solution becomes singular in finite time) (Coppi *et al.*, 1969).

With the addition of the nonconservative terms, closed form solutions no longer exist. However, one can consider an initial situation where the low frequency waves are small and the high frequency wave is large. The equations can then be linearized. This is known as a parametric interaction. Linearizing Eq. (2.29) yields

$$a_i(t) = a_i(0)e^{\gamma_i t}. \quad (2.33)$$

Equations (2.30) and (2.31) become

$$\dot{a}_j + \gamma_j a_j = K^* a_i(t) a_k^*, \quad (2.34)$$

$$\dot{a}_k^* + \gamma_k a_k^* = K a_i(t)^* a_j. \quad (2.35)$$

Assume that $a_i(t)$ is very slowly varying and substitute in the following

$$a_j = a_j e^{pt}, \quad a_k^* = a_k^* e^{pt}, \quad \gamma = K|a_i(t)|. \quad (2.36)$$

This yields the dispersion relation

$$(p + \gamma_j)(p + \gamma_k) - \gamma^2 = 0. \quad (2.37)$$

The threshold for instability is given by $\gamma > \gamma_j \gamma_k$. For γ slowly growing there will always be an instability. Ultimately nonlinear theory is required to determine the fate of the waves.

The nonlinear 3WI in time only was studied by Vyshkind and Rabinovich (1976), Wersinger, Finn and Ott (1980), Meunier, Bussac and Laval (1982). In those studies the damping rates of the two low frequency waves were chosen to be equal. With this assumption these two waves evolve in step and can be set equal (i.e. $a_j = a_k$).

Rescaling time with $t \rightarrow t/\gamma_i$ and transforming the amplitudes with $a_l = u_l \exp(i\phi_l)$ yields the equations

$$\dot{u}_i = u_i - u_j^2 \cos \phi, \quad (2.38)$$

$$\dot{u}_j = -u_j(\Gamma - u_i \cos \phi), \quad (2.39)$$

$$\dot{\phi} = -\Delta - (2u_i - u_j^2/u_i) \sin \phi, \quad (2.40)$$

where $\phi = \phi_i - 2\phi_j$, $\Delta = \delta/\gamma_i$, $\Gamma = \gamma_j/\gamma_i$. The 3WI reduces to three coupled ODE's with two parameters Γ and Δ .

Equations (2.38)-(2.40) have two fixed points. One is the trivial fixed point $u_i = u_j = 0$ which is always unstable. The other is given by

$$u_i = \Gamma / \cos \phi, \quad (2.41)$$

$$u_j = -\Gamma^{1/2} / \cos \phi, \quad (2.42)$$

$$\phi = \tan^{-1}[\Delta/(1 - 2\Gamma)]. \quad (2.43)$$

Linearizing about this fixed point shows that it is stable within the region defined by $\Delta^2 > \Delta_0^2 \equiv \alpha(\alpha + 1)(\alpha - 3)^{-1}$, where $\alpha \equiv 4(\Gamma - 1/2)^2$. For $\Gamma < 1.37$ the system is always unstable. It can also be shown that for $\Delta = 0$ there cannot be any nonlinear saturation. However when Δ decreases through Δ_0 a Hopf bifurcation ensues. Wersinger *et al.* (1980) and Meunier *et al.* (1982) have mapped out portions of the parameter plane (Γ, Δ) in some detail. A Poincaré surface of section can be constructed by recording u_i and u_j at a time t_m defined by ϕ passing through values $\phi_0 + 2\pi m$ where ϕ_0 is an arbitrary constant. They found that the parameter plane is divided into three main regimes: the basin of the stable fixed point, an unbounded regime and a regime of nonlinear saturation. The latter is the interesting regime where a period doubling route to chaos and intermittency are observed. The surface of section shows the transition from periodic orbits to strange attractors. The resulting strange attractor has a very strong attraction in one direction and almost resembles a one dimensional structure. Using this fact as a cue, Bussac (1982) was able to reduce the three dimensional flow to a one dimensional map which exhibited the same route to chaos.

2.3 Spacetime Parametric Interaction

In spacetime the linearized parametric instability where the low frequency waves are initially small can be studied as in the time only case (see for instance Bers, 1975). However, in spacetime a localized, pulsed disturbance in an unstable medium can evolve in two ways (see Bers, 1983): (a) the pulse can grow and propagate away from its origin, so at a fixed point in space the disturbance decays in time – this is a convective instability; or (b) the pulse can encompass more and more of space, so at every point in space the disturbance grows in time – this is an absolute instability. Transforming to the frame of the high frequency wave ($v_i = 0$) and for $a_i(t) \gg a_j, a_k$ (a_i can then be considered constant), Eqs. (2.25) and (2.26) can be linearized (Bers, 1975; Bers, 1983)

$$(\partial_t + v_j \partial_x - \gamma_j) a_j = \gamma a_k^*, \quad (2.44)$$

$$(\partial_t + v_k \partial_x - \gamma_k) a_k = \gamma a_j^*, \quad (2.45)$$

where $\gamma = |K^* a_i|$, and γ_l are dissipation coefficients (the second order diffusive term is ignored). Only one spatial dimension is considered. The high frequency wave is called the pump in the parametric interaction. The dispersion relation is simply

$$D = (\omega - kv_j + i\gamma_j)(\omega - kv_k + i\gamma_k) + \gamma^2 = 0. \quad (2.46)$$

There is a threshold of instability

$$\gamma^2 > \gamma_j \gamma_k \equiv \gamma_c^2. \quad (2.47)$$

For $v_j v_k > 0$ this is a convective instability. For $v_j v_k < 0$ there is an additional threshold for an absolute instability

$$\frac{\gamma}{|v_j v_k|^{1/2}} \equiv \alpha > \frac{1}{2}(|\alpha_j| + |\alpha_k|), \quad (2.48)$$

where $\alpha_l = \gamma_l / v_l$.

If the pump is spatially varying then one must solve the boundary value problem for Eqs. (2.44) and (2.45). For $v_j v_k < 0$ the condition for an absolute instability is the

existence of a growing normal mode. For a slowly varying pump with one extremum and classical turning points the WKB condition for n growing modes is given by

$$\left(n - \frac{1}{2}\right) \pi \leq \int_a^b [\alpha^2 - (|\alpha_j| + |\alpha_k|)^2/4]^{1/2} dx \leq \left(n + \frac{1}{2}\right) \pi, \quad (2.49)$$

where a and b are turning points for a localized pulse. For the situation where the damping on the two daughter waves are equal ($\alpha_j = \alpha_k$) the condition for an absolute instability is then given by

$$\int_a^b [\alpha^2 - |\alpha_j|^2]^{1/2} dx \geq \frac{\pi}{2}. \quad (2.50)$$

2.4 The Inverse Scattering Transform Solution

The conservative 3WI is integrable by use of inverse scattering transforms (IST). This technique was first developed by Gardner, Greene, Kruskal and Miura (1967) for the KdV equation. Lax (1968) developed an approach that could be applicable to other nonlinear PDE's and Zakharov and Shabat (1972) used the method to solve the NLS equation. Ablowitz, Kaup, Newell and Segur (1974), generalized the method and coined the term IST because of the analogy to Fourier transforms.

The general strategy of IST is the same as any transform method – a transformation is made into a space where the time evolution is simple. After time evolving the initial data in the associated space an inverse transformation is made to obtain the solution. The transformed space for the IST method is defined by the asymptotic scattering properties of the eigenfunctions of an associated eigenvalue or scattering problem. The field of the nonlinear evolution equation serves as a potential function of the scattering equation. The original equation is an integrability condition for this scattering equation and a linear time evolution equation. The initial data are transformed into ‘scattering data’ by ‘forward scattering’. The scattering data are evolved in time and then transformed back by ‘inverse scattering’. The difficult part of the procedure is in the inverse scattering which involves the solution of integral equations known as the ‘Gelfand-Levitan-Marchenko’ equations. The Schrödinger equation for instance is the scattering problem used to solve the KdV equation. It is actually a

special case of the second order Zakharov-Shabat (ZS) problem (Zakharov and Shabat, 1972). The sine-Gordon (SG), modified KdV and NLS equations among many others are solved using the ZS problem. An outline of the ZS problem is given in Appendix B. No attempt will be made to present a review of IST. Several comprehensive texts on the subject of solitons and the IST exist (Ablowitz and Segur, 1981; Eckhaus and Van Harten, 1981; Dodd *et al.*, 1982; Drazin and Johnson, 1989).

An outline for the IST solution of the 3WI in one spatial dimension was first presented by Zakharov and Manakov (1973). They showed that the appropriate scattering problem is the third order Zakharov-Manakov (ZM) problem (Zakharov and Manakov, 1973), outlined in Appendix A. They later made a more detailed study of the IST solution (Zakharov and Manakov, 1975). Numerical integration of the 3WI (Bers and Reiman, 1975; Reiman and Bers, 1975) showed the existence of solitons for separated envelope interactions and thresholds for explosive instabilities in spacetime. Based on this, the problem was fully solved by Kaup (1976a), and he also discovered that for most situations of interest the solution of the 3WI could be solved using the simpler ZS problem instead. The numerical and analytical results were shown to coincide in several specific interactions of the 3WI by Bers, Kaup and Reiman (1976). Later Reiman, Bers, and Kaup (1977) conducted a study of the 3WI in an inhomogeneous medium. Kaup (1980) later solved the 3WI in three spatial dimensions. A complete review of the solution and properties of the 3WI in one spatial dimension is given by Kaup, Reiman and Bers (1979). The ensuing review of the IST solution and the accompanying appendices follow directly from this reference, Kaup (1976a) and Reiman (1977). The conservative 3WI in an inhomogeneous medium has been reviewed by Reiman (1979). Two cases of the 3WI directly applicable to the nonintegrable models studied in this thesis are covered in some detail. Formal IST concepts are introduced only when necessary.

The 3WI has different behaviour depending on the relative order of the group velocities and signs of the wave energies. When the energy of the highest-frequency wave has the opposite sign to the lower frequency waves and it also has the middle group velocity then a singularity may arise in finite time. This is known as the

explosive instability. Unlike the time only case discussed in Section. 2.2, an area threshold must be exceeded before the interaction is unstable. When all the waves have energies of the same sign and the highest-frequency wave has middle group velocity interesting soliton solutions exist. This case is known as the Soliton Exchange or Soliton Decay Interaction (SDI). The case where the energies are of the same sign and the highest frequency wave has the highest (or lowest) group velocity is known as the Stimulated Backscatter Interaction. In physical systems the resonance conditions are usually easier to satisfy for the latter case. In this thesis it will be used to model Langmuir Decay Instability and Stimulated Brillouin Scattering. The nonconservative forms of Soliton Decay and Stimulated Backscatter will be considered in this thesis so a more detailed review of their properties are given in the following.

2.4.1 The Soliton Decay Interaction

The existence of solitons is usually synonymous with integrability and IST. In fact it was the discovery of the soliton in the KdV equation by Zabusky and Kruskal (1965) that spurred the development of IST. Solitons play an important role in the 3WI in one spatial dimension when the high frequency wave has the middle group velocity. As will be seen, the high frequency wave has a tendency to give up solitons to the low frequency waves precipitating the name Soliton Decay. As outlined in Appendices A and B, when the envelopes have negligible overlap each can be treated separately with its own ZS scattering problem.

Solitons in the 3WI are a little different from the more familiar solitons in the KdV or NLS equations. In those systems the solitons arise out of a balance between the dispersion and the nonlinearity. Also solitons have velocities proportional to their amplitudes, larger solitons being faster than smaller ones. Collisions involve larger solitons overtaking smaller ones and preserving their forms with only a shift in position after interacting. The 3WI is nondispersive and all waveforms travel at the group velocity of the wave. Collisions only occur between the different waves. Solitons in the 3WI are localized structures in the wave envelopes that preserve their form after interaction with solitons in the other waves. An interesting property of the

3WI is that solitons can be exchanged between the envelopes. The high frequency wave has a tendency to give up its solitons to the lower frequency waves. Because of this property the high frequency wave is referred to as the parent wave and the low frequency waves are referred to as the daughter waves.

In the IST framework solitons are given by the bound states of the associated scattering problem. As shown in Appendix A when the three envelopes are separated or have negligible overlap then each envelope can be treated individually with its own ZS problem. Bound states of the ZS problem indicate solitons in the given envelope. Depending on the group velocity ordering and wave energies each envelope may or may not possess bound states and hence solitons. Using the notation of Appendix A, for the SDI case $(v_i - v_j)(v_k - v_i) > 0$, $(\gamma_1, \gamma_2, \gamma_3) = (-, -, -)$ and $(i, j, k) = (2, 1, 3)$. From Appendix A, this shows all three envelopes may contain solitons. The continuous spectrum of the scattering problem is called the 'radiation'. The IST solution is divided into solitons and radiation. The radiation is the nonlinear extension of the Fourier transform; the solitons have no linear counterpart.

If at some time the envelopes are separated, the scattering data for each envelope can be obtained by forward scattering their respective ZS equations. When the envelopes interact, the evolution must be described by the full ZM equation. However, at a later time after mutual interaction the three envelopes may again be separated and the reduction to three ZS equations applies again. Inverse scattering can be applied to these equations to obtain the time evolved envelopes. Equations (A.27)-(A.29) show the relation between the initial and final scattering data. If the daughter waves initially contain solitons then they will after interacting. However the parent wave will give up its solitons.

The parent wave acts as a filter for solitons. The soliton content of the parent wave is transferred to the daughters leaving the radiation behind. Certain potential functions such as a square wave can be easily solved to yield the scattering data. Thus given an initial condition where the parent wave is a square well, the ZS eigenvalue problem can be solved for the continuous spectrum and the bound states. For arbitrary shaped pulses WKB theory may be applicable. Given a well that is slowly

varying, with one extremum and classical turning points the eigenvalues of the bound states can be found from the Bohr quantization condition

$$\int_a^b (q^2 - \eta^2)^{1/2} dx = \pi \left(n + \frac{1}{2} \right), \quad (2.51)$$

where a and b are the turning points, q is the ZS potential (proportional to the wave envelope), η is the eigenvalue and n is an integer. Setting $\eta \rightarrow 0$ gives the total number of solitons, N , contained in an envelope

$$N < \int_a^b |q| dx + \frac{1}{2}. \quad (2.52)$$

The daughter waves inherit solitons from the parent. For the situation where the parent envelope contains one bound state with eigenvalue $\lambda^{(i)}$ each daughter envelope will obtain a soliton with eigenvalues $\lambda^{(j)}$, $\lambda^{(k)}$ where the eigenvalues are related to one another through Eqs. (A.19), (A.21), (A.23). Single solitons for envelope l have the form

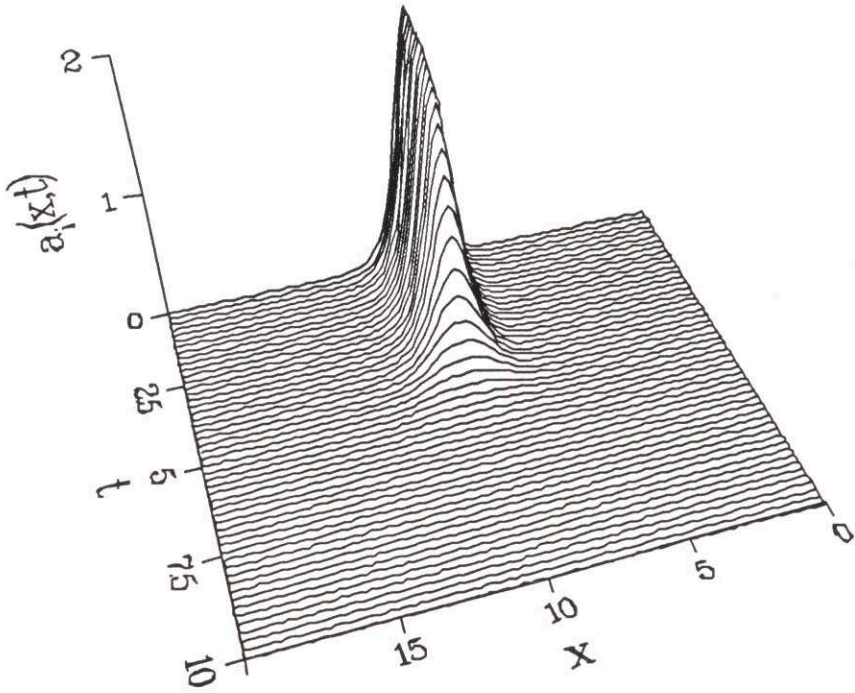
$$|q^{(l)}| = 2\lambda^{(l)} \operatorname{sech}[2\lambda^{(l)}(x - vt - x_0)], \quad (2.53)$$

where v is the group velocity of the envelope and x_0 is a phase that is determined by IST. The ZS potentials $q^{(l)}$ are related to the wave envelopes through Eqs. (A.19), (A.21), (A.23).

Figure 2-1 shows a numerical simulation of the decay of a soliton in the parent wave (no radiation) into solitons in the daughters. The group velocities are given by $v_i = 0$, $v_j = -v_k = -1$. For this choice $\lambda^{(j)} = \lambda^{(k)} = \lambda^{(i)}/2$. Only one of the daughters a_j is shown. The other will be the same under a transformation $x \rightarrow -x$. Up to this point the reference to solitons has only been made with respect to the ZS problems for each envelope. However, in truth the solitons are given by the bound states of the ZM problem. The 3WI soliton is actually the combination of the three envelopes. Equations (3.32)-(3.34) give the analytic expression for the soliton decay shown in Fig. 2-1. However whenever the term soliton is used it will implicitly refer to the ZS solitons corresponding to each envelope.

A point that will be very important when the nonconservative case is considered in Chapter 3, is that the parent wave will not give up its solitons to the daughters

(a)



(b)

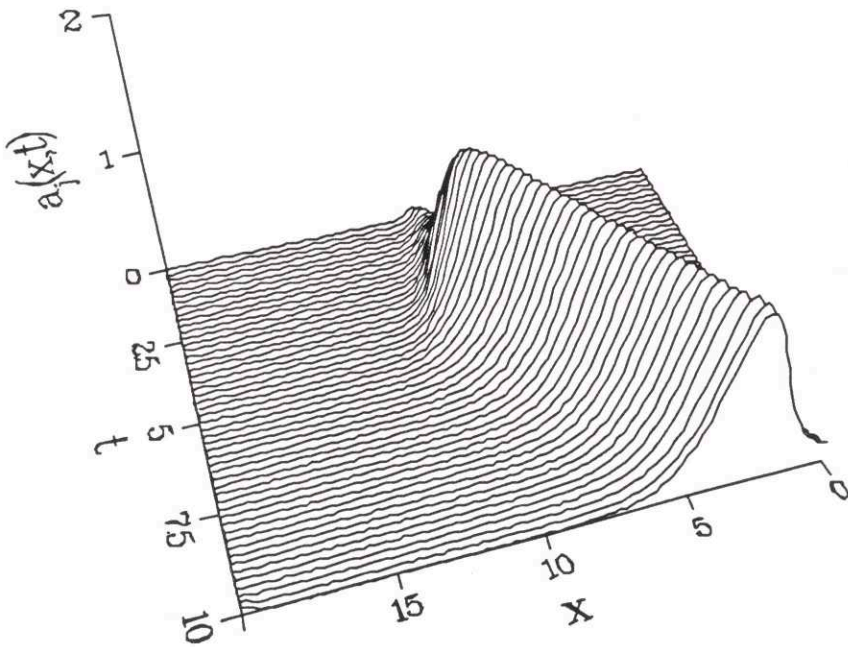


Figure 2-1: Soliton solution of (a) parent wave and (b) daughter wave

if it is completely isolated. This is easily seen in Eq. (2.24). The pulse will simply propagate along the characteristic. However if a bound state does exist it is unstable and a collision with or the initial presence of a daughter envelope, however small, is necessary to trigger the decay. If the parent contains more than one bound state, all of them will be transferred to the daughters and multi-soliton configurations will form in the daughters. If two arbitrarily shaped daughter pulses happen to collide many interesting things occur. If both do not contain any solitons they will interact and deposit some of their energy into the parent. The waves will then separate and all three waves will be distorted. If two daughter pulses each containing one soliton dressed in radiation collide, they will transfer their soliton content and some radiation to the parent, shed the rest of the radiation in the collision, and emerge delayed in time as pure solitons. If two colliding solitons are resonant (having identical bound state ZS eigenvalues) then they will create a parent soliton which will persist until it is induced to decay. All of the various interesting behaviour for the SDI are reviewed extensively in Kaup et al. (1979).

2.4.2 The Stimulated Backscatter Interaction

Without loss of generality the high frequency wave can be taken to have the highest group velocity. For this case the following applies in Appendix A: $(i, j, k) = (3, 2, 1)$, $(\gamma_1, \gamma_2, \gamma_3) = (-, -, +)$. The terminology of laser-plasma interactions (stimulated Brillouin scattering) is often convenient to use. The high frequency wave is referred to as the pump wave (PW), the middle group velocity wave is referred to as the ion-acoustic wave (AW) and the slow wave is referred to as the backscattered wave (BW). From Eqs. (A.18)-(A.23) it is clear that only the the BW can contain solitons so soliton exchange effects do not play a role. This implies that the interesting effects are radiation dominated and due to the collisions between the envelopes. Figures 2-2 - 2-4 show a numerical simulation of the spacetime evolution for the collision of a large square PW with a small AW wave. The group velocities are $v_i = 0$, $v_j = -1$, $v_k = -2$. The interaction between the AW and the PW generates the BW hence the name Stimulated Backscatter. The waves show a decimated structure after the

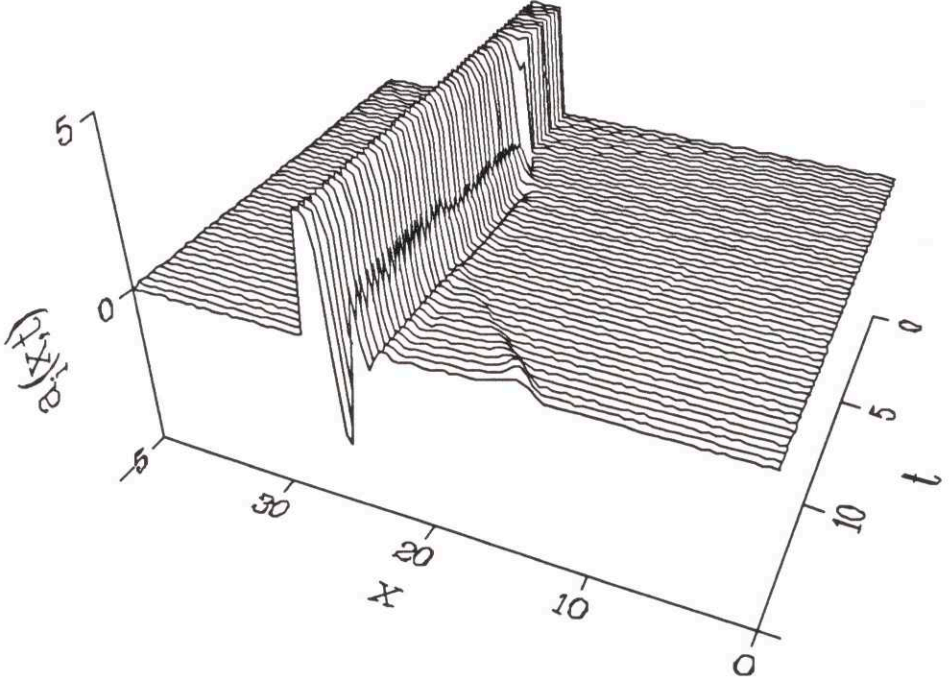


Figure 2-2: SBI solution of the PW, $a_i(x, t)$

interaction. Other simulations show that the wavelength of the oscillation decreases as the size of the initial PW increases.

Closed form analytic results cannot be obtained for this case as in the SDI case because the behaviour is radiation dominated. However the IST solutions can deduce some of the properties of the envelopes. The reflection coefficient $\rho(\lambda)$ defined in Eq. (B.8) and the density of radiation

$$\Gamma(\lambda) = [1 \pm |\rho(\lambda)|^2]^{\mp} - 1, \quad (2.54)$$

are the important quantities, where λ is the eigenvalue of the ZS equation. The density of radiation Γ is analogous to a ‘power spectrum’ of the linear theory. When the initial pulses are square pulses closed form solutions for Γ can be found. From Appendix B and Kaup *et al.* (1979) with the choice $c_1 = -c_3$ and $c_2 = 0$,

$$\Gamma_0^{(3)}(\lambda) = A_3^2 G(L^2 \lambda^2 - A_3^2), \quad (2.55)$$

$$\Gamma_0^{(2)}(\lambda) = A_2^2 G(4l^2 \lambda^2 - A_2^2), \quad (2.56)$$

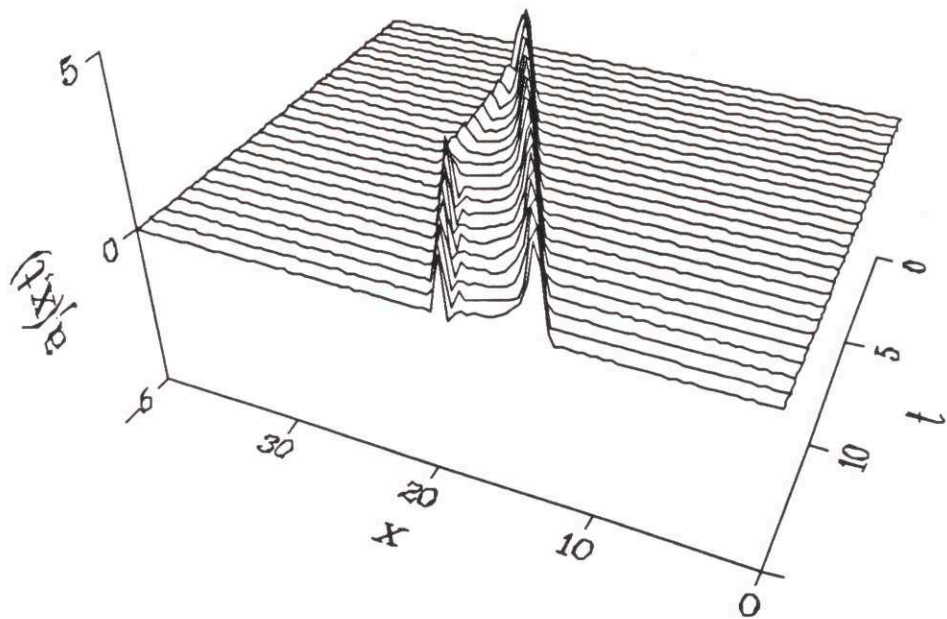


Figure 2-3: SBI solution of the AW, $a_j(x, t)$

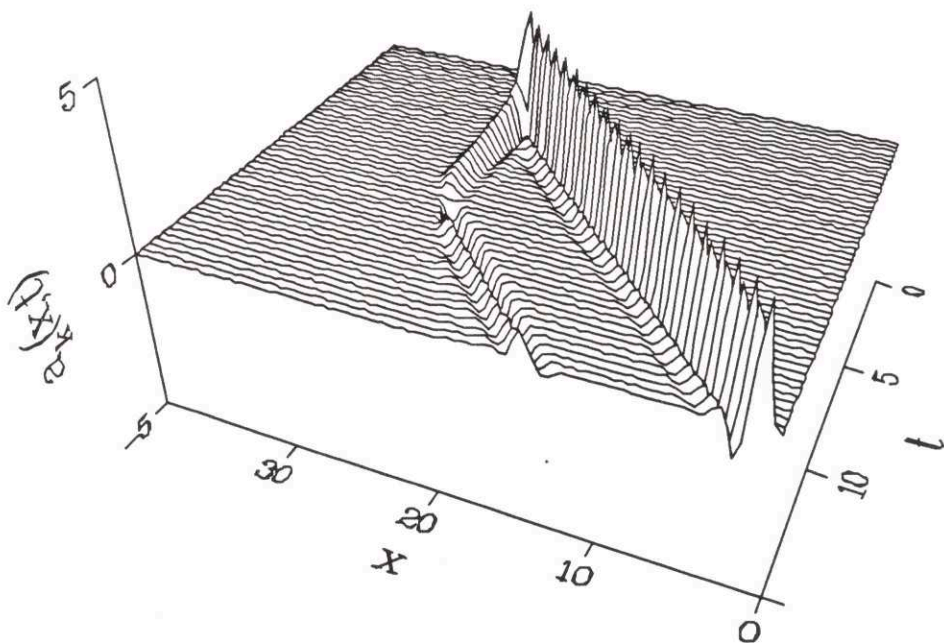


Figure 2-4: SBI solution of the BW, $a_k(x, t)$

where $\lambda = \lambda^{(1)}$, $L(l)$ is the length of the LW(AW) pulse, $A_3(A_2)$ is the area of the PW(AW) pulse and

$$G(x) = \begin{cases} \sinh^2(-x)^{1/2}/(-x) & \text{if } x < 0 \\ \sin^2(-x)^{1/2}/(-x) & \text{if } x \geq 0 \end{cases}. \quad (2.57)$$

Using Eqs. (A.27)-(A.29) for $\Gamma_0^{(1)} = 0$ (BW initially zero) the final reflection coefficients can be derived

$$|\rho_f^{(1)}|^2 = \frac{\Gamma_0^{(2)}\Gamma_0^{(3)}}{1 + \Gamma_0^{(2)}}, \quad (2.58)$$

$$|\rho_f^{(2)}|^2 = \frac{\Gamma_0^{(2)}(1 + \Gamma_0^{(3)})}{1 + \Gamma_0^{(2)}(1 + \Gamma_0^{(3)})}, \quad (2.59)$$

$$|\rho_f^{(3)}|^2 = \frac{\Gamma_0^{(3)}}{(1 + \Gamma_0^{(3)})(1 + \Gamma_0^{(2)})}. \quad (2.60)$$

The basic structure of the BW can be inferred from $\rho_f^{(1)}$. The Fourier transform of $\rho_f^{(1)}$ gives the wave envelope in the linear limit but qualitative results should apply in the nonlinear regime. When the areas of the AW and PW are small, $|\rho_f^{(1)}| \simeq \Gamma_0^{(2)}\Gamma_0^{(3)}$ has a $(\sin x/x)^2$ behaviour when the initial conditions are square pulses. This would give a triangular shaped pulse. A large area AW pulse will not fundamentally alter the reflection coefficient because of the denominator in Eq. (2.58), but a large area PW pulse will. For example, from Eqs. (2.55) and (2.56), if A_3 increases from 1 to 10, then at $\lambda = 0$, $\Gamma_0^{(3)}$ rises from an order unity to an order of e^{20} . For $\lambda > A_3/L$, $\Gamma_0^{(3)}$ is bounded by A_3 , while for $0 < \lambda < A_3$, $\Gamma_0^{(3)}$ becomes of order e^{2A_3} . Thus given $A_3 \gg 1$, $\Gamma_0^{(3)}$ and hence $|\rho_f^{(1)}|^2$ becomes almost square shaped with a width $A_3/L \equiv Q_3$. The Fourier transform of a square wave is a sinc function. Thus the wavelength of the oscillations of the BW structure are inversely proportional to the initial height of the PW. Causality will chop off the forward half of the behaviour. Also since $\rho_f^{(1)}$ is continuously differentiable, the corners of the square pulse are rounded and this implies the Fourier transform will fall off faster than any power of x as $x \rightarrow \infty$. This is approximately what is observed in the simulations.

Similar analyses can be made with the AW and the PW. However the estimates will not be as concrete as for the BW. For the AW initially small the final reflection

coefficient of the PW from Eq. (2.60) behaves approximately as $|\rho_f^{(3)}|^2 \simeq \Gamma_0^{(3)}/(1 + \Gamma_0^{(3)})$. For $A_3 \gg 1$, $|\rho_f^{(3)}|^2 \simeq 1/(1 + \Gamma_0^{(2)})$ in the region $0 < \lambda < A_3$. Outside this region $|\rho_0^{(3)}|$ goes to zero. The qualitative shape of the reflection coefficient is a symmetric function that rises from zero to an amplitude of unity, then dips in the center with a width of Q_3 . The Fourier transform of such a function will be roughly some localized structure with a characteristic width given by $2\pi/Q_3$. For large PW, the reflection coefficient of the AW, Eq. (2.59) is also unity in the region $0 < \lambda < A_3$ and behaves as $\Gamma_0^{(2)}/(1 + \Gamma_0^{(2)})$ outside of this region. For small initial AW the Fourier transform will behave somewhat like that of the BW. Collisions with varying initial amplitudes and between the BW pulse and the PW yield similar results. Kaup *et al.* (1979) present a detailed discussion of these and other results.

Chapter 3

The Nonintegrable Soliton Decay Interaction

3.1 The Model

A nonintegrable form of SDI that exhibits spatiotemporal chaos (STC) is considered in this chapter. The 3WI is used to model the nonlinear saturation of a linearly unstable high-frequency wave by coupling to two damped low-frequency daughter waves. The high-frequency wave has the middle group velocity. The dynamics are constrained to one spatial dimension. An example of a physical application would be the decay of an unstable lower hybrid wave to two daughter lower hybrid waves in magnetic plasmas (Reiman, 1977). However, the model applies to any generic situation that satisfies the given conditions. The equations are a special case of the general 3WI nonconservative equations (2.24)-(2.26). Numerical simulations are combined with linear and perturbation analyses in order to understand the STC manifested in SDI. The IST solutions for the conservative SDI are described in Section 2.4. The solutions involve the exchange of solitons between the three waves. The IST solutions are essential to understanding the behaviour of the nonintegrable SDI, and provide nonlinear solutions to perturb around.

The equations in one spatial dimension x and time t are

$$\partial_t a_i + v_i \partial_x a_i - D \partial_{xx} a_i - \gamma_i a_i = -K a_j a_k, \quad (3.1)$$

$$\partial_t a_j + v_j \partial_x a_j + \gamma_j a_j = K^* a_i a_k^*, \quad (3.2)$$

$$\partial_t a_k + v_k \partial_x a_k + \gamma_k a_k = K^* a_i a_j^*. \quad (3.3)$$

The γ 's have been chosen to be positive. The high frequency wave labelled by subscript i will be referred to as the parent wave and the other two waves will be referred to as the daughter waves. The group velocities satisfy the condition $v_k > v_i > v_j$. All three waves have positive wave energy. The parent wave has growth and the daughter waves are damped. The diffusive term in the parent wave Eq. (3.1) is the second order term in the slow variation of the imaginary part of the frequency and provides a cutoff in wave number for the growth in the parent. This term is extremely important for nonlinear saturation of the system and in determining the long time behaviour. The waves are in perfect resonance. Unlike the spatially uniform case considered in Section 2.2, dephasing is not required for saturation. In fact simulations seemed to indicate that it did not have a major effect on the behaviour at all.

These equations (3.1)-(3.3) are further simplified. A transformation into the frame of the parent wave is made via $x \rightarrow x - v_i t$. In this frame the group velocities of the daughter waves are chosen to be opposite and equal with a magnitude of v . The damping coefficients of the daughters are also chosen to be equal yielding

$$\partial_t a_i - D \partial_{xx} a_i - \gamma_i a_i = -K a_j a_k, \quad (3.4)$$

$$\partial_t a_j - v \partial_x a_j + \gamma_j a_j = K^* a_i a_k^*, \quad (3.5)$$

$$\partial_t a_k + v \partial_x a_k + \gamma_j a_k = K^* a_i a_j^*. \quad (3.6)$$

The number of free parameters can be further reduced by rescaling the length, time and amplitudes with: $a_l \rightarrow (\gamma_j/K) a_l$, $t \rightarrow t/\gamma_j$, $x \rightarrow (v/\gamma_j)x$, $\gamma_i \rightarrow \gamma_i/\gamma_j$ and $D \rightarrow (v^2/\gamma_j)D$ to yield

$$\partial_t a_i - D \partial_{xx} a_i - \gamma_i a_i = -a_j a_k, \quad (3.7)$$

$$\partial_t a_j - \partial_x a_j + a_j = a_i a_k^*, \quad (3.8)$$

$$\partial_t a_k + \partial_x a_k + a_k = a_i a_j^*. \quad (3.9)$$

Notice that the phase of the coupling coefficient K has been absorbed into the amplitudes. The daughter waves satisfy a parity symmetry where the equations are invariant under the transformation $x \rightarrow -x$, $a_j \rightarrow e^{i\phi} a_k$, and $a_k \rightarrow e^{-i\phi} a_j$ where ϕ is an arbitrary constant phase. The equations look deceptively simple. The linear part of Eq. (3.7) is a diffusion equation with growth. The linear parts of Eqs (3.8) and (3.9) are damped free streaming equations.

In the normalized form given by Eqs. (3.7)-(3.9), there are two free parameters: the normalized growth rate γ_i and the normalized diffusion coefficient D . Different regimes of the parameter plane (γ_i, D) yield different behaviour. Three different cases exhibiting STC are considered. Results of numerical simulations are presented then analysed. The first case is nearly integrable with weak growth and weak diffusion. This allows the nonconservative terms to be treated as perturbations about the integrable 3WI and much can be understood about the dynamics. The second case has strong growth and the third has strong diffusion. Both of these cases are not as easily tackled by perturbation theory so analytic results are not as complete as in the nearly integrable case.

3.2 The Nearly Integrable Regime

3.2.1 Simulation Results

Equations (3.7)-(3.9) were numerically simulated with periodic boundary conditions on the domain $x \in [0, L)$. The 3WI is a hyperbolic PDE. It lends itself fairly easily to numerical integration because the characteristic curves are straight lines. Each envelope is first transformed to its characteristic moving frame. A fixed spatial grid is then laid out for each envelope and the PDE is reduced to coupled ODE's. The spatial grid was chosen to be able to resolve the smallest structures that may result. The specific details of the numerical method is in Appendix C.

The long time, large system dynamical behaviour was of interest. In each simulation, the complete spatiotemporal history of each envelope was recorded. The integrated energy $U_l(t) = \int_0^L |a_l(x,t)|^2 dx$ was monitored. The saturated state was considered to be reached when the integrated energy began to fluctuate about some average value. The correlation function $S_l(x,t) = \langle a_l(x-x',t-t')a_l^*(x',t') \rangle$, where the angled brackets denote time averages, was then constructed (See Appendix C for the numerical procedure). Actual spatiotemporal profiles proved to be of great use in comprehending the dynamics. In all the simulations, random real initial conditions were chosen. The correlation function for different runs and runs of varying length were compared to ensure the results were consistent. Conservation laws for the integrated energy are derived in Section 3.2.3. Compliance with these laws was a measure of the veracity of the simulations.

The parameters for the nearly integrable case were $D = 0.001$, $\gamma_i = 0.1$, and $L = 20$. This case exhibits STC and falls into the regime where perturbation theory can be used to explain the behaviour (Chow *et al.*, 1991b). Fig. 3-1 shows the spatiotemporal evolution profile of the parent. The length shown is one half the simulation system size and $t = 0$ is an arbitrary time well after the transients have decayed. The profile of the parent is irregular yet spatial and temporal scales can be observed. There are coherent structures of a definite length scale that are seen to grow, deplete and collide with one another. The corresponding daughter profile is shown in Fig. 3-2. A sea of structures is seen convecting to the left. The structures are of a definite size and are constantly being created. They then damp as they propagate. Only daughter $a_j(x,t)$ is shown. The other will be similar but with structures propagating to the right because of the parity symmetry discussed in the introduction of this chapter.

The correlation function for the parent is given in Fig 3-3. It clearly shows decorrelation for long times and lengths. The spatial direction shows a definite length scale that was observed in Fig. 3-1. Correlations fall off gradually in the time direction. This is a clear signature of STC. There is a well defined correlation length and beyond this length the dynamics are decorrelated. Further information is gained by Fourier transforming $S_l(x,t)$. The spectrum of static fluctuations $S_i(q,t=0)$ for the parent

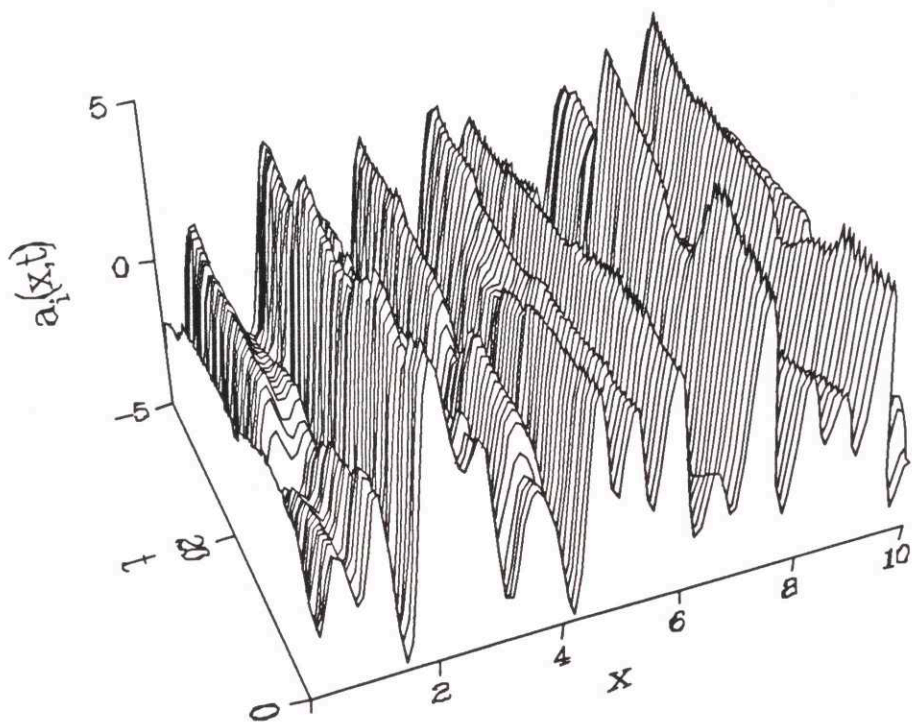


Figure 3-1: Spatiotemporal profile of the parent wave a_i .

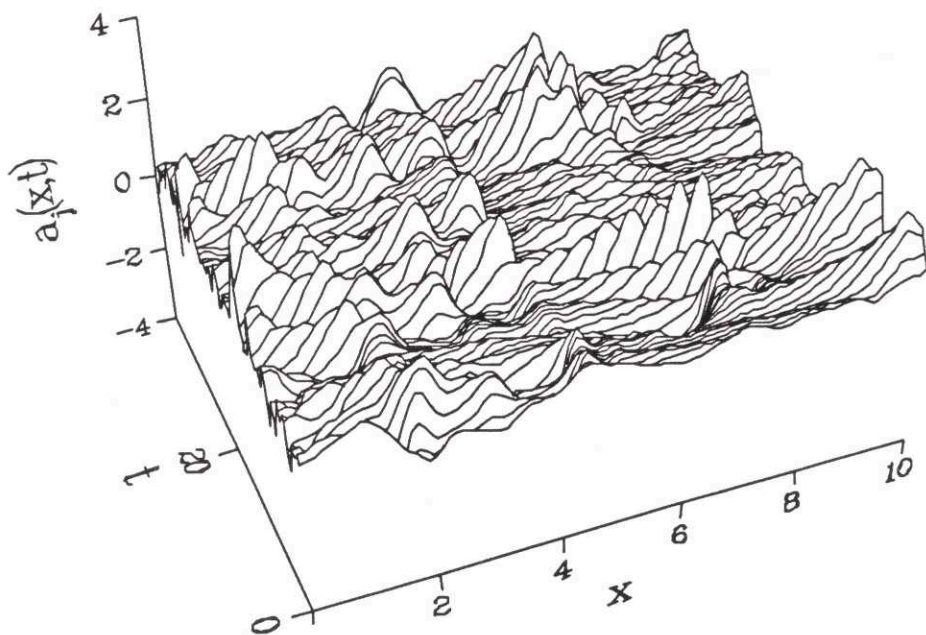


Figure 3-2: Spatiotemporal profile of the daughter wave a_j .

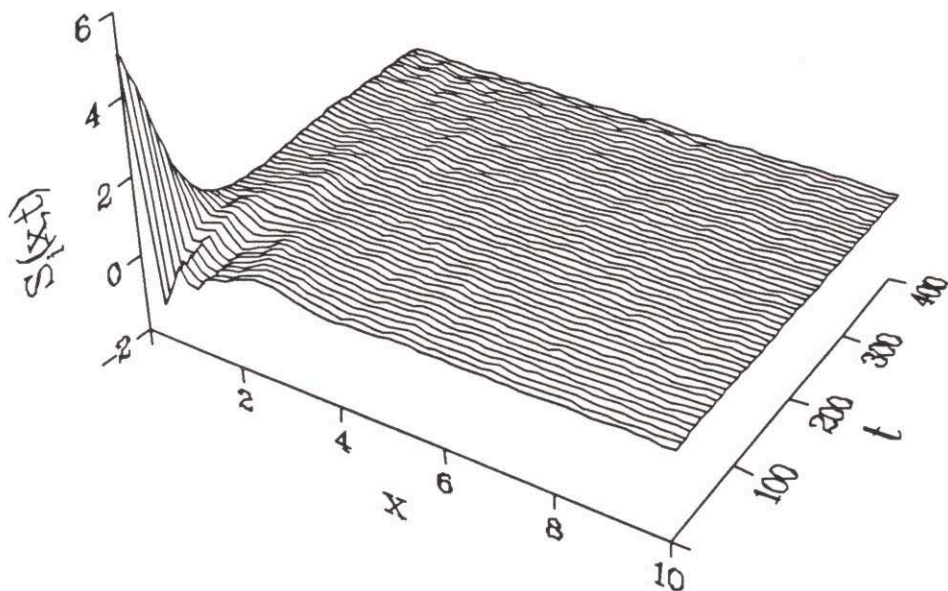


Figure 3-3: Correlation function $S_i(x, t)$ of the parent wave a_i .

wave is shown in Fig. 3-4. There is a cutoff near $q \simeq 10$ and a range of modes show up as a prominent hump. The cutoff reflects the length scale seen in the spacetime profile and in the correlation function. The hump in the spectrum indicates weak periodicity. The spectrum becomes flat for wavenumbers below the hump indicating decorrelation. The local power spectrum $S_i(x = 0, \omega)$ given in Fig. 3-5 shows two time scales. The spectrum bends over near $\omega \simeq 0.02$ which gives a long time scale and a shoulder at $\omega \simeq 0.3$ gives a short time scale. Longer runs with the same parameters hint that there may be a slow power law rise of undetermined exponent for frequencies below the low ω bend similar to that observed in the Kuramoto-Sivashinsky equation (Zaleski, 1989). The short time scale appears as the growth and depletion cycle observed in the spatiotemporal profile Fig. 3-1.

The daughter correlation function is shown in Fig. 3-6. It is calculated along the characteristic curve $x = -t$. There is an abrupt drop in the time direction (direction along characteristic) followed by a very slow and long decay. In space there is a definite length scale where the correlation function drops to zero but then along the x axis a very small but nonzero correlation is observed over the entire length. The

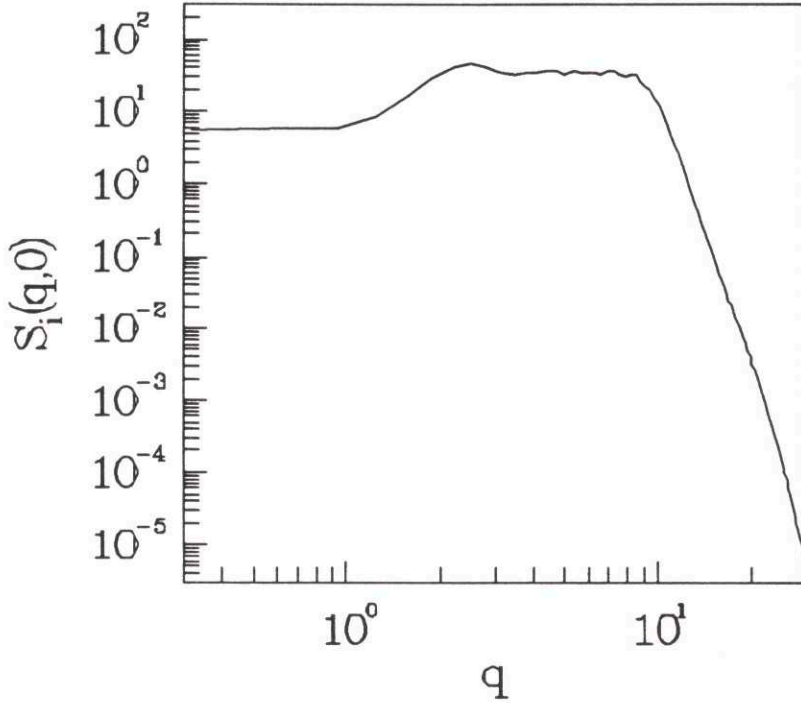


Figure 3-4: Spectrum of static fluctuations $S_i(q, t = 0)$ of the parent wave a_i .

temporal decay rate is of order $t \sim O(1)$ and cannot be resolved at the scale of the plot. The spectrum of static fluctuations $S_j(q, t = 0)$ is shown in Fig. 3-7. It shows a softer cutoff than the parent wave around $q \simeq 6$ giving the correlation length observed in Fig. 3-6. For wavenumbers lower than the cutoff the spectrum flattens out. The local power spectrum $S_j(x = 0, \omega)$ is shown in Fig. 3-8. The spectrum shows two peaks at high ω . One is where the shoulder of the parent wave power spectrum is and the other is at twice the frequency. For low frequencies the spectrum begins to bend over at $\omega \simeq 0.007$. This bend is more pronounced in longer runs. It is not known whether the spectrum becomes flat below this bend or has a power law rise like that in the parent wave. The time series for the integrated energy U_l is shown for all of the waves in Fig. 3-9. The upper curve is the parent wave; the two daughter waves are perfectly synchronized in the lower curve. The power spectrum for the parent energy is shown in Fig. 3-10 (a). There is a prominent peak at the location of the shoulder in the local power spectrum (Fig. 3-5). The power spectrum of the daughter energy

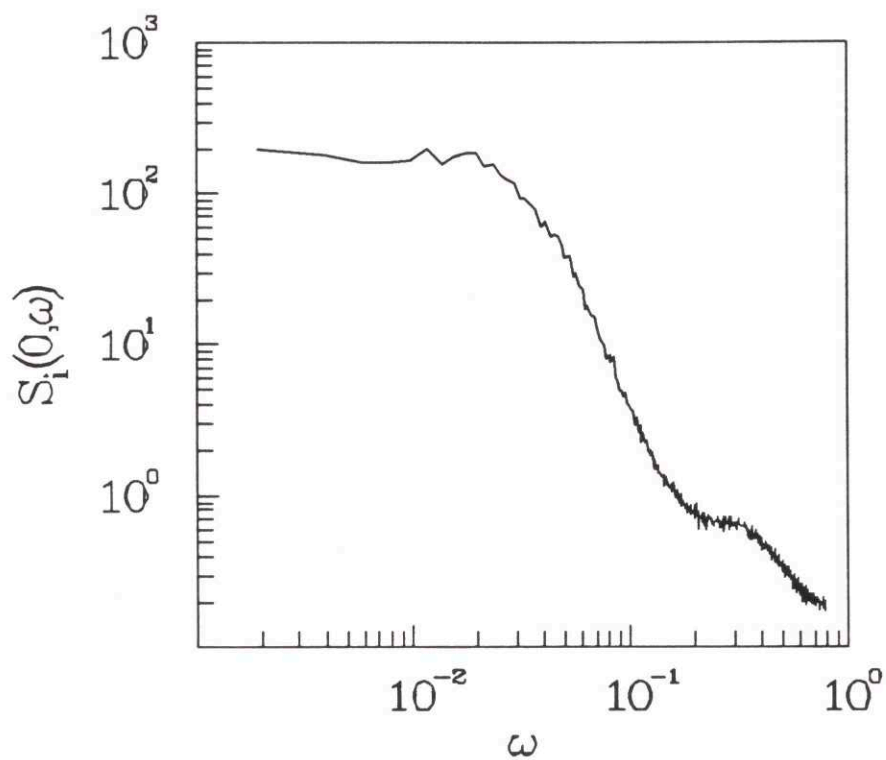


Figure 3-5: Local power spectrum $S_i(x = 0, \omega)$ of the parent wave a_i .

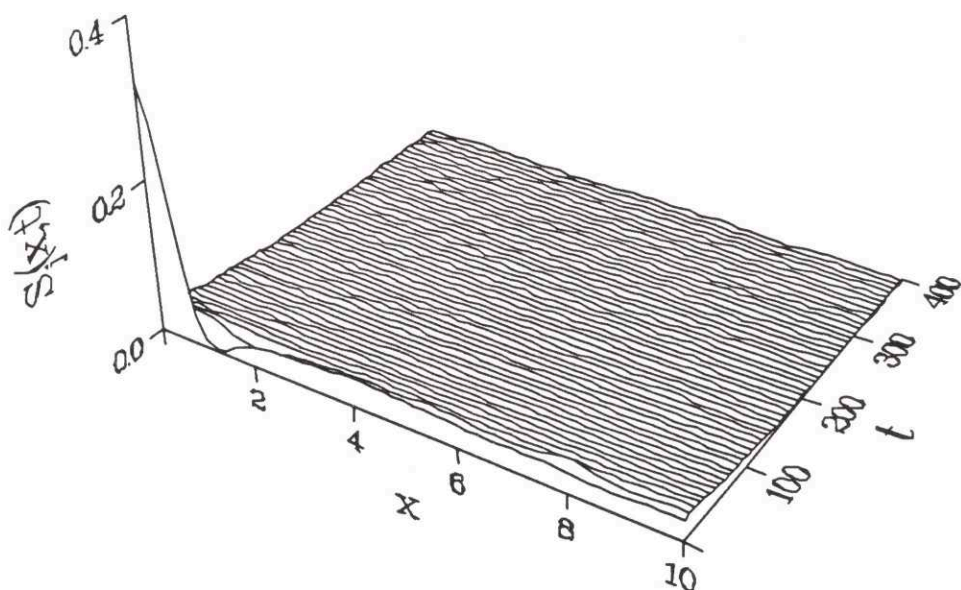


Figure 3-6: Correlation function $S_j(x, t)$ of the daughter wave a_j .

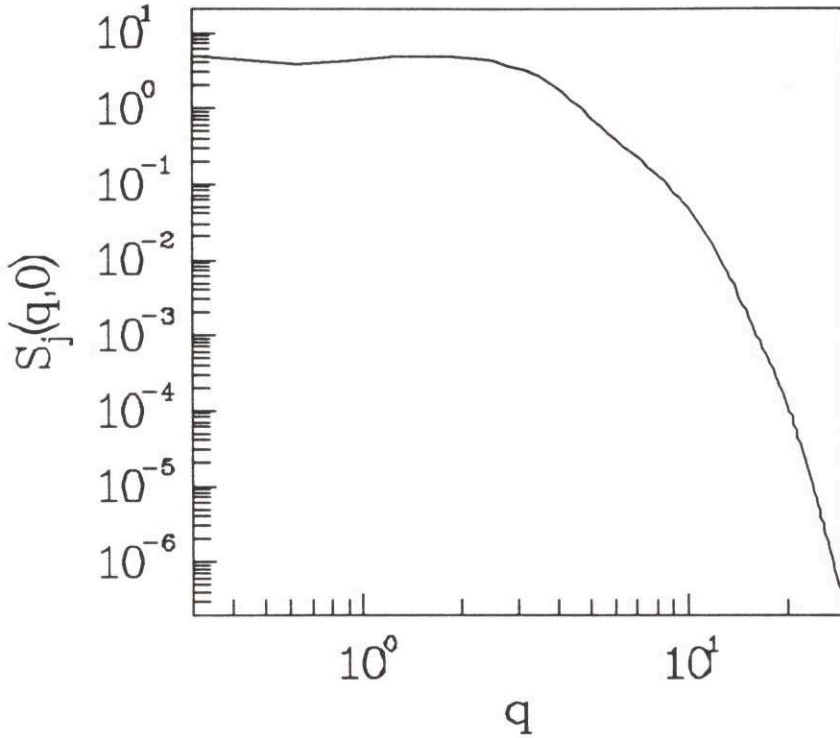


Figure 3-7: Spectrum of static fluctuations $S_j(q, t = 0)$ of the daughter wave a_j .

in Fig. 3-10 (b) shows a similar picture.

The dynamics clearly fall into the realm of STC. There are coherent structures of a definite length scale that interact chaotically. Correlation functions are well defined in space and time and provide a good description of STC. The parent wave is composed of coherent structures that grow and deplete on a short time scale and drift and diffuse on a longer time scale. The daughter waves are composed of damped drifting structures. They are created at intervals of the short time scale seen in the parent wave and have very long correlation times. An analysis of the observed dynamics is presented in the ensuing sections.

3.2.2 Qualitative Description of the Dynamics

The main features of the dynamics can be understood in terms of the linearized equations and by considering the growth and dissipation terms as perturbations around the integrable 3WI. The numerical simulations show that the spatiotemporal dynam-

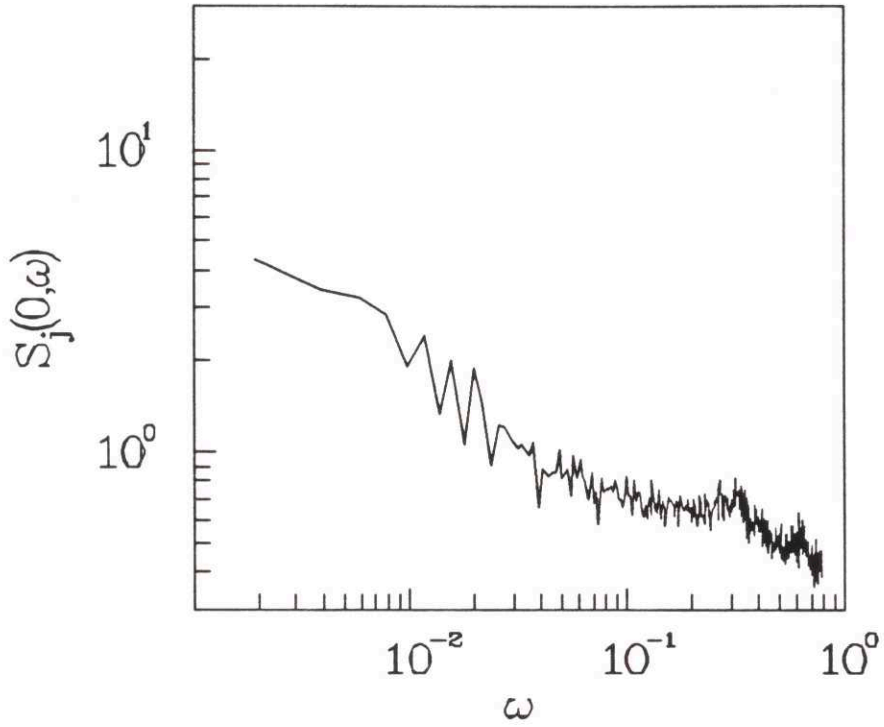


Figure 3-8: Local power spectrum $S_j(x = 0, \omega)$ of the daughter wave a_j .

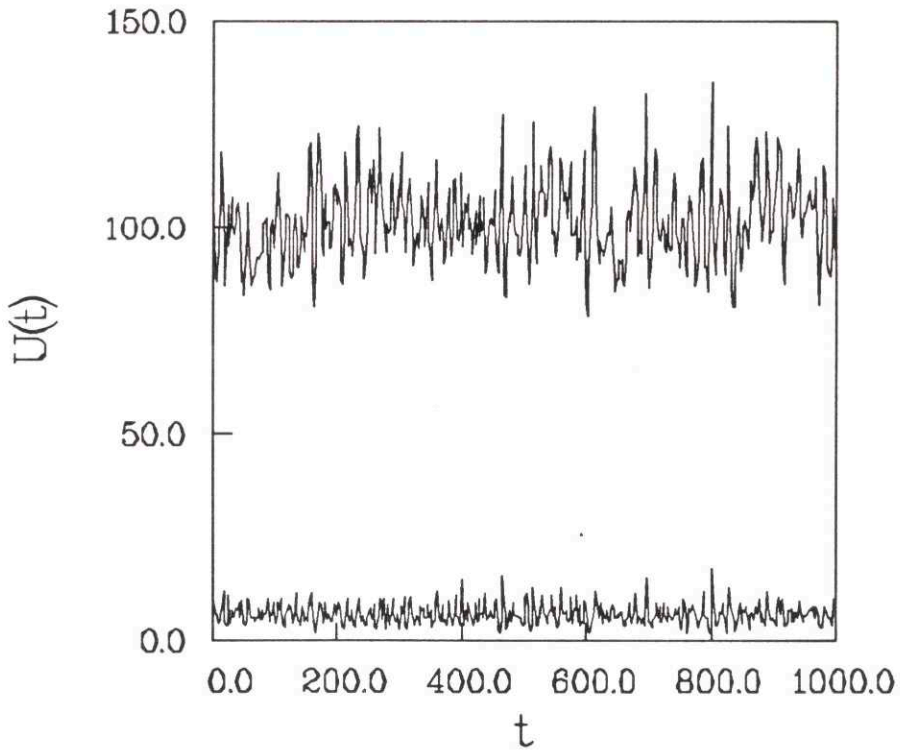


Figure 3-9: Energy time series, $U(t)$. Upper curve is the parent energy; lower curve are the daughter energies.

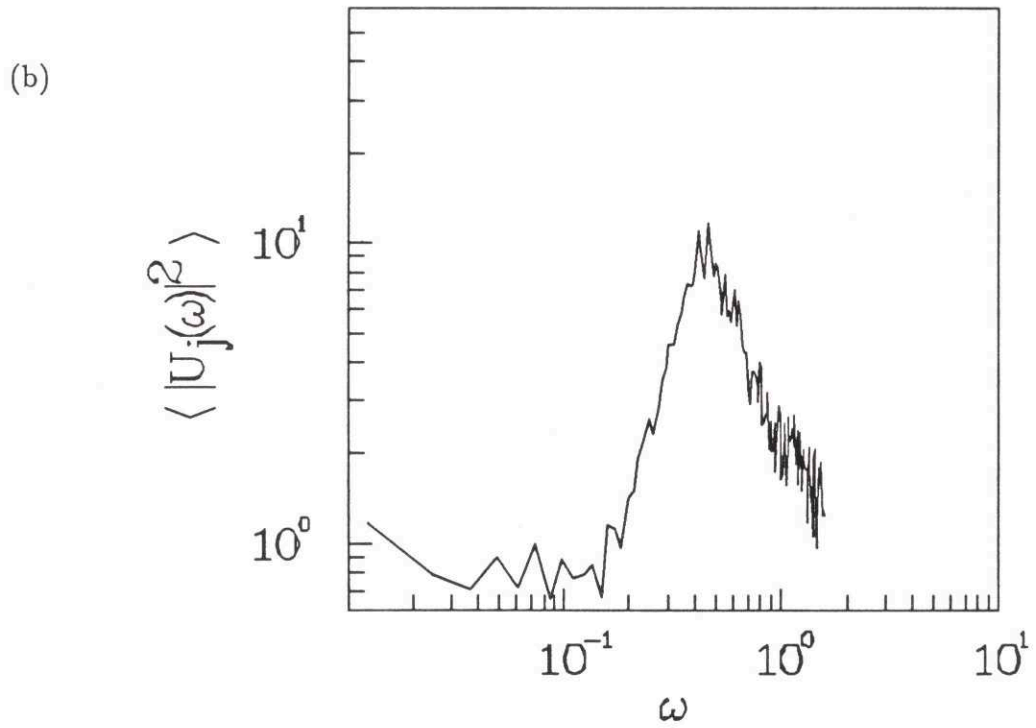
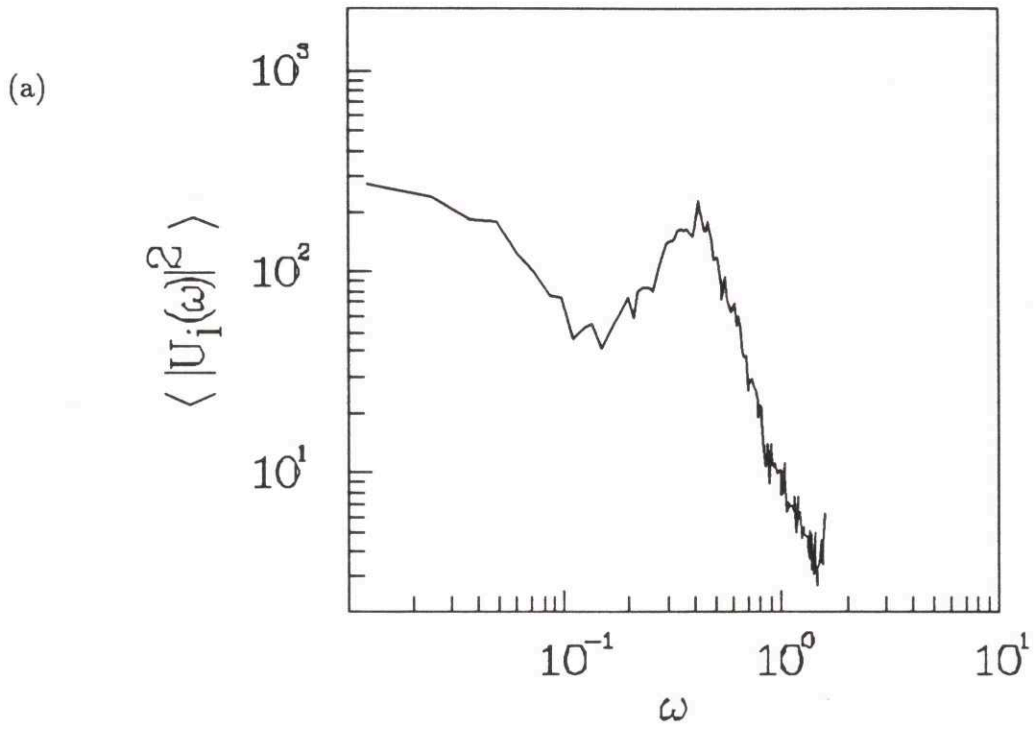


Figure 3-10: Power spectrum of (a) parent energy and (b) daughter energy.

ics exhibits STC and can be described in terms of a correlation function which has a given amplitude (average energy density), and temporal and spatial scales. Combining linear analysis with the IST solutions the correlation lengths for the parent and daughter are derived here.

The trivial fixed state of Eqs. (3.7)-(3.9) found by setting $\partial/\partial t$ to zero is

$$\partial_{xx}a_i + q_0^2 a_i = 0, \quad a_j = a_k = 0, \quad (3.10)$$

where $q_0 = \sqrt{\gamma_i/D}$. The linearized dispersion relation for growth rate s and Fourier mode q for the parent wave obtained by linearizing Eq. (3.7) is

$$s = \gamma_i \left(1 - \frac{q^2}{q_0^2}\right). \quad (3.11)$$

Thus modes $q > q_0$ will damp and those with $q < q_0$ will grow.

Energy is injected into the parent at long length scales. The trivial fixed state is always unstable to long wavelength fluctuations. The nonlinear interaction with the two daughter waves saturates the long wavelength instability. The parametric interaction analysis for a spatially varying pump reviewed in Section 2.3 shows that the daughter waves will be unstable and grow whenever the WKB area threshold equation (2.50) is satisfied. In the notation of this chapter the WKB condition has the form

$$\int_a^b |a_i^2 - \gamma_j^2|^{1/2} dx > \pi/2. \quad (3.12)$$

The IST solution for soliton decay shows that when the parent wave contains a soliton given by the Bohr quantization criterion Eq. (2.51) it will decay into solitons in the daughters. The damping and growth will perturb this decay process but for weak perturbations the essential elements of the interaction remain intact. Instead of decaying into solitons the parent wave will decay into quasi-solitons when the WKB threshold condition is met. A perturbative analysis around the IST soliton decay solution is detailed in section 3.2.4.

The depletion process spatially decimates the pump and saturates the growth of the low q . From any random initial condition, small scales are smoothed out by the diffusion process to length scales on the order of $2\pi/q_0$. The long scales grow until

a local area exceeds the WKB depletion threshold condition Eq. (3.12). The parent wave then depletes to quasi-solitons in the daughters and generates smaller scales or higher q in the process. The steady state is attained when a balance between the nonlinear conversion of long length scales to small length scales and the linear elimination of the small scales is attained. Spatially the parent wave will be composed of long wavelength fluctuations about the principal wavelength $2\pi/q_0$. The correlation length for the parent is then

$$\xi_p \simeq 2\pi/q_0. \quad (3.13)$$

The daughters will be composed of quasi-solitons in a constant state of creation and decay. The daughter correlation length will be given by the average quasi-soliton width. In Section 2.4 the soliton width in the integrable equations was shown to be related to the bound state eigenvalue of the parent pulse. This relation is assumed to carry over into the nearly integrable regime. If the average eigenvalue is denoted by η then the daughter correlation length is

$$\xi_d \simeq 2/\eta. \quad (3.14)$$

3.2.3 Conservation Equations

Conservation equations can be formed for Eqs. (3.1)-(3.3) by first forming the complex conjugate equations. Multiplying the original equations by a_i and the conjugate equations by a_i^* and adding yields

$$\partial_t |a_i|^2 + v_i \partial_x |a_i|^2 - 2\gamma_i |a_i|^2 - D(a_i^* \partial_{xx} a_i + a_i \partial_{xx} a_i^*) = -K a_i^* a_j a_k - K^* a_i a_j^* a_k^*, \quad (3.15)$$

$$\partial_t |a_j|^2 + v_j \partial_x |a_j|^2 + 2\gamma_j |a_j|^2 = K a_i^* a_j a_k + K^* a_i a_j^* a_k^*, \quad (3.16)$$

$$\partial_t |a_k|^2 + v_k \partial_x |a_k|^2 + 2\gamma_k |a_k|^2 = K a_i^* a_j a_k + K^* a_i a_j^* a_k^*, \quad (3.17)$$

For a periodic domain $x \in [0, L)$, the equations are integrated over x . Equation (3.16) is added to Eq. (3.15) and Eq. (3.17) is subtracted from Eq. (3.16) to yield the integrated conservation or energy equations

$$\frac{1}{2} \partial_t U_i + \frac{1}{2} \partial_t U_j = \gamma_i U_i - \gamma_j U_j - D \int_0^L |\partial_x a_i|^2 dx, \quad (3.18)$$

$$\frac{1}{2}\partial_t U_j - \frac{1}{2}\partial_t U_k = -\gamma_j U_j + \gamma_k U_k, \quad (3.19)$$

where $U_i = \int_0^L |a_i|^2 dx$. For the conservative 3WI, ($D = \gamma_l = 0$), Eqs. (3.18) and (3.19) are known as the Manley-Rowe relations, usually rewritten in the form $\partial_t(U_i + U_j) = 0$, $\partial_t(U_i + U_k) = 0$. The Manley-Rowe relations are two of the infinite conserved quantities associated with integrable partial differential equations (Ablowitz and Segur, 1981). Equation (3.19) shows that if the damping coefficients of the daughters are equal ($\gamma_j = \gamma_k$) then the energies of the daughters will approach one another exponentially.

In the saturated state the energy U_i is composed of an average part plus a fluctuating part, $U_i = \langle U_i \rangle + \delta U_i$, where $(1/L) \langle U_i \rangle = S_i(0, 0)$. Inserting this into Eqs. (3.18) and (3.19) and taking the time average yields

$$\langle U_i \rangle - \frac{D}{\gamma_i} \int_0^L \langle |\partial_x a_i|^2 \rangle dx = \frac{\gamma_j}{\gamma_i} \langle U_j \rangle, \quad (3.20)$$

$$\langle U_j \rangle = \frac{\gamma_k}{\gamma_j} \langle U_k \rangle. \quad (3.21)$$

Applying Parseval's theorem to the integral in Eq. (3.20) gives

$$\int_0^L \langle |\partial_x a_i|^2 \rangle dx = \int_0^\infty q^2 \langle |a_i(q, t)|^2 \rangle dq, \quad (3.22)$$

where the convention $f(x) = \frac{1}{2\pi} \int e^{iqx} F(q) dq$ is used. Note the right hand side of Eq. (3.22) is really a sum rather than an integral. However for $L \gg \xi_p$, where ξ_p is the correlation length, this approximation is fairly good. For the STC regime $\langle |a_i(q)|^2 \rangle$ is approximately constant up to the highest unstable mode $q_0 = \sqrt{\gamma_i/D}$. This allows the integral to be evaluated yielding

$$\int_0^L \langle |\partial_x a_i|^2 \rangle dx = \left[\frac{q^3}{3} \langle |a_i(q)|^2 \rangle \right]_0^{q_0} \quad (3.23)$$

$$\sim \frac{1}{3} \frac{\gamma_i}{D} \langle U_i \rangle, \quad (3.24)$$

since $U_i \simeq q_0 |a_i(q_0)|^2$. Reinserting into Eq. (3.20) yields the relation

$$\langle U_i \rangle \simeq \frac{3}{2} \frac{\gamma_j}{\gamma_i} \langle U_j \rangle. \quad (3.25)$$

3.2.4 Short Time Behaviour

The short time scale observed in the simulation was due to the constant growth and depletion of the parent wave into quasi-solitons. This time scale is contingent on several factors. The IST soliton decay solution shows that the soliton content of the parent is completely transferred to the daughters. The perturbing terms will convert some of this soliton content into radiation. The result is that the depleted parent will have some remaining area after depletion. This remaining area will then grow until it attains the threshold for depletion and repeat the process. The threshold area depends on the initial amplitude of the daughters. If the daughter amplitudes are zero, Eq. (3.7) shows that the parent pulse cannot deplete. Some nonzero amplitude is required to seed the depletion. Colliding daughter waves provide this stimulus for decay. A closed loop follows. Depleting parent pulses generate quasi-solitons which collide with other parent structures causing decays in a continual fashion.

Perturbation theory is used to answer two questions involved in this process: a) Given that the parent depletes from some initial area (ZS eigenvalue), what is the remaining area after depletion (leftover radiation) ? b) What threshold area (threshold eigenvalue) is required for the parent to deplete? The first question is addressed with a multiple-time scale analysis around the IST solution for soliton decay. The IST one soliton decay solution shows that a soliton in the parent wave decays to solitons in the daughters with a characteristic decay time. The growth and dissipation are relevant on a slower time scale. The second question is answered with a perturbation expansion in the ZM scattering space. A threshold condition on the parent wave bound state eigenvalue for the emission of a daughter quasi-soliton is derived. Many of the IST concepts dealt with in this section are outlined in Section 2.4 and Appendices A and B.

The main results are summarized here. Again let η be the average threshold bound state eigenvalue of a localized parent structure. The remaining area after depletion can be represented by an 'effective eigenvalue' η' . This is the amount of soliton content converted to radiation and not transferred to the daughters. If the effect of diffusion is considered small then the time required to grow back to threshold after a depletion

is given by

$$t_g \simeq \frac{1}{\gamma_i} \ln \frac{\eta}{\eta'}. \quad (3.26)$$

The cycling time t_c would then be the decay time plus t_g . The IST solutions (see Section 3.2.5) show that the decay time is on the order of $1/(2\eta)$. However for weak growth, $\gamma_i \ll 2\eta$, the decay time can be neglected with respect to the growth time and $t_c \simeq t_g$. In Section 3.2.5 a multiple scale perturbation expansion about the IST decay solutions is used to estimate η' . The calculation relies on the ordering $\gamma_i \ll 1 \ll 2\eta$ and the result obtained is

$$\eta' \simeq (2 + \gamma_i) \ln(3)/2. \quad (3.27)$$

A comparison of the Bohr quantization condition (2.51) with the WKB condition for decay (3.12) shows that $\eta > \gamma_j$ is necessary for a parent pulse to decay. Once η exceeds this critical value it will decay if a quasi-soliton collides with it. A more careful analysis is given in Section 3.2.6 where a perturbation expansion in scattering space is developed. The depleting parent structures generate quasi-solitons on average at intervals of $t \simeq t_c$. These quasi-solitons then collide with other parent structures triggering further depletions in a self consistent loop. The complex dynamics is a result of this feedback loop. Assuming that depletions are triggered by two colliding quasi-solitons generated two correlation lengths away gives an estimate of

$$\eta \simeq 2\gamma_j + 4\xi_p \gamma_i. \quad (3.28)$$

This estimate does not take into account of radiation and diffusion effects which can delay the decay. It must be considered more of a lower bound for ideal circumstances.

3.2.5 Multiple Scale Analysis

For simplicity consider only real envelopes and write the 3WI as

$$u_t = -vw + \epsilon\sigma u + \epsilon D u_{xx}, \quad (3.29)$$

$$v_t = v_x + uw - \epsilon v, \quad (3.30)$$

$$w_t = -w_x + uv - \epsilon w, \quad (3.31)$$

where $u = a_i$, $v = a_j$, and $w = a_k$. It can be shown that if the amplitudes are initially real, they remain so for all time (Kaup *et al.*, 1979). Numerically, it was found that the results for complex envelopes and real envelopes were similar. A small parameter $\epsilon \ll 1$ has been scaled out. The parameters σ and D will also be considered small. An ordering of $D \ll \sigma \ll \epsilon \ll 1$ is chosen. The effects of diffusion and growth are considered to be smaller than that of damping which is already considered small. It is a simple task to transform back to the form Eqs. (3.1)-(3.3) where the damping was scaled to unity. For $\epsilon = 0$ the equations (3.29)-(3.30) are integrable by IST.

The IST solutions show that a single soliton in the parent wave will decay to solitons in the daughter waves. This was discussed in Chap. 2 and in Appendix A in terms of ZS solitons. However the same situation can be solved exactly in terms of the ZM problem. This solution corresponds to two bound states where a_{11} and a_{33} in the ZM scattering matrix Eq. (A.16) are zero in their respective upper half planes. This was explicitly computed by Kaup (1976a) for the case where two daughter solitons at $t = -\infty$, one at $x = -\infty$ and one at $x = \infty$, collide. If the two daughter solitons are nonresonant (i.e. different eigenvalues) they pass through one another with only a phase shift. However if the two are resonant then they form a soliton in the parent. The time reversed version of this solution is of interest – a parent soliton decaying to daughter solitons.

The soliton solution for a degenerate ZM eigenvalue $\xi = i\eta$ is given by

$$u = \frac{4\eta}{e^{2\eta x} + e^{-2\eta x} + e^{2\eta t}}, \quad (3.32)$$

$$v = \frac{2\sqrt{2}\eta e^{-\eta(x-t)}}{e^{2\eta x} + e^{-2\eta x} + e^{2\eta t}}, \quad (3.33)$$

$$w = \frac{2\sqrt{2}\eta e^{\eta(x+t)}}{e^{2\eta x} + e^{-2\eta x} + e^{2\eta t}}. \quad (3.34)$$

For $t \rightarrow -\infty$ the solution is

$$u = 2\eta \operatorname{sech}(2\eta x), \quad (3.35)$$

$$v = w = 0, \quad (3.36)$$

and for $t \rightarrow \infty$ the solution is

$$u = 0, \quad (3.37)$$

$$v = \sqrt{2\eta} \operatorname{sech}(\eta(x+t)), \quad (3.38)$$

$$w = \sqrt{2\eta} \operatorname{sech}(\eta(x-t)), \quad (3.39)$$

The spectral parameter η is arbitrary for now, but will be estimated in Section 3.2.6. Notice in Eqs. (3.32)-(3.34) that the characteristic time scale for the decay process is $t \simeq 1/2\eta$. The effect of the perturbations on this soliton solution is examined. With growth and dissipation, the parent soliton will not completely transfer its energy to the daughters. This remaining area is the desired result.

Consider for the moment an isolated soliton governed by the linearized equation

$$q_t + cq_x = -q \quad (3.40)$$

For a soliton initial condition $q(x, t = 0) = q_0 \operatorname{sech} q_0(x)$ the equation (3.40) can be solved to yield the solution $q = q_0 e^{-t} \operatorname{sech} q_0(x - ct)$. Notice that only the amplitude is damped but the width of the soliton remains unaffected. With this in mind consider perturbed solutions of the form

$$u = \frac{A(x, t)}{e^{2\eta x} + e^{-2\eta x} + e^{2\eta t}}, \quad (3.41)$$

$$v = \frac{B(x, t)e^{-\eta(x-t)}}{e^{2\eta x} + e^{-2\eta x} + e^{2\eta t}}, \quad (3.42)$$

$$w = \frac{C(x, t)e^{\eta(x+t)}}{e^{2\eta x} + e^{-2\eta x} + e^{2\eta t}}. \quad (3.43)$$

with the choice $A = 4\eta$, $B = C = 2\sqrt{2}\eta$ at $t = 0$. Plugging this into Eqs. (3.29)-(3.31) yields the result

$$A_t = \frac{2\eta A - BC}{S + e^{2\eta t}} e^{2\eta t} + \epsilon \sigma A + \epsilon D \partial_{xx} u, \quad (3.44)$$

$$B_t - B_x = \frac{AC - 4\eta B}{S + e^{2\eta t}} e^{2\eta t} - \epsilon B, \quad (3.45)$$

$$C_t - C_x = \frac{AB - 4\eta C}{S + e^{2\eta t}} e^{-2\eta t} - \epsilon C, \quad (3.46)$$

where $S = e^{2\eta x} + e^{-2\eta x}$. Since $D \ll \epsilon$ was chosen the effects of diffusion will be ignored. The diffusion term is only relevant for long time scales. The problem has two time scales, the soliton decay time given by $t \simeq 1/2\eta$ and the damping time given by $t \simeq 1/\epsilon$. The growth time scale will always be smaller than the damping time

scale. For a separation of time scales $2\eta \gg \epsilon$, a multiple-time scale perturbation analysis can be considered. By a simple rescaling of time and distance the eigenvalue η can always be adjusted to be of order unity. The validity of the perturbation theory is then given by $\epsilon \ll 1$. When comparing with numerical results the parameters will be rescaled so that ϵ will be unity. This just implies that $\eta \gg 1$. For bookkeeping purposes η will be carried throughout the calculation and is considered an $O(1)$ quantity.

Fast and slow time variables are assigned

$$\tau_0 = t, \quad \tau_1 = \epsilon t, \quad (3.47)$$

so that

$$d/dt = d/d\tau_0 + \epsilon d/d\tau_1. \quad (3.48)$$

Consider perturbation expansions to first order

$$A = A_0(x, t) + \epsilon \mu, \quad (3.49)$$

$$B = B_0(x, t) + \epsilon \nu, \quad (3.50)$$

$$C = C_0(x, t) + \epsilon \omega. \quad (3.51)$$

Plug everything into Eqs. (3.44)-(3.46) and take order by order in ϵ :

$O(1)$:

$$\frac{\partial A_0}{\partial \tau_0} = 0, \quad (3.52)$$

$$\frac{\partial B_0}{\partial \tau_0} = 0, \quad (3.53)$$

$$\frac{\partial C_0}{\partial \tau_0} = 0. \quad (3.54)$$

$O(\epsilon)$:

$$\begin{aligned} \frac{\partial \mu}{\partial \tau_0} - (4\eta\mu - C_0\nu - B_0\omega) \frac{e^{2\eta\tau_0}}{S + e^{2\eta\tau_0}} = \\ - \frac{\partial A_0}{\partial \tau_1} + \frac{1}{\epsilon} (4\eta A_0 - B_0 C_0) \frac{e^{2\eta\tau_0}}{S + e^{2\eta\tau_0}} + \sigma A_0, \end{aligned} \quad (3.55)$$

$$\begin{aligned} \frac{\partial \nu}{\partial \tau_0} - \frac{\partial \nu}{\partial x} - (C_0\mu - 4\eta\nu + A_0\omega) \frac{e^{2\eta\tau_0}}{S + e^{2\eta\tau_0}} = \\ - \frac{\partial B_0}{\partial \tau_1} + \frac{1}{\epsilon} (A_0 C_0 - 4\eta B_0) \frac{e^{2\eta\tau_0}}{S + e^{2\eta\tau_0}} - B_0, \end{aligned} \quad (3.56)$$

$$\begin{aligned} \frac{\partial \omega}{\partial \tau_0} + \frac{\partial \omega}{\partial x} - (B_0 \mu + A_0 \nu - 4\eta \omega) \frac{e^{-2\eta x}}{S + e^{2\eta x}} = \\ - \frac{\partial C_0}{\partial \tau_1} + \frac{1}{\epsilon} (A_0 B_0 - 4\eta C_0) \frac{e^{-2\eta x}}{S + e^{2\eta x}} - C_0. \end{aligned} \quad (3.57)$$

Notice that the following ordering is imposed

$$2\eta A_0 - B_0 C_0 \sim O(\epsilon), \quad (3.58)$$

$$A_0 C_0 - 4\eta B_0 \sim O(\epsilon), \quad (3.59)$$

$$A_0 B_0 - 4\eta C_0 \sim O(\epsilon). \quad (3.60)$$

Recall that for the unperturbed situation the left hand sides of the above equations are identically zero. The $O(1)$ equations reveal that A_0 , B_0 and C_0 are independent of the fast time scale τ_0 . The $O(\epsilon)$ equations form an inhomogeneous system of equations with time dependent coefficients for the first order amplitudes. The $O(\epsilon)$ equations can be written in the simplified form

$$\left(\frac{\partial}{\partial \tau_0} + L \right) \phi = F, \quad (3.61)$$

where ϕ is a column vector of the first order amplitudes, F is the vector formed by the right hand side of the $O(\epsilon)$ equations and L is the spatial differential operator of the system. Ideally one would like to solve for the eigenstates of L , expand F in those states then remove the secularities as was done by Kaup (1990) for the nonlinear Schrödinger equation. In this manner the parts of F orthogonal to L which do not contribute secularities are identified. However the complexity and time dependence of L makes this proposition difficult. With this caveat in mind, the secularities of the $O(\epsilon)$ equations were eliminated equation by equation. The justification comes a posteriori by comparing with numerical results.

Removing the secular terms yields the set of slow modulation equations

$$\frac{\partial A_0}{\partial \tau_1} = (2\eta A_0 - B_0 C_0) \frac{e^{2\eta x/\epsilon}}{\epsilon(S + e^{2\eta x/\epsilon})} + \sigma A_0, \quad (3.62)$$

$$\frac{\partial B_0}{\partial \tau_1} - \frac{\partial B_0}{\partial x} = -B_0, \quad (3.63)$$

$$\frac{\partial C_0}{\partial \tau_1} - \frac{\partial C_0}{\partial x} = -C_0. \quad (3.64)$$

Equations (3.63)-(3.64) are readily solved to yield

$$B_0 = 2\sqrt{2}\eta e^{-\tau_1}, \quad (3.65)$$

$$C_0 = 2\sqrt{2}\eta e^{-\tau_1}, \quad (3.66)$$

since at $t = 0$, $B_0 = C_0 = 2\sqrt{2}\eta$. These results are then plugged into the modulation equation for A_0 , Eq. (3.62) to obtain

$$\frac{\partial A_0}{\partial \tau_1} = (2\eta A_0 - 8\eta^2 e^{-2\tau_1}) \frac{e^{2\eta\tau_1/\epsilon}}{\epsilon(S + e^{2\eta\tau_1/\epsilon})} + \sigma A_0. \quad (3.67)$$

This is a first order linear differential equation. It can be immediately solved to yield

$$A_0 \frac{e^{-\epsilon\sigma t}}{S + e^{2\eta t}} = -8\eta^2 \int^t dt \frac{e^{2\eta t} e^{-\epsilon(2+\sigma)t}}{(S + e^{2\eta t})^2} + R, \quad (3.68)$$

where the substitution $\tau_1 = \epsilon t$ was made and R is an integration constant. The integral on the right hand side of Eq. (3.68) can be integrated by parts twice to obtain an expansion to first order in ϵ . The expression for A_0 is then

$$A_0(x, t) = 4\eta e^{-2\epsilon t} - 2\epsilon(2 + \sigma) \frac{(S + e^{2\eta t})}{S} \left[\ln(1 + S e^{-2\eta t}) e^{-2\epsilon t} - \ln(1 + S) e^{\epsilon\sigma t} \right], \quad (3.69)$$

where the initial condition $A_0(x, t = 0) = 4\eta$ has been applied. Recall that the full perturbed solution for the parent is given by expression (3.41). Plugging in A_0 from Eq. (3.69) yields

$$u = \frac{4\eta e^{-2\epsilon t}}{S + e^{2\eta t}} - \frac{2\epsilon(2 + \sigma)}{S} \left[\ln(1 + S e^{-2\eta t}) e^{-2\epsilon t} - \ln(1 + S) e^{\epsilon\sigma t} \right]. \quad (3.70)$$

The daughters can be considered separated from the parent for times $t \geq 1/2\eta$. Thus, at separation the expression for the parent solution to first order in ϵ is

$$u \simeq \frac{2\epsilon(2 + \sigma) \ln(1 + S)}{e^{2\eta x} + e^{-2\eta x}}. \quad (3.71)$$

This is the remaining part of the parent after depletion to daughter solitons. Since $\ln(1 + S)$ is slowly varying compared to the denominator, simply evaluate it at $x = 0$, which gives $S = 2$. Notice that Eq. (3.71) has the form

$$u \simeq Q \operatorname{sech}(2\eta x), \quad (3.72)$$

where

$$Q = \epsilon(2 + \sigma) \ln(3). \quad (3.73)$$

The asymptotic solution for u has the form of a soliton with reduced amplitude!

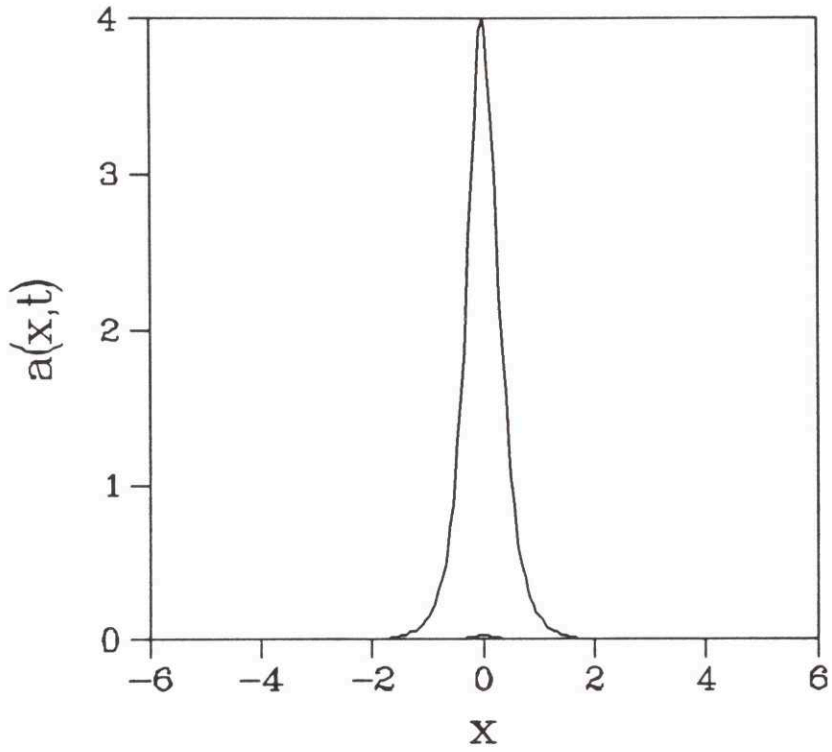
The cycling time for a growth and depletion cycle is given by the time it takes the amplitude Q to reach 2η , its initial value. Imposing this gives the expression

$$t_c \simeq \frac{1}{\epsilon\sigma} \ln \frac{2\eta}{\epsilon(2 + \sigma) \ln(3)}. \quad (3.74)$$

The total cycling time will actually be the depletion time plus this time (3.74). If the depletion time is much smaller than t_c it can be ignored.

The calculation was tested numerically. An initial condition of a parent soliton with eigenvalue $\eta = 2$ and small daughter pulses was taken to represent the ZM soliton solution Eqs. (3.32)-(3.34). Figure 3-11 shows the initial and final configurations for this case with $\eta = 2$, $\epsilon = 1$ and no growth. The remnant of the parent wave after the daughters have damped away has a reduced soliton shape as predicted by Eq. (3.72). The amplitude is a little less than the predicted value of $Q \simeq 2$ from Eq. (3.73). Other simulations with different damping rates consistently have amplitudes that are close to but a little less than predicted by the calculation. This may be due to the order ϵ perturbations in Eqs. (3.49)-(3.51) that were not included. However, it works reasonably well. Figure 3-12 shows the initial and final configurations for $\eta = 2$, $\epsilon = 1$ and $\sigma = 0.1$. Again the final result agrees fairly well with the calculation. However, as the growth is increased the calculation begins to fail. Again this may be due to the order ϵ perturbations. The calculation can only be trusted for very weak growth.

(a)



(b)

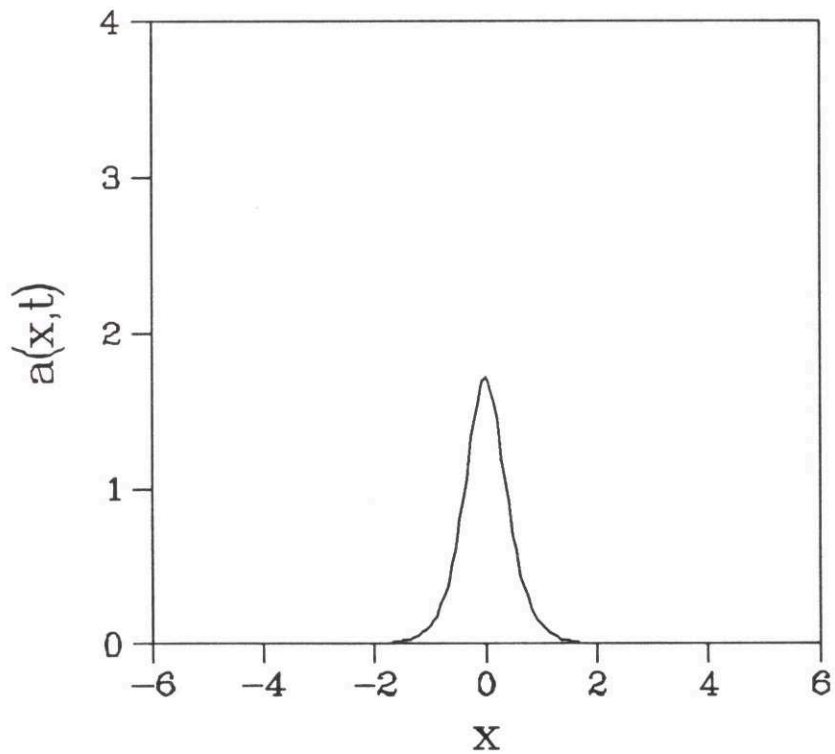


Figure 3-11: Soliton decay with $\eta = 2$, $\epsilon = 1$, and no growth; (a) initial configuration, (b) final configuration.

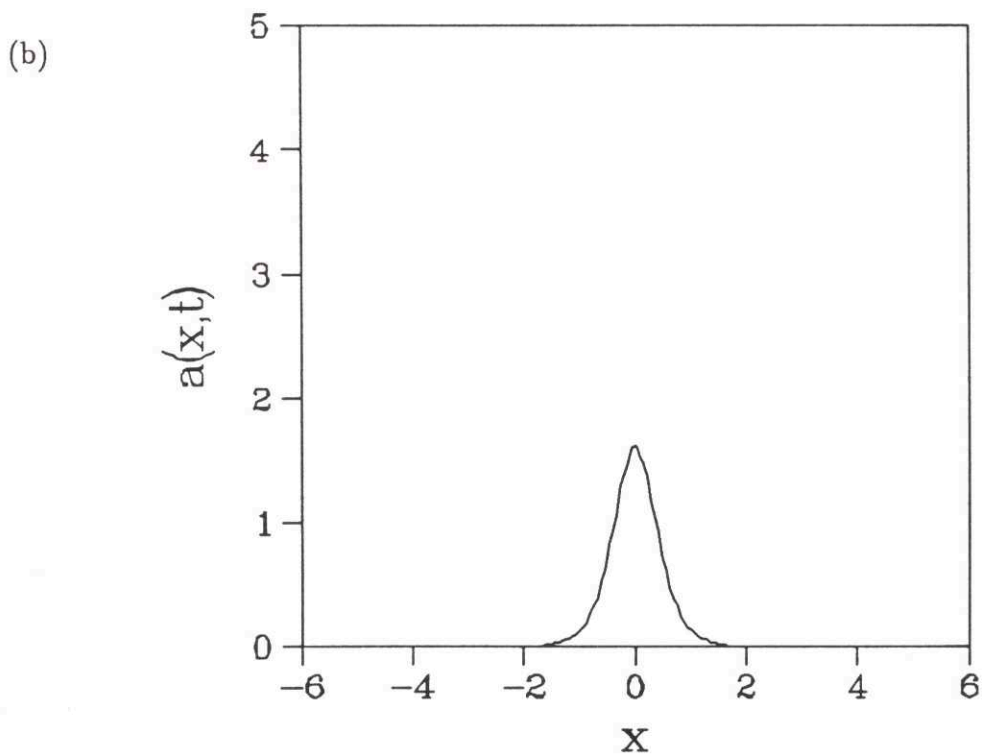
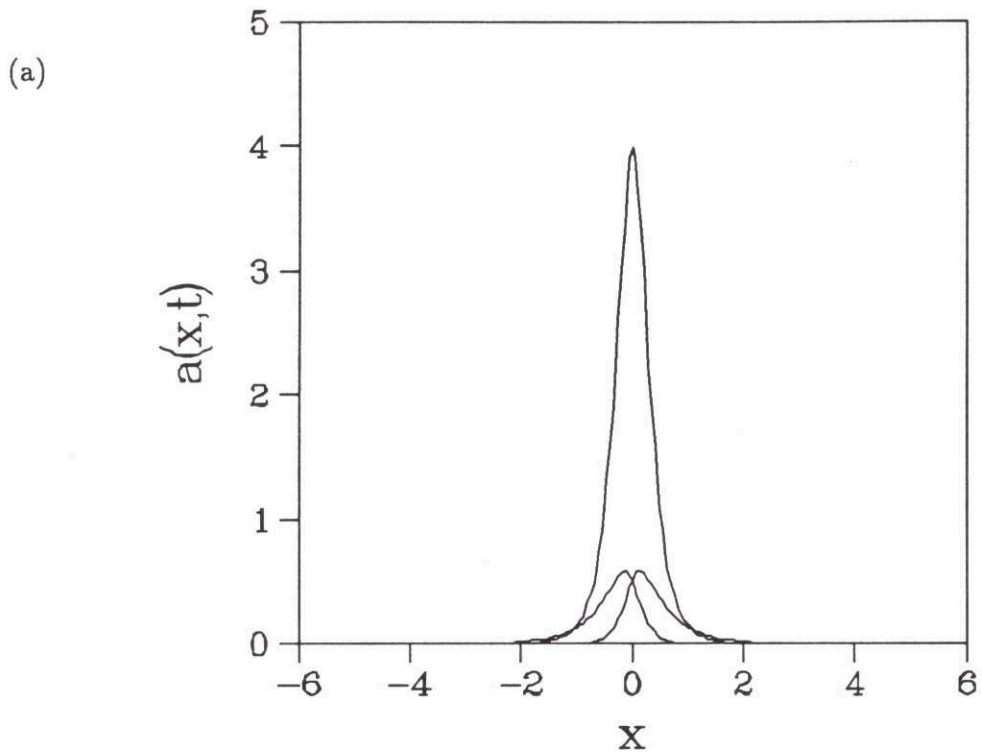


Figure 3-12: Soliton decay with $\eta = 2$, $\epsilon = 1$, and $\sigma = 0.1$; (a) initial configuration, (b) final configuration.

3.2.6 Scattering Space Perturbation Theory

In order to estimate the threshold eigenvalue, a perturbation expansion in scattering space, first developed by Kaup (1976b) and expanded by Kaup and Newell (1978) is employed. This subject has recently been reviewed by Kivshar and Malomed (1989). The following calculation is a time dependent version of the one given in Kaup *et al.* (1979), to estimate the threshold for noise induced decay of a soliton in the conservative 3WI. Those ideas have been used to construct a perturbation expansion to estimate the threshold for decay of the 3WI with growth and damping induced by collisions with daughter quasi-solitons.

The parametric interaction introduced in Section 2.3 has shown that a parent pulse is unstable to decay when it exceeds a critical threshold Eq. (3.12). However, a non-zero daughter amplitude (however small) is still required to induce the decay. The question of what threshold area or eigenvalue is required for the decay to occur remains. Many of the concepts and notation in this section are in Section 2.4 and Appendices A and B.

The specific question addressed is the decay of the parent into the daughter. For this the separation property of the ZM problem into three separate ZS problems will be used, see Kaup *et al.* (1979) and Appendix A. Since the pump decays into the two daughters symmetrically it is necessary to consider only one of them $q^{(3)}$, where $q^{(n)}$ are the corresponding ZS potentials for the n th envelope detailed in Appendix A. In accordance with the notation of Kaup *et al.* (1979), the envelopes are indexed by (1,2,3) with index 1 corresponding to the lowest group velocity, index 2 corresponding to the middle group velocity and index 3 corresponding to the highest group velocity. As $t \rightarrow \infty$ the envelopes will be separated and a ZS reflection coefficient for $q^{(3)}$ (right going daughter wave) is defined as (see Appendix B)

$$\rho^{(3)} = \frac{b^{(3)}}{a^{(3)}} = \frac{b_{21}}{b_{11}}. \quad (3.75)$$

Of interest is the soliton produced in $q^{(3)}$ by the decay of the parent $q^{(2)}$. The one

soliton solution for the ZS equation with eigenvalue $\lambda^{(3)} = i\xi$ has the form

$$q^{(3)}(x) = 2D_k^{(3)} \frac{e^{-2\xi x}}{1 + \frac{D_k^{(3)2}}{4\xi^2} e^{-4\xi x}}, \quad (3.76)$$

where

$$D_k^{(3)} = -i \frac{b^{(3)}}{a^{(3)}} \Big|_k \equiv -i \frac{b_{21}}{b'_{11}} \Big|_k, \quad (3.77)$$

is given by Eq. (B.11). The magnitude of the soliton solution Eq. (3.76) can be written as

$$|q^{(3)}(x)| = 2\xi \operatorname{sech}[2(\xi - \Gamma)], \quad (3.78)$$

where

$$|D_k^{(3)}| = 2\xi e^\Gamma. \quad (3.79)$$

The average position of the soliton is then given by

$$x^{(3)} = \frac{\Gamma}{2\xi}. \quad (3.80)$$

This gives the asymptotic position of the soliton after it has separated from the parent. An estimate of when the soliton was emitted can be found by extrapolating the position of the soliton to the position of parent soliton $q^{(2)}$, where it was initially emitted. For a parent soliton with zero group velocity ($c_2 = 0$) located at the origin, this would imply

$$\Gamma = \ln \left[\frac{D_k^{(3)}(t)}{2\xi(t)} \right] = 0. \quad (3.81)$$

From this, the threshold condition for soliton emission is found to be

$$D_k^{(3)}(t) = 2\xi(t). \quad (3.82)$$

For the integrable case ξ is constant, and $\partial_t D_k^{(3)}(t) = 2\xi D_k^{(3)}(t)$. The perturbing terms evoke a time variation. Scattering space perturbation theory is employed to determine the time dependence.

In addition to the ZM eigenfunctions given in Appendix A, define the eigenfunctions $\Psi^{(j)}$ with the following boundary conditions:

$$\Psi_n^{(j)} \rightarrow \delta_n^j e^{-ic_j x} \quad \text{as } x \rightarrow \infty, \quad (3.83)$$

A set of adjoint eigenfunctions for the associated adjoint problem can also be defined (Kaup, 1976a; Kaup *et al.*, 1979)

$$\epsilon^{ijk} \Phi_n^{(k)A} = -c_n \sum_{m,p=1}^3 \epsilon_{nmp} \Phi_m^{(i)} \Phi_p^{(j)} e^{i\zeta x(c_1+c_2+c_3)}, \quad (3.84)$$

and correspondingly for $\Psi_n^{(k)A}$, where ϵ_{ijk} is the totally antisymmetric tensor of rank three. Defining $[b_{ij}]$ to be the inverse of $[a_{ij}]$, Kaup *et al.* (1979) found the time evolution of the inverse of the scattering data to be

$$b_{ij,t} = -I[\Phi^{(j)}, \Psi^{(i)}], \quad (3.85)$$

where

$$I[U, W] = i \int_{-\infty}^{\infty} \tilde{U}^A C^{-1}(V_t) W dx, \quad (3.86)$$

where the $\tilde{}$ denotes matrix transpose, and the notation $C \equiv \text{diag}[c_1, c_2, c_3]$, $V \equiv [V_{ij}]$ has been used. The ZM potentials V_{ij} are defined in Eqs. (A.10)-(A.12). Equation (3.85) relates the time evolution of the scattering data directly to that of the potential. From Eq. (A.17) the time evolution of the scattering data for the integrable 3WI has the simple form

$$b_{ij,t} = i\zeta c_1 c_2 c_3 \left(\frac{1}{c_i} - \frac{1}{c_j} \right) b_{ij}. \quad (3.87)$$

Using Eqs. (A.10)-(A.12) with Eqs. (3.29)-(3.31) the perturbed 3WI can be rewritten as an equation for the ZM potentials V . In generalized notation this takes the form

$$V_t = F_0(V) + \epsilon F_1(V), \quad (3.88)$$

where F_0 represents the unperturbed parts and F_1 represents the first order perturbation (terms of $O(\epsilon)$). Kaup's (1976b) strategy was to use this in Eq. (3.85) to construct an expansion in ϵ for the time dependence of the scattering data. To first order Eq. (3.85) becomes

$$b_{ij,t} = -I^{(0)}[\Phi^{(j)}, \Psi^{(i)}] - \epsilon I^{(1)}[\Phi^{(j)}, \Psi^{(i)}], \quad (3.89)$$

where in $I^{(1)}$ the perturbed part of Eq. (3.88) F_1 , is used in combination with the unperturbed eigenfunctions.

The emitted soliton is given by a zero in the upper half ζ plane of b_{11} . Here ζ is the ZM eigenvalue. At a zero of b_{11} designated by ζ_k the total derivative is also zero so

$$\left. \frac{db_{11}}{dt} \right|_{\zeta=\zeta_k} = \left(\frac{\partial b_{11}}{\partial t} \right)_{\zeta_k} + \left(\frac{\partial b_{11}}{\partial \zeta} \right)_{\zeta_k} \frac{d\zeta_k}{dt} = 0. \quad (3.90)$$

Rearranging and using Eqs. (3.89) with (3.90) gives

$$\frac{d\zeta_k}{dt} = -\frac{1}{(b'_{11})_k} \left(\frac{\partial b_{11}}{\partial t} \right)_{\zeta_k} \quad (3.91)$$

$$= \frac{1}{(b'_{11})_k} I[\Phi^{(1)}, \Psi^{(1)}; \zeta_k], \quad (3.92)$$

where $(b'_{11})_k = (\partial b_{11}/\partial \zeta)|_{\zeta_k}$, and the third variable in I implies evaluation at $\zeta = \zeta_k$. Eq. (3.92) is the time dependence of the eigenvalue induced by the perturbing terms. To obtain the time evolution of the residue of $\rho^{(3)}$ it is necessary to account for the time variation of ζ_k . Thus

$$\partial_t \left(\frac{b_{21}}{b'_{11}} \Big|_{\zeta=\zeta_k} \right) = \left[\partial_t \left(\frac{b_{21}}{b'_{11}} \right) + \zeta_{k,t} \partial_\zeta \left(\frac{b_{21}}{b'_{11}} \right) \right] \Big|_{\zeta=\zeta_k}. \quad (3.93)$$

Since $D_k^{(3)} = -i(b_{21}/b'_{11})$ the time evolution for $D_k^{(3)}$ is

$$D_{k,t}^{(3)} = (b'_{11})_k^{-2} \left\{ -(b''_{11})_k D_k^{(3)} I[\Phi^{(1)}, \Psi^{(1)}; \zeta_k] - i \frac{c_2 - c_1}{2} J[\Phi^{(1)}, \chi; \zeta_k] \right\}, \quad (3.94)$$

where $\chi = b_{21}\Psi^{(1)} - b_{11}\Psi^{(2)}$ and

$$J[U, W; \zeta_k] \equiv i \int_{-\infty}^{\infty} \partial_\zeta [\tilde{U}^A C^{-1}(V_t)W] \Big|_{\zeta=\zeta_k}. \quad (3.95)$$

This was found by using Eq. (3.85) in Eq. (3.93).¹

Assume at $t = 0$, $q^{(1)} = q^{(2)}$ are small and $q^{(2)}$ is a soliton located at $x = 0$ with eigenvalue $\zeta = \zeta_1 = i\eta$. Let the group velocities be $c_3 = -c_1 = 1, c_2 = 0$. From Eq. (A.23) this gives $\xi = \eta/2$. To lowest order the integrals in Eq. (3.94) can be evaluated with the unperturbed pure soliton states. For this initial condition (Kaup, 1976b; Kaup *et al.*, 1979)

$$b_{11} = \frac{\zeta - \zeta_1}{\zeta - \zeta_1^*}, \quad (3.96)$$

¹There is a typographical error in Eq. F18 in Kaup *et al.* (1979). The factor b''_{11} is missing.

$$I = - \int_{-\infty}^{\infty} \frac{dx}{e^{2\eta x} + e^{-2\eta x}} q_t^{(2)}, \quad (3.97)$$

$$J = \frac{1}{i\eta} \int_{-\infty}^{\infty} \frac{dx}{e^{2\eta x} + e^{-2\eta x}} \left(e^{\eta x} q_t^{(1)} + e^{-\eta x} q_t^{(3)} \right). \quad (3.98)$$

From Eq. (3.29) the evolution equation of $q^{(2)}$ has the form

$$q_t^{(2)} = \epsilon \sigma q^{(2)} + \epsilon D q_{xx}^{(2)} + \dots, \quad (3.99)$$

where only the perturbing terms are shown. Again, consider the diffusion to be so small that it can be neglected on the short time scales. Equation (3.99) with $q^{(2)} = 2\eta \text{sech}(2\eta x)$ is then plugged into Eq. (3.97) and integrated to yield for the $O(\epsilon)$ term

$$\epsilon I^{(1)} = -\epsilon \sigma. \quad (3.100)$$

From Eqs. (3.29) and (3.30) the evolution equations for the two daughters have the form

$$q_t^{(1)} = -\epsilon q^{(1)} + \dots, \quad (3.101)$$

$$q_t^{(3)} = -\epsilon q^{(3)} + \dots \quad (3.102)$$

Let the initial conditions of the daughters have the form of amplitude reduced solitons

$$q^{(1)} = B \text{sech}(\eta x), \quad (3.103)$$

$$q^{(3)} = C \text{sech}(\eta x), \quad B, C \ll \eta. \quad (3.104)$$

Plugging into Eq. (3.98) yields for the $O(\epsilon)$ term

$$\epsilon J^{(1)} = \frac{-\epsilon}{2i\eta} \int_{-\infty}^{\infty} dx \text{sech}(2\eta x) \text{sech}(\eta x) (B e^{\eta x} + C e^{-\eta x}). \quad (3.105)$$

If $B = -C$ then $J^{(1)} = 0$. This implies that two daughter pulses of opposite phase will not deplete the parent. This fact is seen in the evolution Eqs. (3.7)-(3.9) where opposite phased daughters make a positive parent grow rather than deplete. Consider the case where $C = B$. Then Eq. (3.105) is integrated to yield

$$\epsilon J^{(1)} = \frac{-\epsilon \pi B}{i\eta^2}. \quad (3.106)$$

This situation gives the maximum depletion initial condition. Plugging into Eq. (3.94), with the knowledge of the unperturbed part yields

$$D_{1,t}^{(3)} = \eta D_1^{(3)} + 2\epsilon\sigma D_1^{(3)} - \epsilon \frac{\pi B}{2}. \quad (3.107)$$

Plugging into the eigenvalue evolution equation (3.92) yields

$$i\eta_t = 2i\epsilon\sigma\eta, \quad (3.108)$$

which integrates to

$$\eta = \eta_0 e^{2\epsilon\sigma t}. \quad (3.109)$$

In the STC situation, the parent pulse decays and emits quasi-solitons which damp as they propagate. They can then collide with another parent pulse and trigger a second decay. With this in mind B is written in the form

$$B = \eta e^{-\phi}, \quad (3.110)$$

where $e^{-\phi}$ represents the damping experienced by the quasi-soliton before it collides with the parent pulse. Note that B differs from the daughter soliton amplitudes $B_0/2$ in Eq. (3.65) by a factor of $\sqrt{2}$. This is because for the group velocities chosen the wave amplitudes and the corresponding ZS potentials differ by a factor of $\sqrt{2}$.

Of course in this calculation the parent pulse is a soliton. For very slow growth this should be a reasonable approximation because it is the soliton content of the pulse that is involved in the decay. The growth may cause some of the soliton content to be transformed into radiation but if it is slow the effect should not alter the results drastically. Plugging Eq. (3.108) into Eq. (3.107) yields

$$D_{1,t}^{(3)} = \eta_0 e^{2\epsilon\sigma t} D_1^{(3)} + 2\epsilon\sigma D_1^{(3)} - \epsilon\pi(\eta_0/2)e^{-\phi} e^{2\epsilon\sigma t}. \quad (3.111)$$

This is a first order linear equation which can be integrated to yield

$$D_1^{(3)} e^{-\frac{\eta}{2\epsilon\sigma} e^{2\epsilon\sigma t}} e^{-2\epsilon\sigma t} = -\epsilon\pi \frac{\eta_0}{2} e^{-\phi} \int e^{-\frac{\eta}{2\epsilon\sigma} e^{2\epsilon\sigma t}} dt + R, \quad (3.112)$$

where R is an integration constant. The integral on the right hand side of Eq. (3.112) can be expanded in powers of $2\epsilon\sigma/\eta_0$ by integrating by parts twice. Performing this

operation yields

$$D_1^{(3)} = \epsilon \frac{\pi}{2} \left(1 - 2 \frac{\epsilon \sigma}{2} e^{-2\epsilon \sigma t} \right) + R e^{-\frac{\eta}{2\epsilon \sigma} e^{2\epsilon \sigma t}} e^{2\epsilon \sigma t}. \quad (3.113)$$

At this point the initial condition must be applied. The initial condition also splits into a zeroth order term plus a first order term. The zeroth order contribution is identically zero since the unperturbed state was chosen to be a single parent soliton. The first order contribution is due to the small but non-zero initial amplitudes of the daughters. Thus following the same calculation as above (see Kaup *et al.*, 1979) except for a variation in $D_1^{(3)}$ due to the perturbation it can be shown that initially

$$D_1^{(3)}(t=0) = \frac{\pi B}{2}. \quad (3.114)$$

Using this in Eq. (3.113) and applying the threshold condition Eq. (3.82) yields

$$\begin{aligned} \eta_0 e^{2\epsilon \sigma t} = \frac{\epsilon \pi}{2} e^{-\phi} \left(1 - 2 \frac{\epsilon \sigma}{\eta_0} e^{-2\epsilon \sigma t} \right) \\ + \pi e^{-\phi} \left(\frac{\eta_0}{2} - \frac{\epsilon}{2} \left(1 - 2 \frac{\epsilon \sigma}{\eta_0} \right) \right) e^{-\frac{\eta}{2\epsilon \sigma} e^{2\epsilon \sigma t} - 1} e^{2\epsilon \sigma t}. \end{aligned} \quad (3.115)$$

One observes immediately from the threshold equation (3.115) that for $\eta_0 < \epsilon$ the parent will not decay. The damping will be sufficiently strong to suppress the decay. This agrees with the conclusion deduced from the WKB threshold condition Eq. (3.12). The solution set (η_0, t) could be found numerically although care must be taken to ensure the correct branch is chosen. However, an analytic expression would be very useful.

The eigenvalue η grows at a rate $e^{2\epsilon \sigma t}$. If $\eta_0 < \epsilon$ then the decay will not occur and the eigenvalue will continue to grow until another collision occurs. On average nearest neighbor pulses will be depleting at roughly t_c intervals generating quasi-solitons that may induce the decay of the pump. Suppose that $\eta_0 \sim 2\epsilon$ at a collision with a daughter pulse. Self consistency can be checked for a posteriori. Then a lowest order estimate of η can be made. Plugging in $\eta_0 \sim 2\epsilon$ into Eq. (3.115) yields

$$2\epsilon \simeq \frac{\epsilon \pi}{2} e^{-\phi} e^{-2\epsilon \sigma t} + \frac{\pi}{2} e^{-\phi} e^{\frac{1}{\sigma} (e^{2\epsilon \sigma t} - 1)}. \quad (3.116)$$

Terms of $O(\sigma)$ have been dropped; this approximation is valid in the weak growth limit. Furthermore consider the limit where $2\epsilon\sigma t \ll 1$ (short times), so the exponentials in Eq. (3.116) can be expanded in a Taylor series. Truncating to first order and solving for t yields the result

$$t \sim \frac{1}{2\epsilon} \ln \left(\frac{4}{\pi} e^{-\phi} \left(1 - \frac{\pi}{4} e^{-\phi} \right) \right). \quad (3.117)$$

This value for t can then be plugged into the expression for η Eq. (3.109) to obtain

$$\eta \sim 2\epsilon e^{\sigma \ln \left(\frac{4}{\pi} e^{-\phi} \left(1 - \frac{\pi}{4} e^{-\phi} \right) \right)}. \quad (3.118)$$

By taking $\phi \gg \ln(4/\pi e^{-\phi} - 1)$, Eq. (3.118) can be expanded to yield the simple form

$$\eta \sim 2\epsilon(1 + \sigma\phi). \quad (3.119)$$

In the STC regime as seen in Section 3.2.1 parent pulses are collided upon more or less randomly by quasi-solitons with random phases. Consider a situation where a collision is due to daughter pulses emitted two correlation lengths ξ_p away. The factor ϕ is then the damping occurred for propagation over this length

$$\phi \sim 2\xi_p \epsilon / c_3 = 2\epsilon\xi_p, \quad (3.120)$$

since c_3 has been scaled to unity. The expression for η now takes the form

$$\eta \sim 2\epsilon(1 + 2\sigma\epsilon\xi_p). \quad (3.121)$$

Plugging this result into the expression for cycling time Eq. (3.74) yields

$$t_c \sim \frac{1}{\epsilon\sigma} \ln \frac{4\epsilon(1 + 2\sigma\epsilon\xi_p)}{\epsilon(2 + \sigma) \ln 3}. \quad (3.122)$$

This expression really should be considered to be a lower bound. It assumes that the daughters collide with equal phases. In the STC situation this would not always hold true. Radiation and diffusion effects will also serve to suppress the decay of the parent pulse. For the parameter regime of the nearly integrable regime the logarithm is of order unity and this expression is simplified to

$$t_c \sim \frac{1}{\epsilon\sigma}. \quad (3.123)$$

3.2.7 Long Time Behaviour and STC

The long time behaviour of SDI stems from the diffusion of the parent wave and the many collisions between the parent structures and the daughter quasi-solitons. The phases of the colliding quasi-solitons are very important for the outcome of the result. Consider real envelopes. From Eq. (3.7) it is apparent that if the two quasi-solitons have opposite sign they reinforce a positive pump and cause a negative one to deplete. Conversely two quasi-solitons of the same sign will deplete a positive pump but feed a negative one. In the STC situation a parent at a given location will be involved with collisions with quasi-solitons at random times with random phases. Certain collisions will cause the parent structure to grow and others will deplete it. Thus the threshold eigenvalue will have a spread around some average value depending on the phases of the quasi-solitons and the frequency of collisions. The parent structures also act as amplifiers for the quasi-solitons. When a quasi-soliton collides with a parent structure of the right phase it can trigger a depletion and create new quasi-solitons. The quasi-soliton regenerates itself and continues to propagate. By this mechanism the effect of a quasi-soliton could extend over very long distances. During the process there will be a small phase shift due to the time required for decay. So the long correlations will be close to but exactly not along the characteristic curve.

In the STC situation the parent structures are not truly in isolation. Quite to the contrary they are in the close proximity to one another. A more appropriate (although more difficult) way to handle the problem may be to consider the ZS problem with a perturbed periodic potential. The lack of isolation can lead to interesting effects. For instance tunnelling between adjacent parent structures can occur. This could lead to bound states of double or even n -tuple wells. These effects were sometimes observed in the simulations.

If the diffusion coefficient is zero then there will be no nonlinear saturation. The generated high q modes would not be damped. The parent structures would simply cascade to shorter and shorter length scales with higher and higher amplitudes. The diffusion is responsible for the long time behaviour. The parent structures tend to grow and deplete in one location for very long times compared to the cycling time scale

t_c . However the action of the diffusion combined with the growth and depletion will cause them to drift and shift position. A simplistic estimate of the long time scale for the parent τ_p is obtained by considering the diffusion time across a correlation length. Thus

$$\tau_p \simeq D/\xi_p^2 = \frac{(2\pi)^2}{\gamma_i}. \quad (3.124)$$

The long time scale observed in the daughter wave dynamics will be related to the parent correlation time. As the quasi-solitons collide with the parent structures they will deplete creating new quasi-solitons. As the parent structures drift so will the location for creation of the quasi-solitons. However the quasi-solitons have a different width than the parent structures so the long time scale of the daughters τ_d is given by

$$\tau_d \simeq \frac{4}{\eta^2 D}. \quad (3.125)$$

The average saturated energy density can be crudely estimated from the threshold eigenvalue η . Recall that the simulation results show that the saturated state of the parent wave is in the form of coherent structures with the average amplitude related to η . Locally, the shape of the coherent structures are roughly sinusoidal with wavenumber q_0 . Let the parent wave be composed of locally sinusoidal coherent structures of average amplitude a_0 . Then the average energy density $\langle U_i \rangle / L \equiv S_i(0, 0)$ (see Section 3.2.3) is given by

$$S_i(0, 0) \simeq a_0^2/2. \quad (3.126)$$

The average amplitude can be estimated by using the Bohr quantization condition Eq. (2.51). Taking a square wave form with a width given by the correlation length ξ_p gives a condition relating the average amplitude to the average eigenvalue

$$(a_0^2 + \eta^2)^{1/2} \xi_p = \frac{\pi}{2}. \quad (3.127)$$

Solving for a_0 and plugging into Eq. (3.126) yields

$$S_i(0, 0) \simeq \frac{1}{2} \left[\left(\frac{\pi}{2\xi_p} \right)^2 + \eta^2 \right]. \quad (3.128)$$

Given this estimate for $S_i(0, 0)$ the average daughter energy density $S_j(0, 0)$ follows from Eq. (3.25).

3.2.8 Discussion

The analytical estimates can be compared with the simulation results. In the simulation $\gamma_j \equiv \epsilon = 1$, $\gamma_i \equiv \sigma = 0.1$, and $D = 0.001$. From Eq. (3.10) and (3.13), the principal mode is $q_0 = 10$, which gives a correlation length of $\xi_p \simeq 0.6$. The threshold eigenvalue Eq. (3.28) comes out to be $\eta \simeq 2.2$. This then gives a daughter correlation length of $\xi_d \simeq 0.9$ from Eq. (3.14). The cycling time is given by $t_c \simeq 8$ from Eq. (3.74). From Eq. (3.124) the parent correlation time is $\tau_p \simeq 400$. From Eq. (3.125), the correlation time of the daughter is $\tau_d \simeq 800$. To compare with the results of the simulation the values can be expressed in terms of frequencies and wave numbers.

For the parent wave the long time scale τ_p translates to a frequency of $\omega_p \simeq 0.016$ which corroborates with what was observed in the parent power spectrum in Fig. 3-5. The predicted cycling time translates to $\omega_c \simeq 0.78$. This value is high by about a factor of two compared to the shoulder observed in the parent power spectrum. However the spacetime profiles in Fig. 3-1 do show some of the parent structures cycling near the predicted time scale, and Fig. 3-2 shows quasi-solitons being created at a rate close to the predicted value so the calculation does give a lower bound. The daughter power spectrum in Fig. 3-8 showed two peaks in the high frequency regime. The lower frequency one corresponds to the cycling time and the higher frequency one is at twice the frequency and is probably a harmonic of the first. The predicted long time scale translates to a frequency of $\omega_d \simeq 0.008$ which again corroborates well with the simulation result.

The spectrum of static fluctuations in Fig. 3-4 for the parent wave shows a cutoff near $q_0 \simeq 10$ as expected. The daughter wave has a much softer cutoff as seen in Fig. 3-7. Since the correlation length is due to the quasi-soliton width this is expected. The quasi-soliton width is inversely proportional to the threshold eigenvalue η and thus has a spread about an average value. The estimate for the width given by the correlation length ξ_d corresponds to a wave number of $q_d \simeq 7$ which is somewhat high for the same reason the cycling frequency estimate was too high.

The ratio of the parent energy to the daughter energy was predicted to be $U_i/U_j \simeq 15$ from Eq. (3.25). The energy time series in Fig. 3-9 corroborates this. The peak

height of the correlation functions of the parent and daughter waves $S_i(0,0)/S_j(0,0)$ (Figs. 3-3 and 3-6) show the same ratio. The two daughter waves are synchronized as expected from Eq. (3.19). The parent average energy density was calculated to be $S_i(0,0) \simeq 5.8$ from Eq. (3.128) which is quite good considering the cavalier approximations made. The power spectrum of the energy in Fig. 3-10 shows a peak at around $\omega \simeq 5$ which is a little closer to the estimate for t_c . Recall that the cycling time perturbation calculation in Section 3.2.4 was actually done for the eigenvalue or area cycling time.

A word should be said about the system size. It is clear with the very long correlation times for the daughters that they cycle the box many times before correlations decay away. Thus for long times, the temporal correlation function along the characteristic or at a single spatial location would be the same. This was borne out in the simulation. It is unknown what the precise boundary effects are since it would be impossible to numerically test a system large compared to this long time scale. However with other runs of varying length, it was found that the above time scales seem to be unaffected by the system size as long as it is much larger than ξ_p . The power law rise for the parent power spectrum below $2\pi/\tau_p$, seems to decrease in exponent as the system size increases. It appears that the main features of STC in terms of correlation functions can be understood for this parameter regime.

3.3 Other Parameter Regimes

The parameter space is extremely vast. The above parameters were chosen because they exhibited STC and fell into the regime where perturbation theory was possible to provide analytical estimates for the properties of the correlation functions. However the system is very rich and other regimes are equally complex and interesting albeit less tenable to analytical analysis. Two different cases will be shown demonstrating other forms of STC in SDI. These are by no means an exhaustive representation of the behaviour of the system. The regime studied above in this chapter was the weak growth and weak diffusion regime. In this section a case where the growth of the

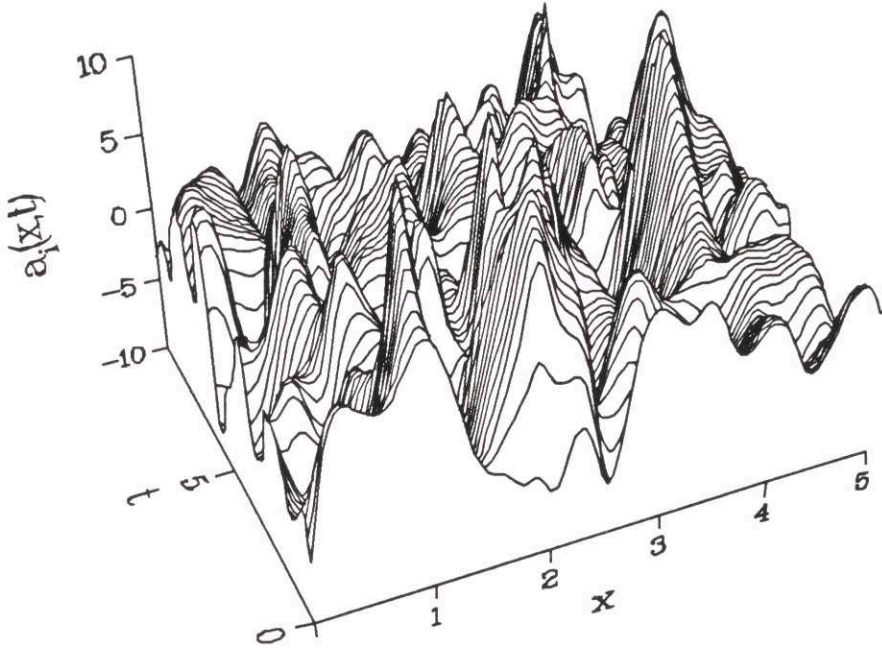


Figure 3-13: Spacetime profile of the parent wave a_i in the strong growth regime.

parent is comparable to the damping and a case where the diffusion is large will be studied.

3.3.1 The Strong Growth Regime

The parameters for this case were $\gamma_i = 1$, $D = 0.01$, $L = 20$. Again the system was numerically simulated and evolved until a saturated state was reached. The correlation functions were measured for each envelope.

Figure 3-13 shows the spacetime profile of the parent wave. As in the nearly integrable case there is still evidence of structures growing and depleting. However, unlike that case the depletions are very violent often destroying the structures. The correlation function $S_i(x, t)$ in Fig. 3-14 shows correlations decaying very rapidly in both space and time indicating STC. Temporally there seems to be a short time scale on the order of $t_p \simeq 1$ with a small tail. A hint of periodicity appears in the space direction with an apparent correlation length around $\xi_p \simeq 1$. The local power

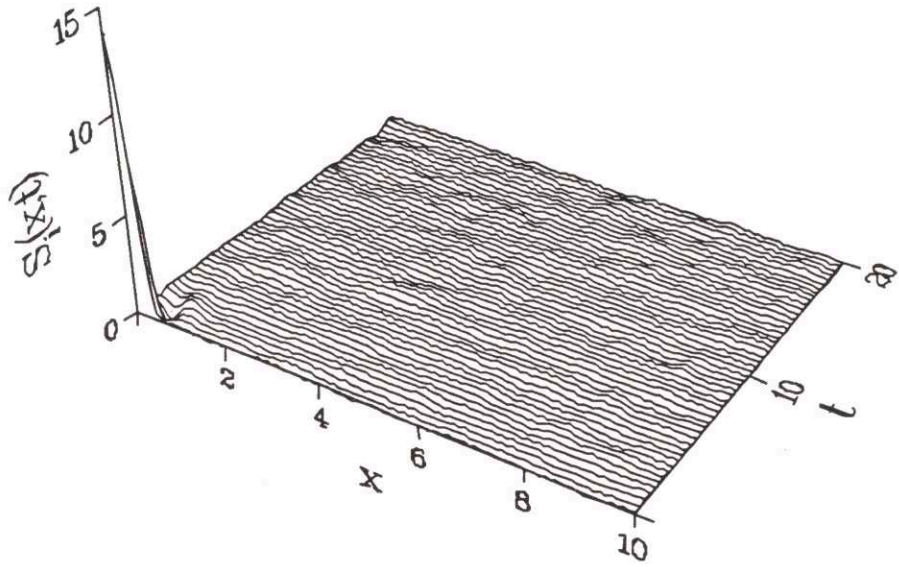


Figure 3-14: Correlation function of the parent wave a_i in the strong growth regime.

spectrum $S_i(x=0, \omega)$ appears in Fig. 3-15. There is a cutoff at approximately $\omega \simeq 2$. This corresponds to a time scale of $t \simeq 3$, which is consistent with the spacetime profile. In the spacetime profile the structures are seen to grow and deplete over a range of times. Many have time scales around $t \simeq 1$, and the number decreases with increasing depletion times. The longest depletion times are around $t \simeq 5$. The shortest depletion time is reflected in the sharp drop in the correlation function. The complete decorrelation of a parent structure seems to require a few depletions and this shows up as the short tail in the correlation function and the correlation time observed in the power spectrum. Fig. 3-16 shows the spectrum of static fluctuations. A cutoff around $q \simeq 8$ is observed. The cutoff is much softer than in the nearly integrable case where a hump was observed. The principal mode for these parameters is $q_0 = 10$. The spacetime profiles show that the violent depletions tend to broaden the widths of the coherent parent pulses.

The spacetime profile of the daughter wave is in Fig. 3-17. The most notable feature is that the amplitudes of the quasi-solitons are of the same order as the parent

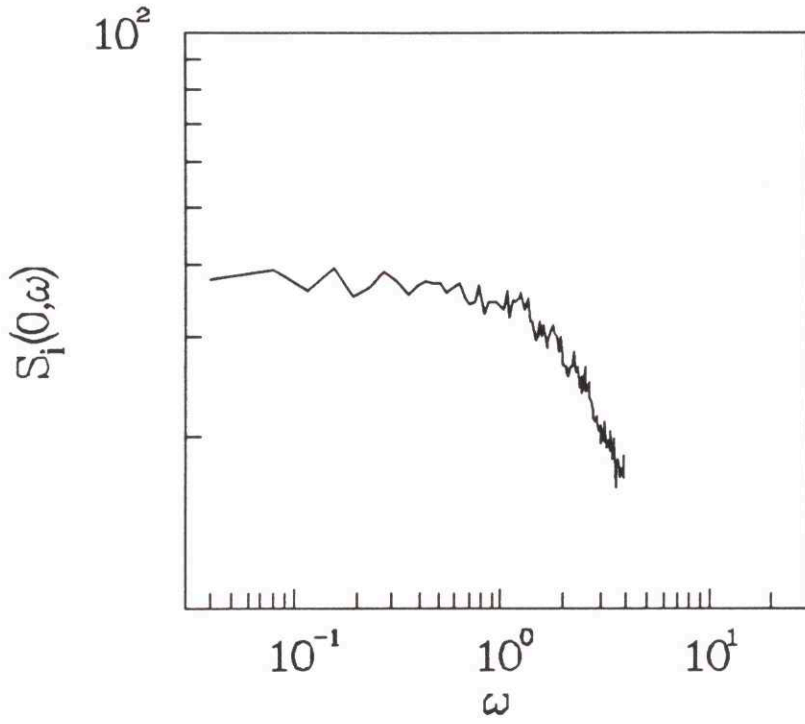


Figure 3-15: Local power spectrum of the parent wave a_i in the strong growth regime.

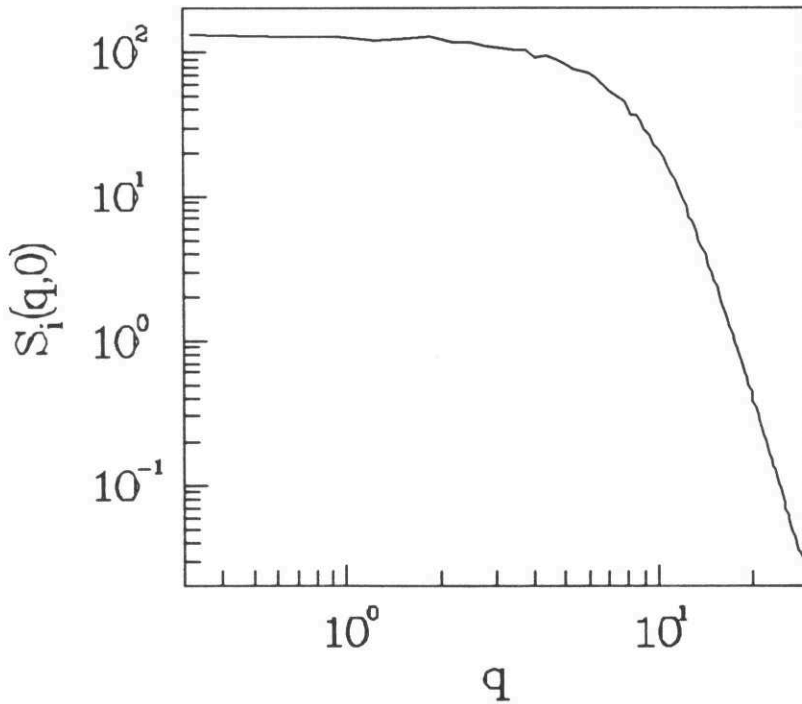


Figure 3-16: Spectrum of static fluctuations of the parent wave a_i in the strong growth regime.

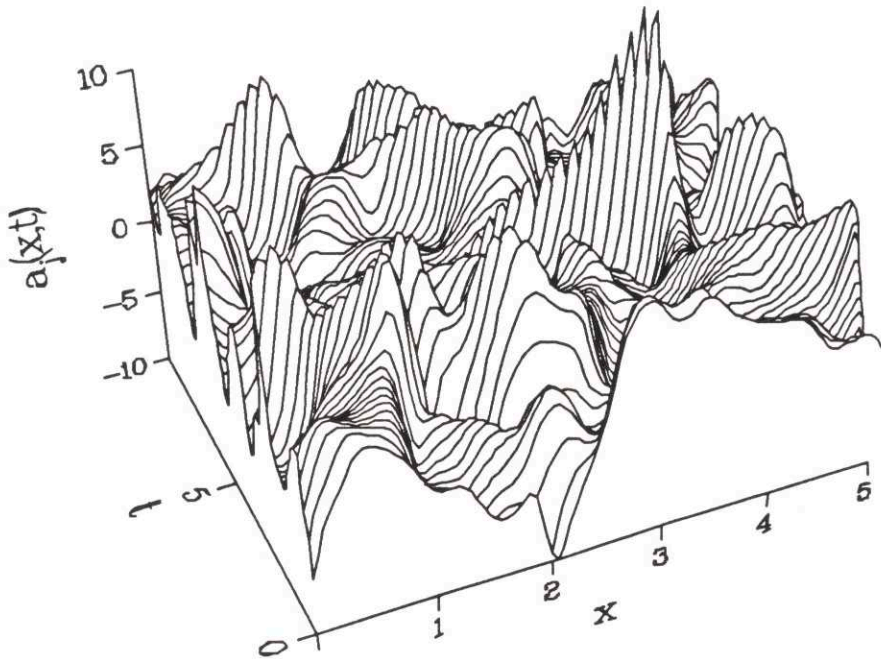


Figure 3-17: Spacetime profile of the daughter wave a_j in the strong growth regime.

structures. This is because the growth rate and the damping rate are equal. Thus the energies will be roughly equal according to Eq. (3.25). The dynamics involve collisions between parent and daughter structures of comparable size so radiation effects are more important than in the nearly integrable case (Kaup *et al.*, 1979). The perturbation results of the nearly integrable case will not apply. The correlation function is shown in Fig. 3-18. It shows definite spatial and temporal scales. The power spectrum is shown in Fig. 3-19. There is a cutoff at approximately $\omega \simeq 3$ corresponding to a time scale of $t \simeq 2$. The spacetime profiles show that decorrelation is due mostly to the damping. The correlation length is around $\xi_d \simeq 1$ as seen in the correlation function and in the spectrum of static fluctuations in Fig. 3-20 as a cutoff around $q \simeq 6$. The energy ratio is $S_i(0,0)/S_j(0,0) \simeq 1.5$ as expected from the conservation condition Eq. (3.25).

Applying the perturbation results of Section 3.2.4, realizing these parameters are beyond its validity yields the results $\eta \simeq 4.5$, $\eta' \simeq 1.6$. This gives $t_c \simeq 1$ and $\xi_d \simeq .4$. The result for the cycling time does agree with the simulation. However the daughter

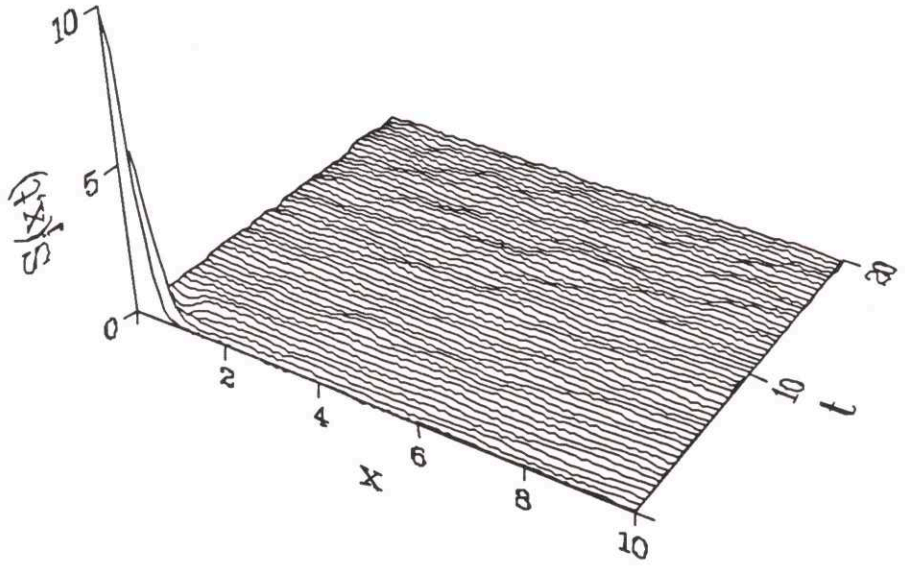


Figure 3-18: Correlation function of the daughter wave a_j in the strong growth regime.

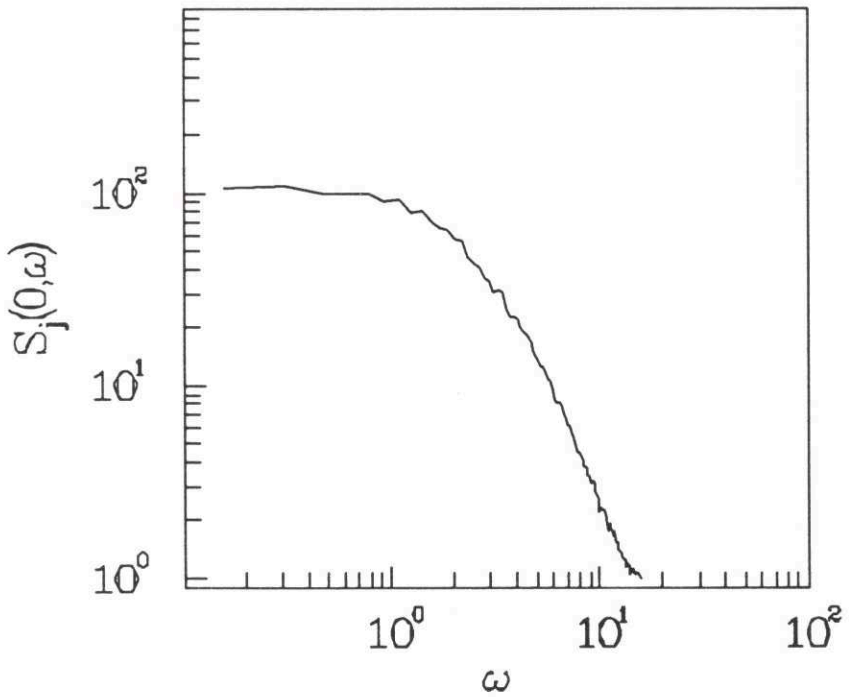


Figure 3-19: Power spectrum of daughter wave a_j in the strong growth regime.

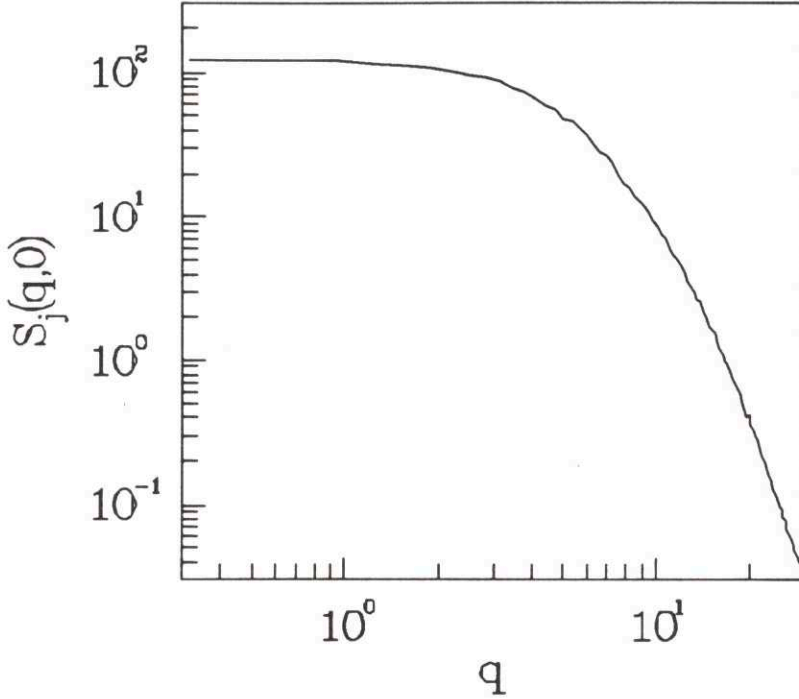


Figure 3-20: Spectrum of static fluctuations of daughter wave a_j in the strong growth regime.

correlation length does not fare as well. The spacetime profile shows that well defined quasi-solitons do not exist as they did in the nearly integrable case.

3.3.2 The Strongly Diffusive Regime

The parameters are $\gamma_i = 0.1$, $D = 0.05$, $L = 80$. The parent spacetime profile is shown in Fig. 3-21. As in the nearly integrable case, there are spatial structures that persist for very long times. The principal mode for these parameters is $q_0 = \sqrt{2}$ corresponding to a length scale of $\xi_p \simeq 4.4$. The spacetime profile shows structures of that size but it is apparent that correlations exist well beyond that scale. There appear to be large compound structures where individual structures are seen to grow and deplete yet remain part of a collective conglomerate. The correlation function in Fig. 3-22 shows long range correlations in both space and time. The spectrum of static fluctuations in Fig. 3-23 corroborates the observation. The spectrum is observed to bend over around the principal mode $q_0 \simeq 1.4$ yet it does not entirely

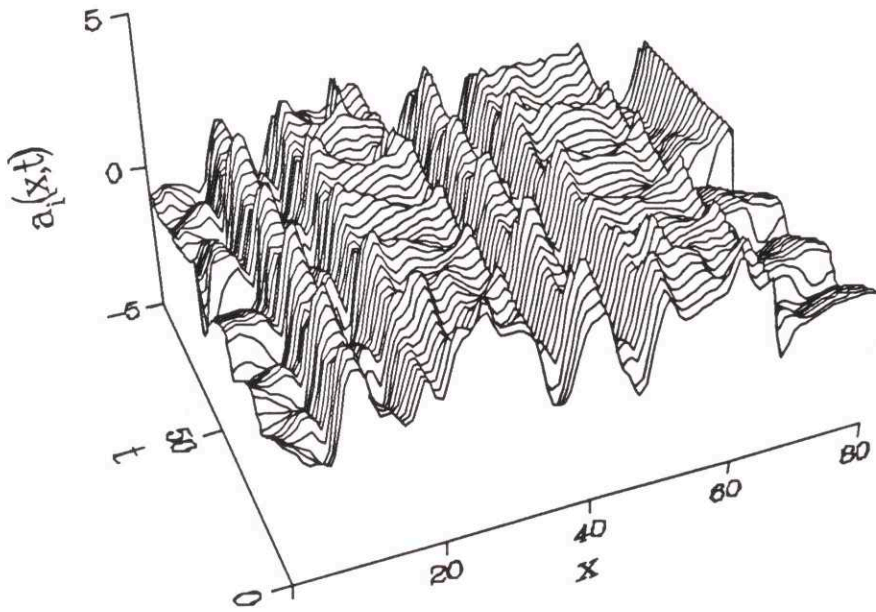


Figure 3-21: Spacetime profile of the parent wave a_i in the strongly diffusive regime

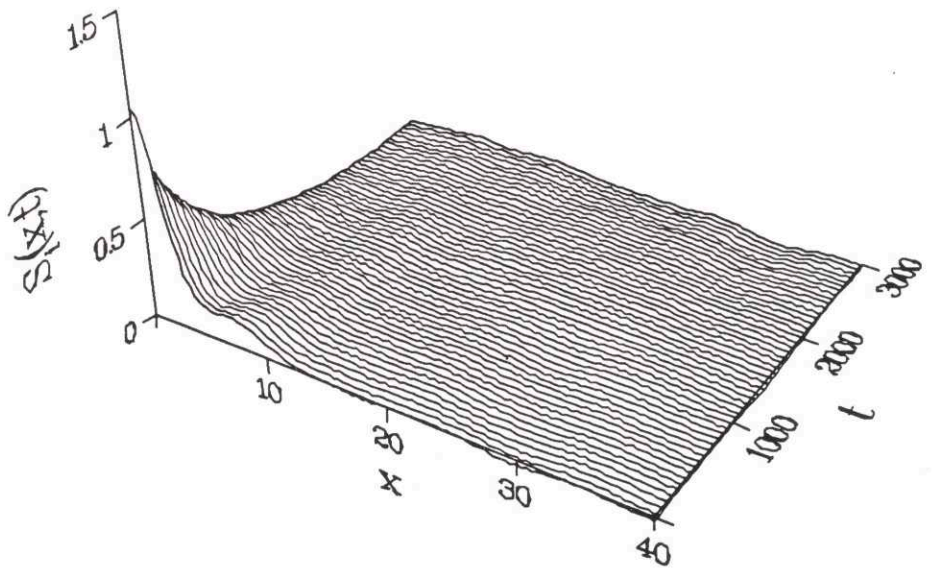


Figure 3-22: Correlation function of the parent wave a_i in the strongly diffusive regime.

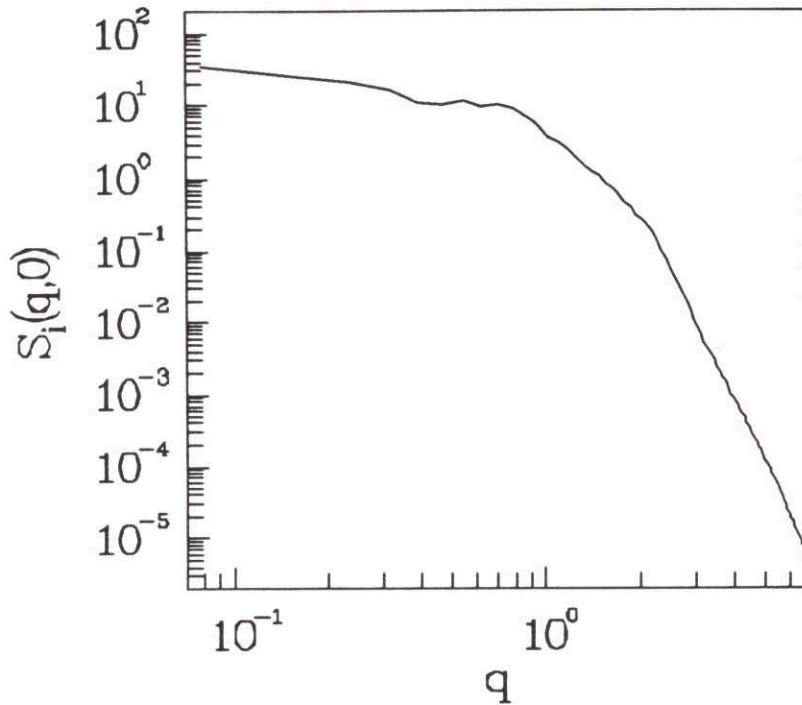


Figure 3-23: Spectrum of static fluctuations of the parent wave a_i in the strongly diffusive regime.

flatten out. It is also clear that correlations exist at the level of the system size. The local power spectrum in Fig. 3-24 shows a very long correlation time as observed in the correlation function and spacetime profile. The cycling time observed in the spacetime profile is at too high a frequency to be resolved in this figure. The spatial alternation between a single structure and a squarish collective structure seems to be a robust state. Different runs with different initial conditions and slight variations in the parameters produced similar looking profiles.

The spacetime profile of daughter wave a_j and a_k are shown in Fig. 3-25. Unlike the nearly integrable case there is not a strong convection along the characteristic. In fact it is difficult to distinguish between the two daughter profiles. The damping length for the daughters is much smaller than the parent structure length scale. Thus the daughter structures only exist within the confines of a parent structure and do not interact very much with neighbouring structures as with weak diffusion. The correlation function for the daughter is shown in Fig. 3-26. The correlation function

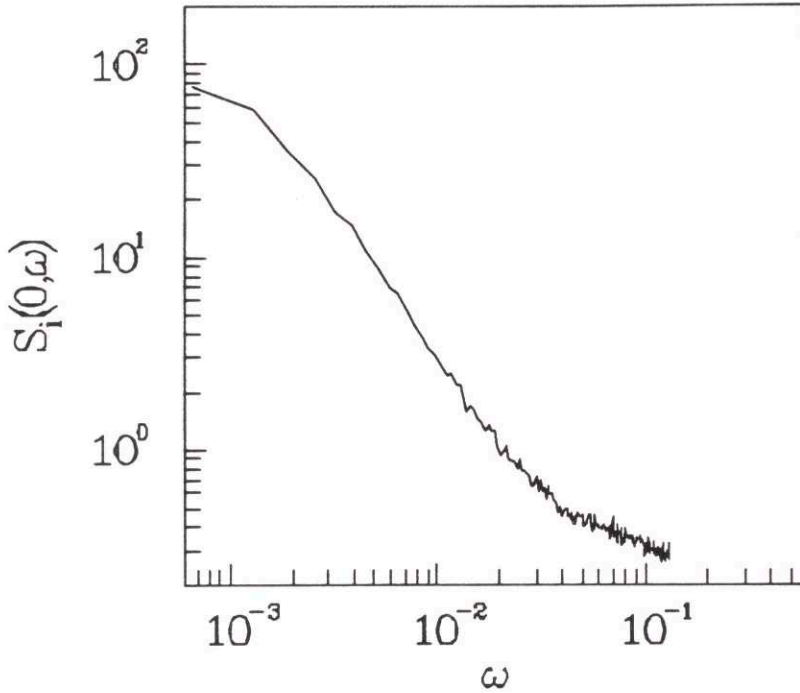
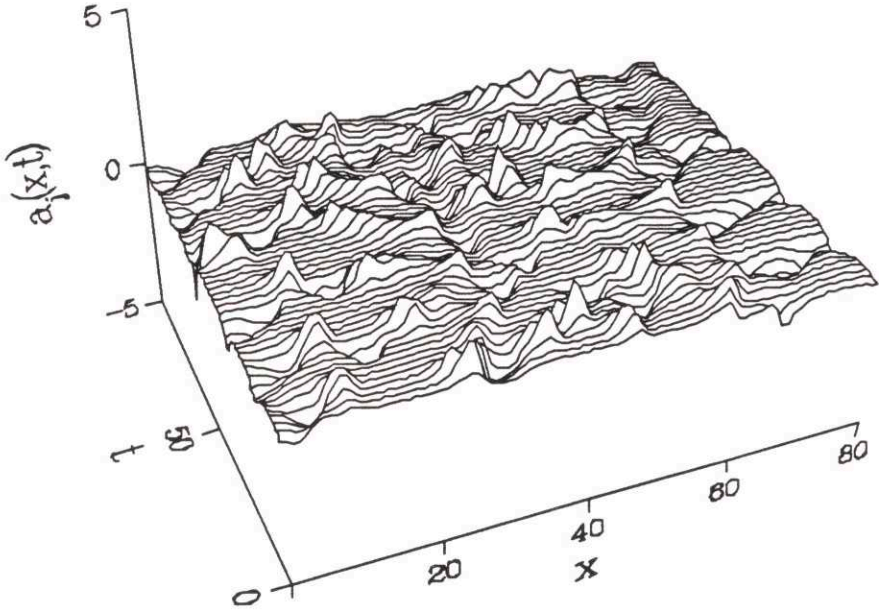


Figure 3-24: Power spectrum of the parent wave a_i in the strongly diffusive regime.

was measured in the frame of reference of the characteristic velocity. The observed ridge is along the $x = 0$ direction of the system frame. It simply indicates that the daughter waves mirror the parent structures. A slight rise in the ridge at about $x \simeq 15$ then again near 35 reflects the cycling time. The power spectrum of a_j in Fig. 3-27 shows two peaks then a rise for low frequencies. Longer runs show the spectrum bends over and begins to flatten out when the parent wave does. The larger peak situated at $\omega \simeq 0.08$ reflects the periodic structures seen in the correlation function. It corresponds to the cycling time of a_j around the simulation box. The smaller peak is a harmonic of the larger peak. The spectrum of static fluctuations in Fig. 3-28 shows the spectrum gradually bending over yet correlations do extend across the whole system.

In this case the daughter waves are slaved to the parent wave. All the spatial scales are much larger than the damping lengths so for all effective purposes the daughters are static and merely react to the parent. However unlike the case of spatially uniform amplitudes the instability can be saturated by forming quasi-solitons. In the

(a)



(b)

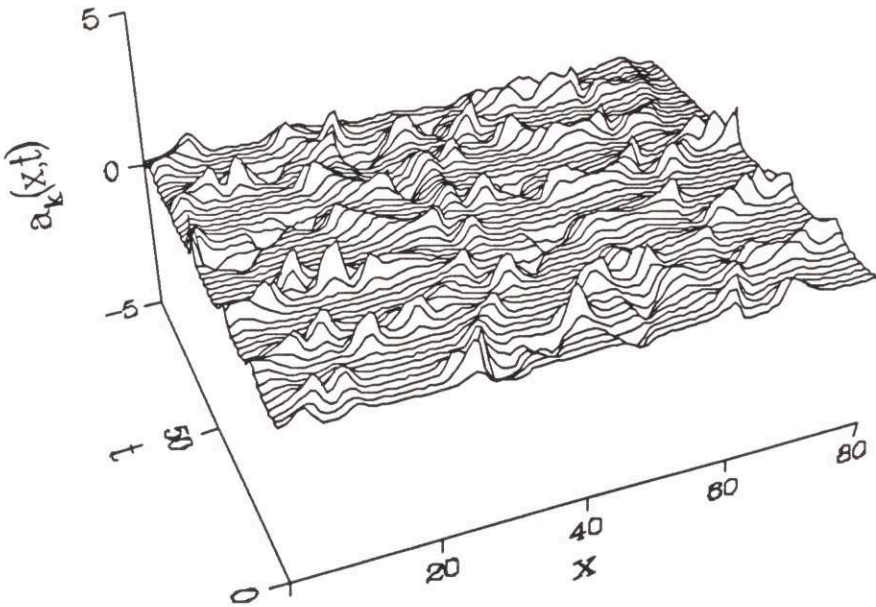


Figure 3-25: Spacetime profiles of daughter wave (a) a_j and (b) a_k in the strongly diffusive regime.

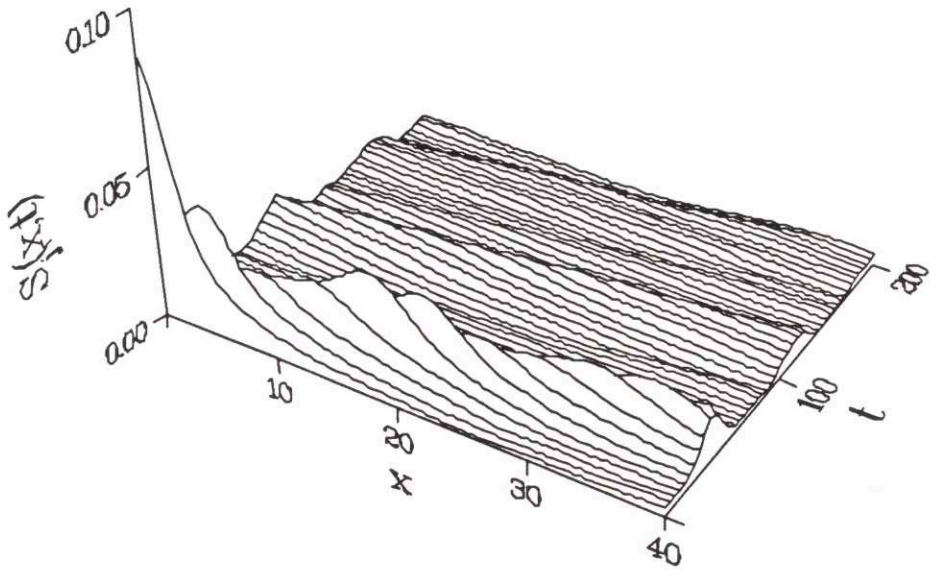


Figure 3-26: Correlation Function of the Daughter Wave a_j in the strongly diffusive regime.

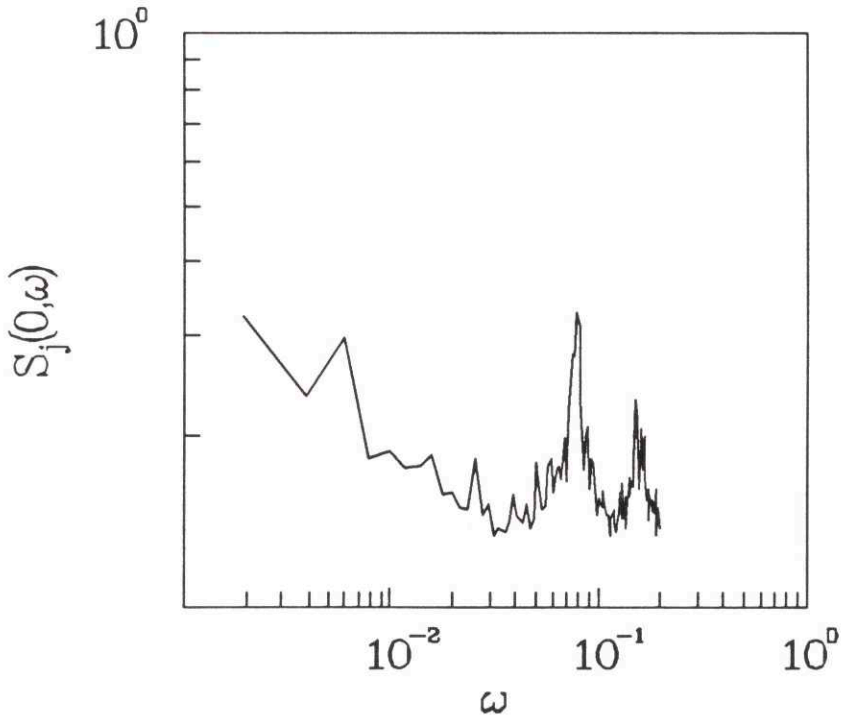


Figure 3-27: Power Spectrum of the Daughter Wave a_j in the strongly diffusive regime.

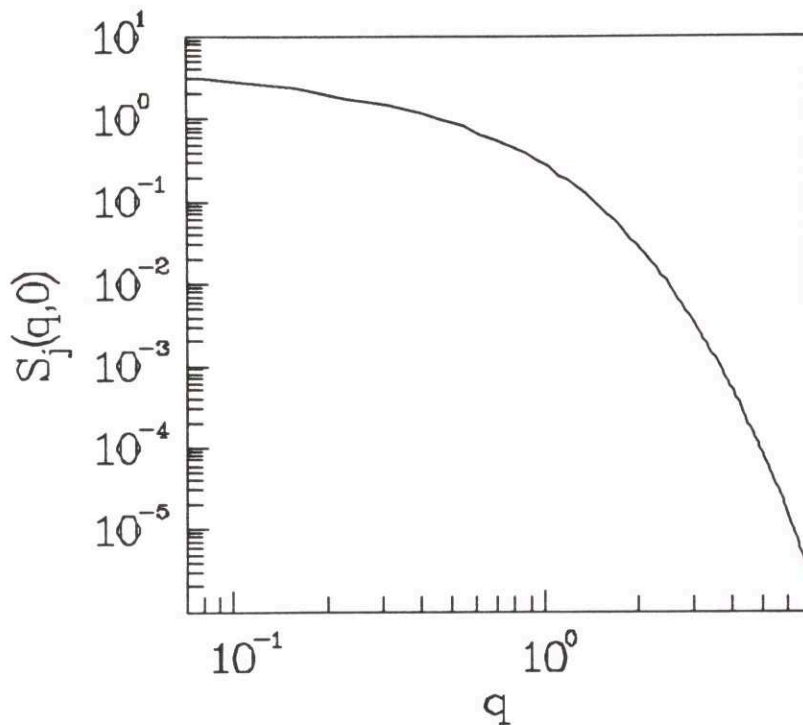


Figure 3-28: Spectrum of Static Fluctuations of the Daughter Wave a_j in the strongly diffusive regime.

nearly integrable case, the daughter waves transferred information between the parent structures, constantly perturbing the parent structures and instigated the diffusion. In the strongly diffusive case, information is transferred very slowly between the parent structures. Hence the extremely long correlation times. However the mechanism for decorrelation is poorly understood. Somehow it must be related to the rate of information transfer between the different structures but no quantitative estimates can be made.

3.4 Conclusions

The SDI case is an excellent paradigm for STC. In its nearly integrable regime, perturbation theory around nonlinear solutions is possible. This is a great aid in understanding the dynamics and for obtaining analytical results. The contrast to low dimensional chaos seen in Section 2.2 is quite clear. Specific routes to chaos, fractals, strange attractors – signatures of low dimensional chaos are not very relevant in the

description of STC. Many degrees of freedom are clearly involved in STC. A description in terms of correlation functions captures much of the behaviour. The language of linear response theory (Martin, 1968; Forster, 1975) may be more appropriate to STC than the language of traditional chaos theory. On the other hand STC is much simpler than fully developed turbulence. There is no inertial range. The chaos is confined to long wavelengths. One could not really describe SDI as having weak turbulence. That term is usually reserved for systems where the nonlinearity is weak compared to the linear effects. In SDI the nonlinearity is essential in establishing the coherent structures.

The results presented in this chapter leave many questions unanswered. The analyses indicate that there are subtle interactions between the waves. Numerical measurements of cross correlations between the waves would certainly yield interesting results. Only a limited number of parameter sets were explored. Wider parameter searches are certainly in order. The simulations seemed to hint that some interesting effects may occur for extremely long times. Longer runs and better statistics are required to check whether or not the power spectra of the waves really show scale invariant behaviour and what exponent characterizes it. This would indicate whether interesting collective behaviour involving the coherent structures exist or not. Higher order moments could be measured to examine the distribution of fluctuations $\delta a_l = a_l - \langle a_l \rangle$ in both real and Fourier space. It could then be checked whether or not the fluctuations of the Fourier modes are Gaussian as discussed in Section 1.2. If this were true then the large-scale governing equations in their simplest form could be linear and relaxational. For instance with the KS equation, progress has been made to deduce an effective equation driven by random noise to describe the large-scale (coarse-grained) dynamics (Yakhot, 1983; Zaleski, 1989). Knowledge of the response function would test whether the SDI dynamics obey a fluctuation-dissipation theorem. This could be measured numerically by taking the average response to an imposed perturbation. This would lead the way for possibly defining a temperature for STC in SDI. The nearly integrable limit could be explored in ZM scattering space. The eigenvalue spectrum could be evaluated numerically. The eigenvalues are

no longer time invariant and may exhibit interesting dynamics. Collisions between eigenvalues or other crises may occur in the eigenvalue plane giving more clues to nonintegrability and STC. This type of analysis has been done with the sine-Gordon equation (Overman II *et al.*, 1986) and has yielded very interesting results.

Chapter 4

Langmuir Decay Instability

4.1 The Model

This chapter studies a nonintegrable form of the stimulated backscatter interaction that exhibits STC. As in Chapter 3 an unstable high-frequency wave, saturates nonlinearly by coupling to two damped low-frequency waves. The only difference being that the high-frequency wave has the largest group velocity. In order to satisfy the resonance conditions (2.9) it is much more common for the high frequency wave to be the fastest wave as well. Thus the model described in this chapter is applicable to many different physical contexts. The title of the chapter – Langmuir Decay Instability (LDI), was chosen because of specific reference to one application in current laser plasma experiments. The STC induced in LDI may explain some recent experimental results. The unstable wave (Langmuir wave) grows because it is the decay product of another three wave interaction (stimulated Raman scattering). The details are in Section 4.4. An unstable Langmuir wave can also result from a beam-plasma interaction. However the same equations are just as readily applied to other phenomena; one example is the interaction of gravity-capillary waves where winds may excite and induce a particular mode to grow which then couples to two other modes (McGoldrick, 1965).

Numerical simulation and analysis is used to understand the dynamics. The IST solutions of the integrable equations described in Section 2.4.2 again will form the

basis for understanding the nonintegrable behaviour. In LDI, solitons do not play a major role. Instead it is the collision of the waves which drive the dynamics. Radiation effects dominate and as a result perturbation theory is not as readily employed compared to SDI. However much can be gleaned from the IST solutions regardless. Some of the analysis of LDI will overlap with that done for SDI.

In normalized form the equations of interest are

$$\partial_t a_i - D \partial_{xx} a_i - \gamma_i a_i = -a_j a_k, \quad (4.1)$$

$$\partial_t a_j - \partial_x a_j + a_j = a_i a_k^*, \quad (4.2)$$

$$\partial_t a_k - 2 \partial_x a_k + a_k = a_i a_j^*. \quad (4.3)$$

These equations are identical to the normalized SDI equations (3.7)-(3.9) except the group velocity of envelope a_k is $v = -2$ instead of $v = 1$. The frame of reference of the unstable wave is again chosen. This small change makes an enormous difference in the results. Just as the order of the group velocities in the integrable equations led to major differences in behaviour so will it affect the nonintegrable equations and the manifested STC. Using laser plasma terminology for LDI, wave a_i is referred to as the pump wave (PW), wave a_j is the acoustic wave (AW) and wave a_k is the backscattered wave (BW).

4.2 Simulation Results

The Eqs. (4.1)-(4.3) were simulated on the domain $x \in [0, L)$ with periodic boundary conditions as in Chapter 3. The long time, large system limit was of interest. Simulations were started with random real initial conditions. As in the SDI case it can be shown that the envelopes remain real for all time (Kaup *et al.*, 1979). The numerical scheme is the same as that used for SDI and is detailed in Appendix C. The spatial and temporal grids were chosen so as to resolve all the dynamics. The integrated energy $U_l = \int |a_l(t)|^2 dx$ was monitored for each run. When it reached a state where it fluctuated about an average value, the saturated state was considered to be attained. The spacetime history was recorded for all the envelopes. In the saturated regime the

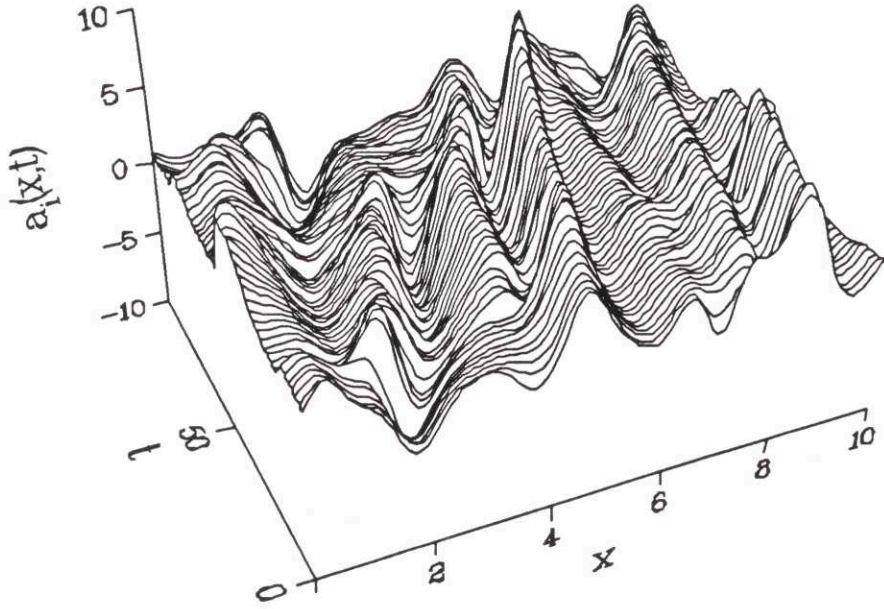


Figure 4-1: Spacetime profile of the PW a_i .

correlation functions $S_i(x, t) = \langle a_i(x - x', t - t') a_i(x', t') \rangle$ where averages are over time, were taken. As in SDI the parameter set is given by (D, γ_i) .

Several different parameter sets were used in the simulations. In the first example the parameters are: $\gamma_i = 0.1$, $D = 0.004$ and $L = 20$. As will be seen later the length plays an important role in the dynamics. The spatiotemporal profile of the PW is shown in Fig. 4-1. Again furrowed ridgelike ‘coherent’ structures observed in the SDI in Chapter 3 are seen but with a definite drift towards the right. There appear to be length and time scales where things are correlated, but beyond which the dynamics becomes chaotic. The correlation function for the PW is shown in Fig. 4-2. The function approaches zero in space and time indicating STC but a nonlinearly induced mode with a definite phase velocity is clearly observed. This effect was observed in the spacetime profiles as the drifting coherent structures. The correlation function shows that these structures are very long lived. Along the x axis, $\sin x/x$ behaviour similar to the SDI is observed. The spectrum of static fluctuations $S_i(q, t = 0)$ is shown in Fig. 4-3. A box like function as expected is observed with a cutoff at approximately

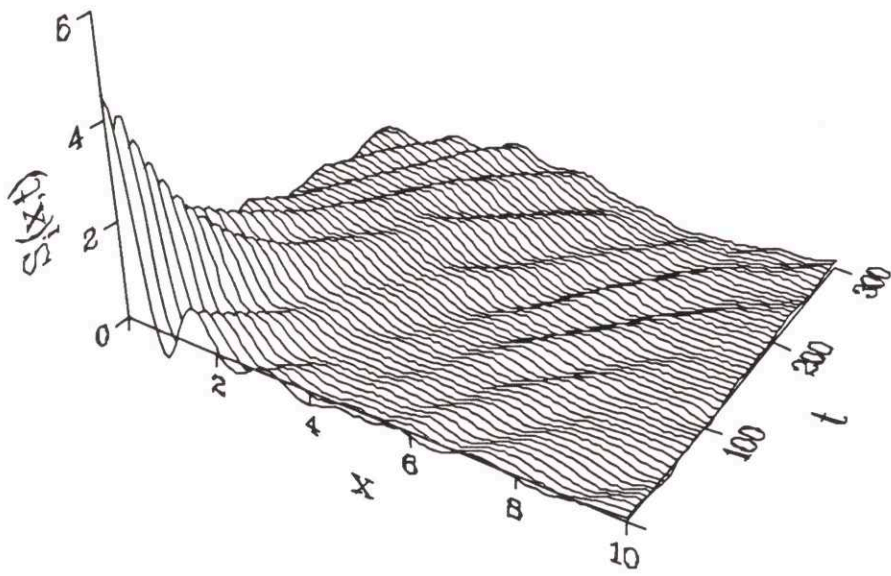


Figure 4-2: Correlation Function of the PW a_i .

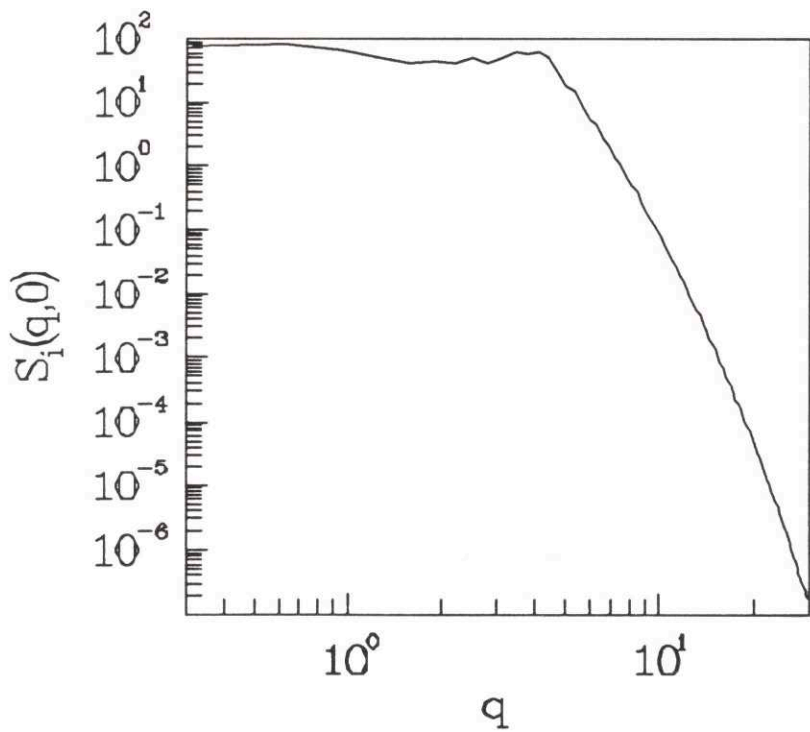


Figure 4-3: Spectrum of Static Fluctuations of the PW a_i .

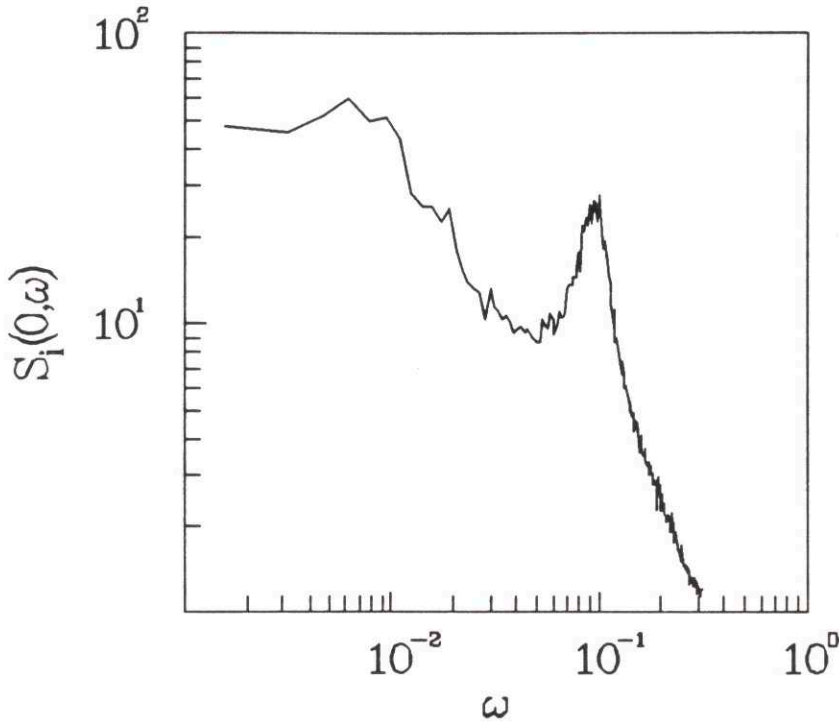


Figure 4-4: Power series of the PW a_i .

$q \simeq 5$, translating to a correlation length of $\xi_p \simeq 1.3$. The local power spectrum $S_i(x = 0, \omega)$ is shown in Fig. 4-4. A definite peak at $\omega \simeq .1$ is observed, the spectrum then flattens out at around $\omega \simeq 0.007$ defining a correlation time.

The spacetime profile of the AW is shown in Fig. 4-5. Ridgeline coherent structures are seen to drift towards the left. For large scales the dynamics are chaotic. The correlation function measured along the characteristic $x = -t$ is given in Fig. 4-6. There is strong decay in space and time confirming STC. However there is a hump located at $S(x \simeq 10, t \simeq 10)$, and another at $S(x \simeq 1, t \simeq 20)$. Note that the correlation function shown is over the entire length of the system, and the periodicity for $t = 0$ is seen. The power spectrum is shown in Fig. 4-7. The correlation time corresponds to a frequency of $\omega \simeq 0.3$. The spectrum of static fluctuations is shown in Fig. 4-8. There is a cutoff at $q \simeq 9$ corresponding to a correlation length of $\xi_a \simeq 0.7$.

The spacetime profile of the BW is shown in Fig. 4-9. Again irregular yet distinct structures are seen to drift towards the left. The correlation function measured along

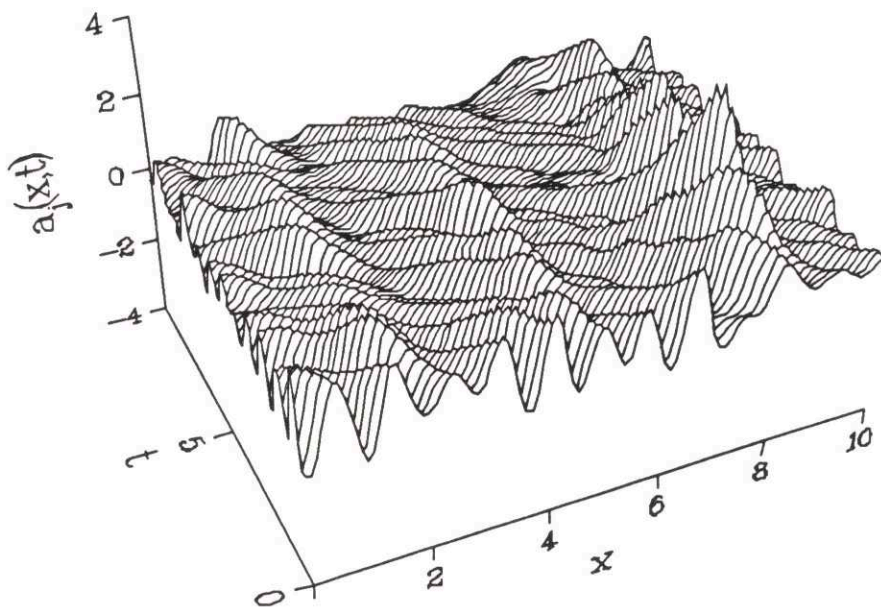


Figure 4-5: Spacetime profile of the AW a_j .

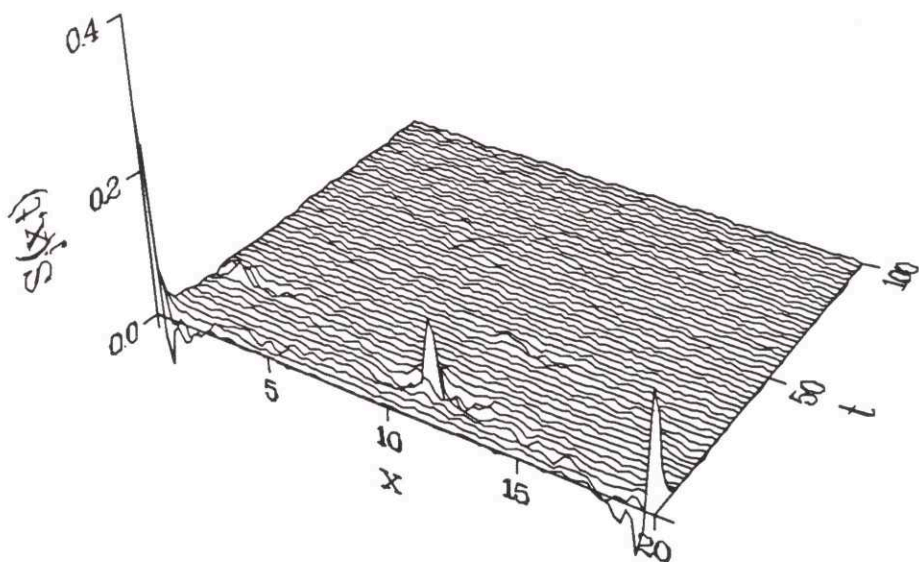


Figure 4-6: Correlation function of the AW a_j .

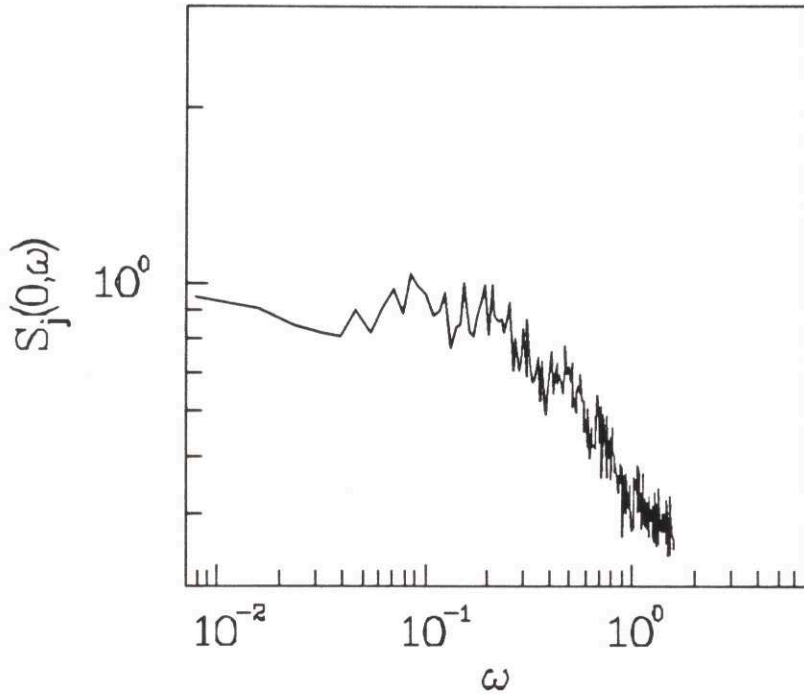


Figure 4-7: Power spectrum of the AW a_j .

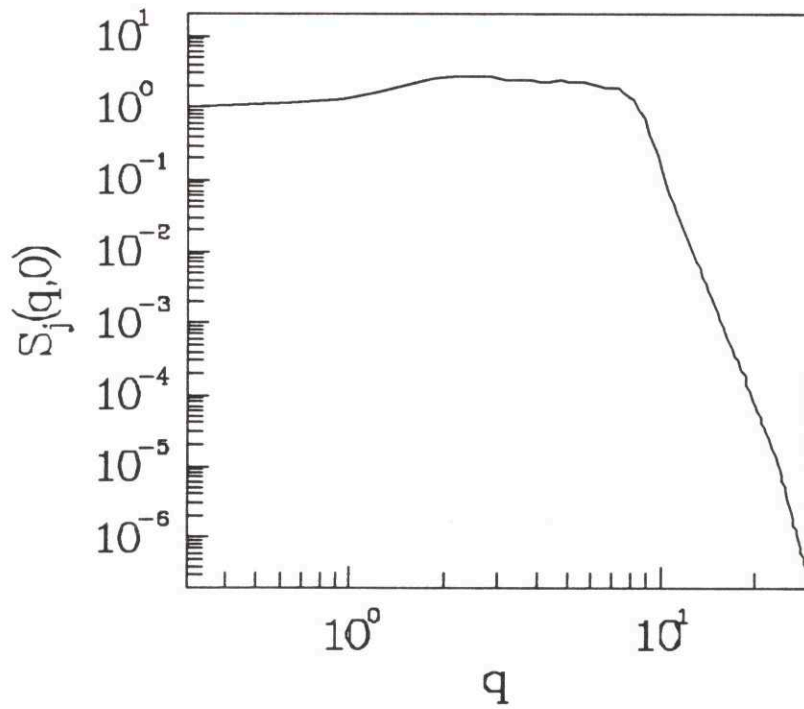


Figure 4-8: Spectrum of static fluctuations of the AW a_j .

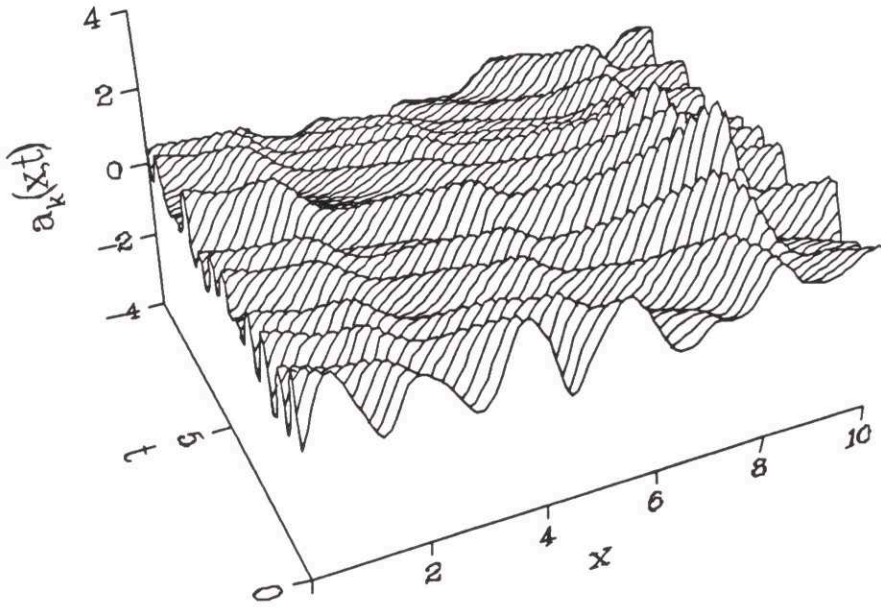


Figure 4-9: Spacetime profile of the BW a_k .

the characteristic $x = -2t$ is shown in Fig. 4-10. Correlations approach zero in space and time indicating STC. A nonlinear mode similar to the parent is also observed. The propagating mode implies that the structures found in Fig. 4-9 are not aligned along the characteristic curve but are actually slightly skewed to the right. The phase velocity in the moving frame $v \simeq 0.1$ indicates that the shift away from the characteristic velocity is not very great. Correlations in the direction of the coherent structures are fairly long compared to the damping times. The power spectrum along the characteristic in Fig. 4-11 shows a cutoff around $\omega \simeq 0.4$. The spectrum of static fluctuations in Fig. 4-12 shows a cutoff around $q \simeq 5$ giving a correlation length of $\xi_b \simeq 1.3$.

A sample time series of the energy $U(t)$ is shown in Fig. 4-13. They fluctuate about an average value. The BW and AW energies are locked together. The average value is independent of the initial conditions.

Different parameter sets were explored and showed similar results. In the cases

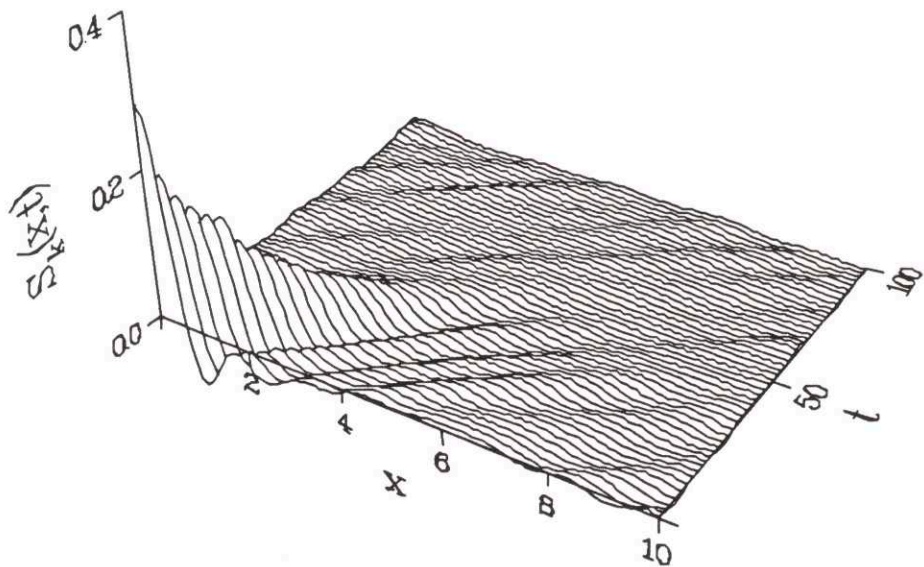


Figure 4-10: Correlation function of the BW a_k .

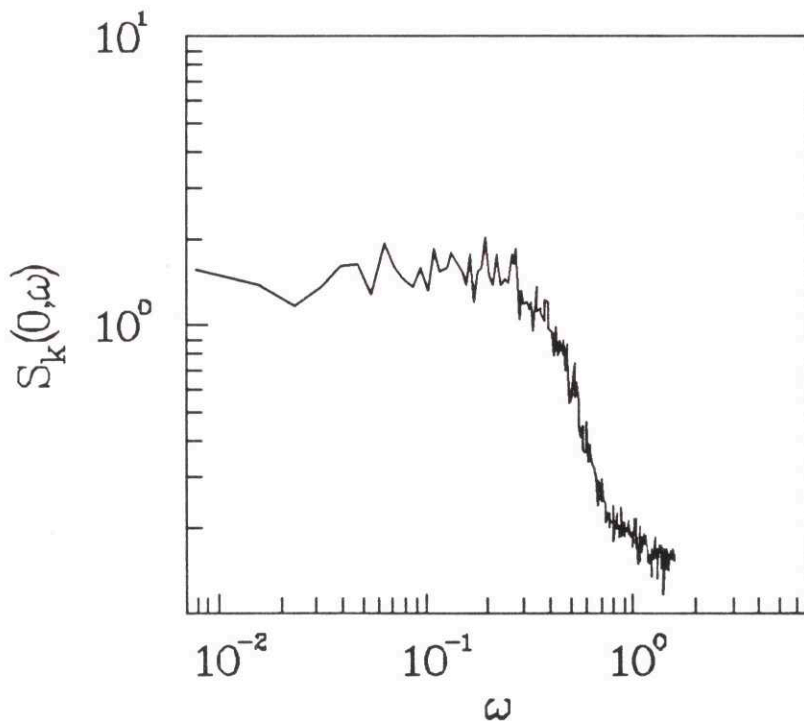


Figure 4-11: Power spectrum of the BW a_k .

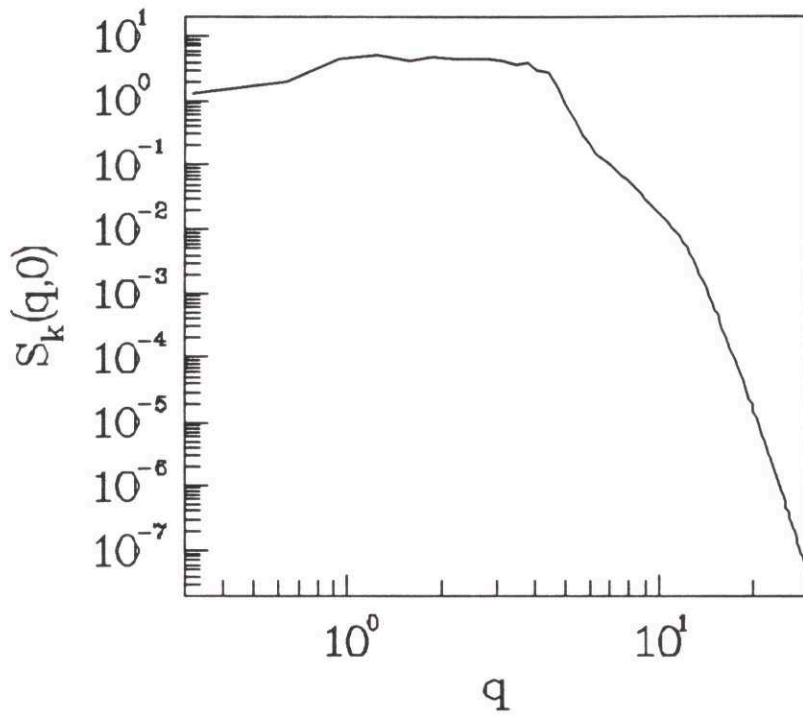


Figure 4-12: Spectrum of static fluctuations of the BW a_k .

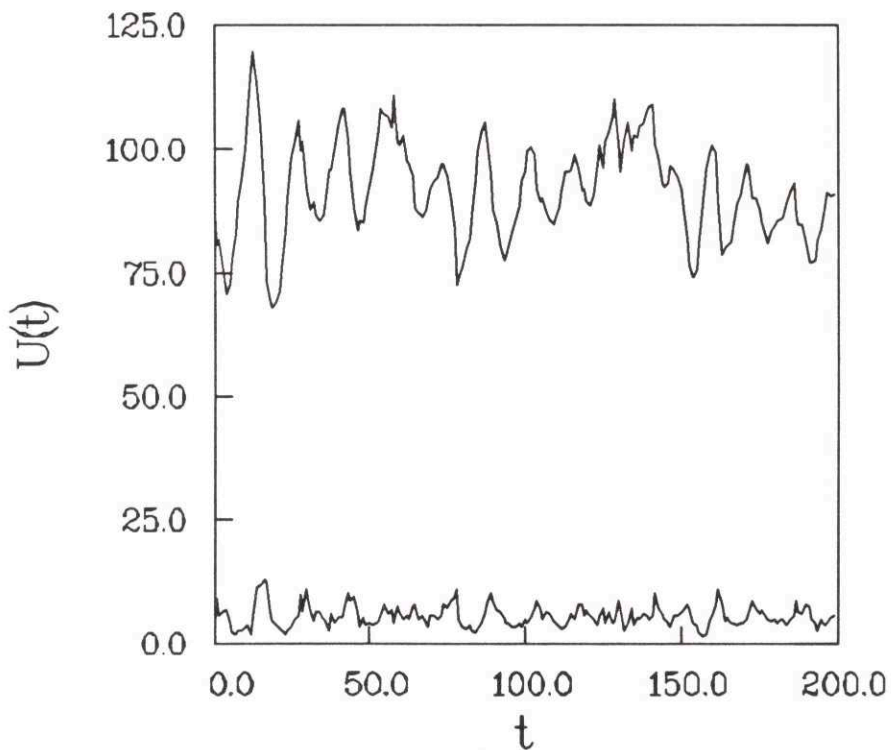


Figure 4-13: Integrated energy $U(t)$.

tested the spacetime profiles all showed drifting coherent structures evolving chaotically. The correlation functions showed qualitatively similar results to those shown here. However these parameter sets were relatively close to the example case. A discussion of the different behaviour that could arise with different parameter sets is given in the next section.

4.3 Analysis and Discussion

The simulation results can be understood with the aid of linear analysis and the IST solutions. The LDI dynamics exhibit STC and are described in terms of correlation functions. The correlation functions have spatial and temporal scales and a definite amplitude. There is also the additional feature of a nonlinear propagating damped mode in the PW and to a lesser extent in the BW.

The linearized equation for the PW (4.1) is exactly the same as that for the parent wave in SDI. The trivial fixed point Eq. (3.10) gives a principal mode for the PW at $q_0 = \sqrt{\gamma_i/D}$. Higher modes are damped and lower modes are growing. As in SDI there is a competition between linear growth and nonlinear saturation. Instead of depletion to quasi-solitons seen in SDI, the saturation mechanism is due to the radiation transferred during collisions between the envelopes. The balance between the competing effects is also responsible for the propagating mode as will be shown.

The IST solutions of the stimulated backscatter interaction (which applies to LDI) in Section 2.4.2, show solitons are not involved. The interesting dynamics are due to collisional radiation effects. A collision between the AW and the PW generates the BW and decimates the waves as seen in Figs. 2-2-2-4. Similar behaviour occurs when the BW collides with the PW. The decimation of the parent wave is always on the side opposite to that of the collision. This is seen in the IST solutions and can be understood from the nonlinear saturation of the corresponding parametric instability. When the AW collides with the PW, the BW and AW grow from the colliding edge as a convective instability. This is because both of their group velocities are in the same direction.

When the two envelopes attain a significant amplitude the PW begins to saturate. However the two daughter waves will continue to grow and continue to take energy from the PW. The area of the PW will be reduced. The depleting pump cuts off the growth of the two daughter waves and they saturate and begin to damp as well. If the original amplitude of the PW was large enough or the growth rate γ_i high enough, the reduction in area continues until the PW becomes negative. This effect was seen in the integrable case in Fig. 2-2. The negative part of the PW can again be a source for a convective instability and the same process ensues. In this way the envelopes are spatially decimated into the oscillatory structures seen in the simulation. The decimation is always on the side of the PW away from the colliding edge. The low q 's are converted to high q 's by this process. Modes higher than q_0 get damped, so the PW will settle into structures of size $\xi_p \simeq 2\pi/q_0$. The values $q_0 = 5$ and $\xi_p \simeq 1.3$, obtained for the simulation parameter set, agree well with the simulation.

The PW equation (4.1) has the form of a growing diffusion equation. Thus any localized pulse will spread and grow. The propagating PW mode is a result of the combination of this spreading effect and the decimation effect. The wavepackets decimate nonlinearly on one side and they spread and grow linearly on the other side. A pulse moves like a sandbar near an ocean shore, building on one side and receding on the other. A parabolic equation does not have a well defined phase velocity yet one was observed in the PW correlation function. However, a 'spreading' velocity can be defined by considering the trajectory of a point of constant amplitude on a localized pulse. The phase velocity of the sandbar mode, as it will be referred to, will then be given by this spreading rate. From the simulations of several different cases it was discovered that the phase velocity behaves as $v_p \simeq \sqrt{D\gamma_i}$.

This dependence can be demonstrated by considering the linearized PW equation

$$\partial_t a_i = \gamma_i a_i + \partial_{xx} a_i. \quad (4.4)$$

The general solution of this equation is given by

$$a_i(x, t) = \frac{1}{2\pi} \int \hat{a}_i(q, t=0) e^{(\gamma_i - Dq^2)t} e^{iqx} dq, \quad (4.5)$$

where $\hat{a}_i(q, t = 0)$ is the Fourier transform of the initial condition. Of interest is the spreading rate of a single parent structure. The simulation shows that the spectrum of static fluctuations is a box function of width $q_0 = \sqrt{\gamma_i/D}$. The inverse Fourier transform is $\sin(q_0 x)/(q_0 x)$ which roughly describes the shape of the PW structures. Therefore taking

$$\hat{a}_i(q) = \begin{cases} A & \text{if } -q_0 < q < q_0 \\ 0 & \text{otherwise} \end{cases} . \quad (4.6)$$

the solution of Eq. (4.5) is

$$a_i(x, t) = \frac{A}{2\pi} \int_{-q_0}^{q_0} e^{(\gamma_i - Dq^2)t} e^{iqx} dq. \quad (4.7)$$

Completing the square and scaling out all the relevant factors yields

$$a_i(x, t) = e^{\gamma_i t - \alpha^2} \frac{A}{2\sqrt{\pi Dt}} \text{erf}(\sqrt{\gamma_i t} - i\alpha), \quad (4.8)$$

where $\alpha = x/\sqrt{4Dt}$. In the limit $\alpha \ll 1$, $\gamma_i t \ll 1$, Eq. (4.8) can be expanded to yield

$$a_i(x, t) \simeq \frac{Aq_0}{\pi} \left(1 + \frac{2}{3}\gamma_i t - \alpha^2\right). \quad (4.9)$$

The ‘spreading’ velocity is defined by considering a point of constant amplitude. Imposing $a_i(x, t) = \text{const.}$ yields

$$\alpha^2 - \frac{2}{3}\gamma_i t = 0, \quad (4.10)$$

giving a velocity of

$$v_p \equiv \frac{x}{t} \simeq \sqrt{\frac{8}{3}D\gamma_i}. \quad (4.11)$$

This does not quite agree with the empirical value of $v_p \simeq \sqrt{D\gamma_i}$. However this may not be so surprising because the nonlinear and linear effects are involved simultaneously. However this simple linear argument seems to capture the essence of the effect.

The peak in the PW power spectrum is given by the frequency of the sandbar mode. Using the relation $\omega = v_p q_0$ the frequency is found to be $\omega \simeq \gamma_i = .1$. This is precisely what was observed in Fig. 4-4. As seen in the correlation function in Fig. 4-2 the structures remain coherent for very long times. The power spectrum in Fig.

4-4 was taken along the time axis. The long time scale observed was actually given by the transit time of the sandbar mode around the box $\tau_P \simeq L/v_p$. It is unknown what the decorrelation mechanism for the PW coherent structures actually is. They persist much longer than the diffusion time across a correlation length.

The saturation energy of the PW can be understood as follows. The competition between the nonlinear and linear effects leads to coherent structures of size $2\pi/q_0$. The IST solutions in Section 2.4.2 show that the nonlinear interaction is radiation dominated so the ZS reflection coefficients for each envelope is the relevant quantity. The reflection coefficients after interaction Eqs. (2.58)-(2.59) show that structures of this size are generated in collisions when the PW has a height of $a_i \simeq q_0$. For taller structures, the collisions with the BW and AW will generate structures with smaller wavelengths. The simulations seemed to indicate that these results of the integrable case carry over to the nonintegrable regime. Then as the PW grows, it gets depleted as it constantly collides with the other waves. If it grows higher than $a_i \simeq q_0$ the generated structures damp away. Thus $a_i \simeq q_0$ will be an upper bound to the height of the PW. For these parameters $q_0 \simeq 5$ and the tallest structures in the spacetime profile are of this order. Given the upper bound for the PW height, the saturated energy density can be estimated as in the SDI case in Eq. (3.126) by considering the PW to be composed of coherent structures locally resembling a sine wave with average amplitude of $q_0/2$. This then gives an average energy density of $S_i(0,0) \simeq q_0^2/4 \simeq 6$. The simulation shows a value of $S_i(0,0) \simeq 5$. Considering the assumptions used in the estimate this is remarkably good.

The features of the BW and AW are also analysed. The correlation lengths of the BW and AW structures are due to radiation effects and cross correlations. The final reflection coefficient of the BW in Eq. (2.60) shows that the wavelength of the decimated BW depends inversely on the height of the PW, and will be approximately the same as the wavelength of the PW. However the AW final width is not as strongly coupled to the widths of the other two waves. Simulations of pulse collisions confirm this fact.

It is significant that the correlation length for the AW is one half the correlation

length of the other two waves. This is due to the fact that its group velocity is half of the BW. As discussed above the PW settles into coherent structures of size ξ_p , and this fixes the size of the BW structures. The AW gets generated wherever the BW collides with the PW. In the time direction, along a PW coherent structure, the BW and AW will tend to have the same number of coherent structures. This can be seen by comparing Fig. 4-5 with Fig. 4-9. However since the AW has a group velocity half that of the BW, if it has the same number of structures in the time direction, it must have twice as many in the spatial direction. In other words the coherent structures of the AW are half the size of the BW. This was observed in the simulation. In the saturated state, a lattice-like structure will become established. Of course it is only for special cases that a regular lattice can be formed. In most cases the lattice will be frustrated. This leads to the lack of regularity and STC observed. It would be very useful in the future to measure the cross correlation function between the waves to better understand these effects.

The propagating mode of the BW seen in the correlation function can also be inferred from the IST solution. The correlation function showed that the propagation velocity of the coherent structures were slightly slower than the characteristic velocity. During a collision between the BW with the PW, the two waves will interact nonlinearly and this process retards the transmission of the BW, slowing the velocity.

The AW spacetime profile in Fig. 4-5 shows a furrowed structure moving to the left like the BW, but the correlation function in Fig. 4-6 does not show the long correlations and evidence of a nonlinear mode like the BW and PW. Correlations are quickly damped out compared to the other waves. This is likely due in part to the fact that since the group velocity is half that of the BW, it experiences twice as much damping between collisions. It may also be that the wave collisions affect the AW more than the other waves. The humps observed in the AW correlation function are due to collisions of the AW with the PW and BW waves. The one at $(x \simeq 1, t \simeq 20)$, is due to repeated collisions of the AW with a particular PW structure. The correlation times of the PW structures are very long. Each time the AW circles the simulation box it will collide with the PW structure. The hump is

slightly off from the characteristic. This is due to the fact that the PW structure is drifting. The hump at $(x \simeq 10, t \simeq 10)$ is due to collisions between a given BW structure and the PW structure. Whenever these two waves collide they generate the AW in the process. The BW has group velocity twice that of the AW and so transits the box in a time $t = 10$. In the frame of the AW the hump gets shifted in x as well.

It would seem that the behaviour observed in Section 4.2 for LDI should persist as the PW growth rate increases or the diffusion decreases. The PW structures would reduce in width and this would lead to an increase in their amplitude. The ratio of the PW energy to the daughters would approach unity. However in the weak growth limit the ratio of the PW energy to the daughter energies would be large. The PW structures would become wider and their amplitudes smaller. The daughter waves would damp more between collisions. The coherence times would likely become longer as in the SDI case. The energies of the daughter waves would also get smaller in comparison to the PW's and the nonlinearity would become less important. Differences in the ratios of the velocity would change the ratio of the sizes of the AW and BW. Differences in the damping rates on the daughters would change the saturation energies. If the disparity were large than the wave with the lower damping would dominate the nonlinear collision processes. These effects were seen in preliminary simulations. A detailed analysis remains to be done.

4.4 Saturation of SRS in Laser Plasma Interactions

In recent years with the advent of high powered lasers and a major thrust into laser fusion, laser-plasma experiments have become commonplace. These experiments provide an excellent opportunity to study examples of parametric decays describable by the nonlinear 3WI. When a laser interacts with a plasma it can induce many interactions. One example is stimulated Raman scattering (SRS) where the laser-light wave, decays into a Langmuir wave (LW) (also called electron plasma wave) in the plasma and a scattered light wave. An understanding of SRS may be very important

for laser fusion. The scattered light can carry energy away from the target and the hot electrons generated preheat the target.

Recent experiments (see Drake and Batha, 1991), suggest that certain aspects of SRS cannot be well explained by the standard linear parametric theory of a convective instability in an inhomogeneous medium of Liu, Rosenbluth, and White (1974). Thus nonlinear mechanisms may be needed to explain the observations. One scenario is that the LW in the SRS interaction, becomes a growing parent wave for another three wave interaction – Langmuir Decay Instability, where the LW generated by SRS decays into a backscattered LW and an ion-acoustic wave (IAW) (Heikkinen and Karttunen, 1986; Bonnaud, Pesme, and Pellat, 1990; Drake and Batha, 1991; DuBois *et al.*, 1991). Drake and Batha (1991) suggest that the saturation of SRS by LDI may explain some of the experimental data. Several investigators have studied the full nonlinear system of SRS coupled to LDI. For strong damping on the daughter waves the LDI is marginally unstable and saturates near threshold (Heikkinen and Karttunen, 1986). With weaker damping there may be weak turbulence (Bonnaud, Pesme, and Pellat, 1990), and for even weaker damping, strong turbulence with Langmuir collapse may result (DuBois, Rose, and Russell, 1991).

It may not be necessary to model the full system to understand the saturation mechanism. A combination of nonlinear and linear theory may suffice. Equations (4.1)-(4.3) are used to model LDI nonlinearly, while SRS is treated linearly. The LDI will occur at a much faster time scale than the SRS. On this short time scale the laser can be treated as a constant pump so the principal SRS interaction can be modelled with the linearized parametric interaction of Section 2.3. For small amplitudes the LW decay product of SRS will be unstable with a growth rate proportional to the amplitude of the laser wave. This is the PW of the LDI discussed in this chapter. The actual growth coefficient of the PW will be the difference between the growth rate due to SRS and the Landau damping on the wave. Also since the instability will be at the principal wave number of the unstable LW, the second order diffusion term in the PW models the increase in damping that would exist away from the principal wave number. The other LW and the IAW are damped. The group velocities of the

two LW's will have approximately the same magnitude with opposite signs while that of the IAW will be almost zero in comparison. Hence in the frame of the PW, the group velocities will obey the ratios used in the simulation.

The results of this chapter show that the LDI exhibits STC and the growing PW saturates. The saturation energy can also be estimated. For very strong damping on the daughter waves (very weak growth) the correlation time scales will be very long and the amplitude of the daughter waves will be very small. The nonlinearity becomes weak and STC is very mild. As the damping weakens the nonlinearity becomes more important and STC begins to dominate. This behaviour portrays the general trend of the simulations of the full system. The advantage of isolating the LDI is that the precise nonlinear mechanism for saturation and generation of STC is more readily understood. However, the 3WI can never represent the regime of strong turbulence and Langmuir collapse. The STC dephases the SRS interaction by providing a spread in wave number and frequency around the principal values. The LDI acts like a sink on the LW of SRS. This corresponds to an effective damping and eventual saturation of the LW. The combination of LW damping and dephasing can be shown to saturate the SRS parametric instability (Bers, 1975).

4.5 Conclusions

In both LDI and SDI, the competition between linear instability and nonlinear saturation leads to the complex behaviour and STC, yet the nonlinear mechanisms responsible are entirely different. Nearly integrable systems are very useful in analysing STC. Perturbation expansions around nonlinear solutions are possible to elucidate the behaviour. Unlike SDI, the IST solution for LDI is radiation dominated and thus closed form solutions to perturb around do not exist. However the IST solutions were still of great use in analytically understanding the dynamics of STC.

The three waves form a frustrated lattice. This is akin to the phase turbulence and misalignment seen in the KS equation (Shraiman, 1985). There may be global stationary solutions where the lattice is perfectly aligned. For instance, if the group

velocity ratios are such that a triangular lattice is formed then a stationary state may be possible. Perturbing around this stationary lattice may yield some useful results. A reduced description of the dynamics driven by frustration could also be used. Some lattice spin model with asymmetric couplings may be designed to capture the essentials of the dynamics.

The long time scales of the coherent structures in the PW and BW are poorly understood and need to be investigated further. Longer simulations are required. A wider parameter search is also required. Many things could be studied in the future. As in SDI the response function could be measured to check whether the dynamics obey the fluctuation-dissipation theorem. Measurements of higher moments test whether the distribution of fluctuations is Gaussian. As mentioned the cross correlations between the envelopes should certainly be measured. The dynamics seemed to be dependent on the system size. Simulations with different sized boxes could explore this.

Chapter 5

Stimulated Brillouin Scattering in a Finite Medium

In the previous chapters, models of the 3WI that exhibited spatiotemporal chaos were studied. In this chapter the 3WI will be used to describe a spatially extended system that manifests low dimensional chaos. STC is conveniently described by the concepts of statistical mechanics and linear response theory. The paradigms of low dimensional chaos such as bifurcation theory, strange attractors, and Lyapunov exponents were not as useful in analysing STC. However, they will make their appearance in this chapter.

5.1 The Model

The model studied is Stimulated Brillouin Scattering (SBS) in a homogeneous finite medium. The dynamics of SBS has captured considerable interest both in laser-plasma interactions (Randall and Albritton, 1984; Sauer and Baumgartel, 1984; Blaha *et al.*, 1988; Hüller *et al.*, 1991) and in optical fibers (Cotter, 1983; Bar-Joseph *et al.*, 1985; Coste and Montes, 1986; Botineau *et al.*, 1989; Harrison *et al.*, 1990; Gaeta and Boyd, 1991).

SBS results from a parametric coupling between electromagnetic (light) and acoustic waves. In an optical fiber, a laser impinges on the fiber, excites an acoustic wave

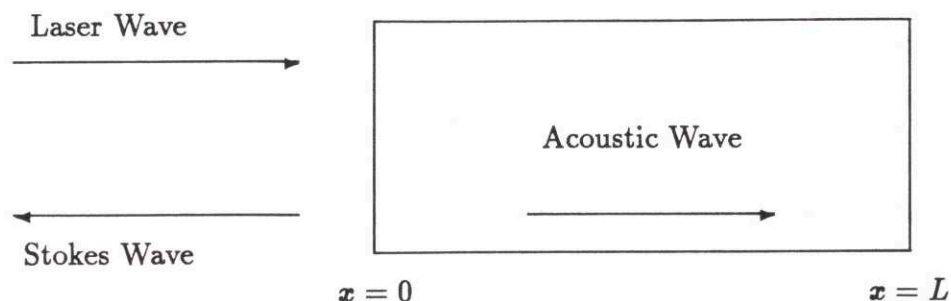


Figure 5-1: Schematic of SBS in a medium of length L .

by electrostriction and scatters back (Stokes wave). In the case of a plasma an ion-acoustic wave is excited. A schematic of SBS in a box of length L is shown in Fig. 5-1. The three wave SBS equations are derived by considering slowly varying amplitudes as in Section 2.1 (Kroll, 1964; Bloembergen, 1965; Kaiser and Maier, 1972).

Nonstationary and chaotic behaviour has been reported in SBS with external feedback such as reflection at the boundaries (Randall and Albritton, 1984; Sauer and Baumgartel, 1984; Hüller *et al.*, 1991) or with models involving more than one pump (Narum *et al.* 1988; Gaeta *et al.*, 1989). Harrison *et al.* (1990) have observed chaotic SBS experimentally in an optical fiber without feedback. Gaeta and Boyd (1991), have performed similar experiments and obtained similar results. They propose that the experimentally observed aperiodic behaviour is due to amplification of noise. They have a stochastically driven model that agrees with the experiments.

In the time only case described in Section 2.2, it was found that the addition of temporal dephasing due to a frequency mismatch is required for chaos. It is shown here that with the addition of temporal dephasing and without feedback the spatiotemporal 3WI modelling SBS can be chaotic in a restricted parameter regime. This appears to be one of the simplest SBS models that exhibits chaos. The question remains as to how a frequency mismatch would occur in a fiber. The experiments were done with narrow linewidth lasers and so the resonance conditions should always be satisfied. Rubenchik (1991) has an argument for how dephasing may arise. The wavelength of the acoustic wave is on the order of the fiber diameter. Thus transverse modes will be set up in the fiber wave guide. The k spectrum will be discrete and so

exact resonance may be impossible.

For SBS in a finite medium with temporal dephasing in one spatial dimension the 3WI, Eqs. (2.24)-(2.26) become

$$\partial_t a_i + v_i \partial_x a_i - \gamma_i a_i = -K a_j a_k \exp(-i\delta t), \quad (5.1)$$

$$\partial_t a_j + v_j \partial_x a_j - \gamma_j a_j = K^* a_i a_k^* \exp(i\delta t), \quad (5.2)$$

$$\partial_t a_k + v_k \partial_x a_k - \gamma_k a_k = K^* a_i a_j^* \exp(i\delta t), \quad (5.3)$$

where power is input through the boundary with $a_i(0) = A_p$. Equations (5.1) and (5.2) describe the evolution of light waves travelling in opposite directions so $v_i = -v_j = c/n$ where c is the velocity of light and n is the index of refraction for the medium. Equation (5.3) describes the evolution of the acoustic wave (ion acoustic wave in a plasma). The group velocity is the sound velocity c_s .

For a typical experiment with fused silica optical fibers and a single-mode argon-ion laser with $\lambda = 514.5\text{nm}$, the parameters are $n = 1.46$, $c_s = 5.96 \times 10^3 \text{ms}^{-1}$, $\gamma_k \simeq 270\text{MHz}$, $K \simeq 66\text{ms}^{-1}\text{V}^{-1}$, and $\gamma_i/\gamma_k \simeq 10^{-3}$ (Cotter, 1983; Cotter, 1987; Harrison *et al.*, 1990; Gaeta and Boyd, 1991).

The equations can be simplified. For a relatively strong pump the interaction time scale for the acoustic wave is given by $\tau = 1/(KA_p)$. This then gives an interaction length of $l \simeq \tau \sqrt{c_s c/n}$. The damping length for the acoustic wave is $l_d \simeq c_s/\gamma_k$. For the case where the damping length is much smaller than the interaction length ($l_d \ll l$) then the convection term in Eq. (5.3) can be ignored. This condition is easily satisfied in optical fibers and can be satisfied in a plasma for heavy ion acoustic wave damping. The damping on the EM waves are weak and can be ignored. Length and time scales are renormalized with $\gamma_k t \rightarrow t$, $x\gamma_k(n/c) \rightarrow x$, $\Delta = \delta/\gamma_k$. The following substitutions are made: $E_0 = a_i K/\gamma_k$, $E_s = a_j K/\gamma_k$, $E_a = (a_k K/\gamma_k) \exp(-i\Delta t)$. The SBS equations become

$$\partial_t E_0 + \partial_x E_0 = -E_s E_a, \quad (5.4)$$

$$\partial_t E_s - \partial_x E_s = E_0 E_a^*, \quad (5.5)$$

$$\partial_t E_a + (1 + i\Delta)E_a = E_0 E_s^*, \quad (5.6)$$

with the boundary conditions $E_0(x = 0, t) = A_p K / \gamma_k \equiv A$, $E_s(x = L, t) = \epsilon$. The scattered wave is assumed to grow from a small noise source ϵ at the right boundary. The laser wave E_0 is referred to as the pump, the scattered light wave E_s is often called the Stokes wave. In terms of a typical optical fiber experiment, $L = 1$ corresponds to 0.75m, $\Delta = 1$ corresponds to 270MHz, and $A = \epsilon = 1$ corresponds to 4MVm^{-1} .

5.2 The Dynamics

Equations (5.4)-(5.6) were numerically simulated using the same method as in the previous two chapters. The only difference was in the handling of the boundary conditions. The details are in Appendix C. For each run the spatiotemporal series was recorded. Diagnostics included monitoring the output time dependence of the waves: $E_0(x = L, t)$, $E_s(x = 0, t)$, $E_a(x = 0, t)$. The phase portrait of $E_a(0, t)$ vs. $E_s(0, t)$ was constructed from this information. As a substitute for a true Poincaré surface of section the phase portrait strobed at the dephasing rate was also constructed, i.e. $E_a(0, t_n)$ vs. $E_s(0, t_n)$ where $t_n = 2\pi n / \Delta$, n is an integer. The system has four free parameters A , Δ , ϵ , and L . However a numerical survey of the parameter space indicated that a two dimensional surface in the parameter space could capture the unfolding behaviour. The Δ - A parameter plane for fixed L and ϵ was chosen.

Figure 5-2 shows the numerically determined unfolding diagram in the Δ - A plane for $L = 40$ and $\epsilon = 0.0025$. Parameters L and ϵ were chosen so that the bifurcation diagram in the Δ - A plane was complete. For small Δ and A there is a stable fixed state. It becomes unstable through a Hopf bifurcation to a periodic state. Then there is a transition to quasi-periodicity and to chaos. Each region will be discussed in detail.

5.2.1 The Fixed State

The system has one fixed state. This is best examined by transforming to modulus-phase form. Substituting the following

$$E_0 = A_0 e^{i\phi_0}, \tag{5.7}$$

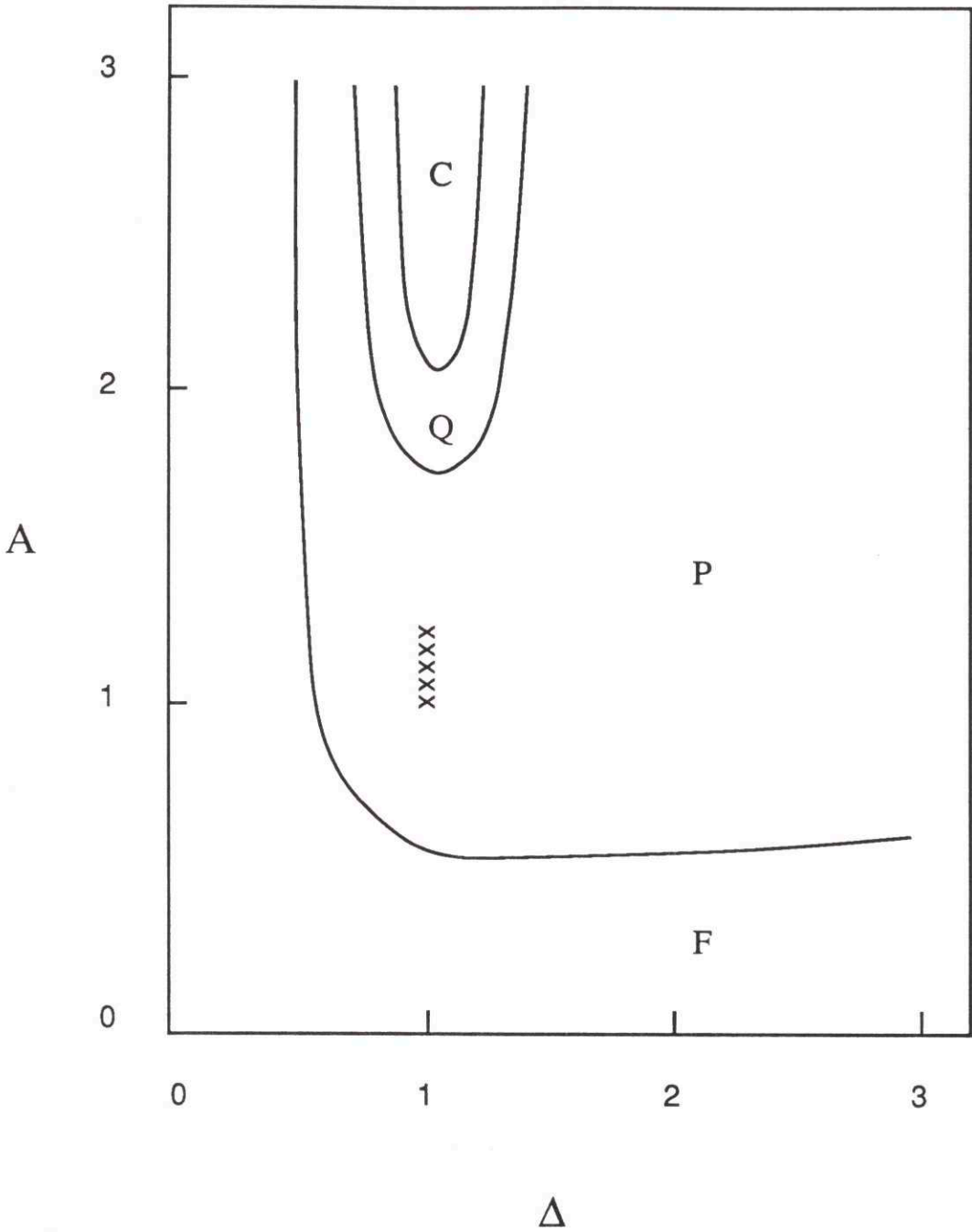


Figure 5-2: Bifurcation diagram in the Δ - A plane for $L = 40$ and $\epsilon = 0.0025$. There are four different phases: F denotes the fixed state, P denotes the periodic orbit, Q denotes quasi-periodicity and C denotes chaos. The line of x's indicate a region of phase coexistence between a periodic and a quasi-periodic orbit.

$$E_s = A_s e^{i\phi_s}, \quad (5.8)$$

$$E_a = A_a e^{i\phi_a}, \quad (5.9)$$

into Eqs. (5.4)-(5.6) yields the equations

$$A_{0,t} + A_{0,x} = -A_s A_a \cos \phi, \quad (5.10)$$

$$A_{s,t} - A_{s,x} = A_0 A_a \cos \phi, \quad (5.11)$$

$$A_{a,t} + A_a = A_0 A_s \cos \phi, \quad (5.12)$$

$$\phi_{0,t} + \phi_{0,x} = -\frac{A_s A_a}{A_0} \sin \phi, \quad (5.13)$$

$$\phi_{s,t} - \phi_{s,x} = -\frac{A_0 A_a}{A_s} \sin \phi, \quad (5.14)$$

$$\phi_{a,t} + \Delta = -\frac{A_0 A_s}{A_a} \sin \phi, \quad (5.15)$$

where $\phi = \phi_a + \phi_s - \phi_0$. The fixed state is obtained by setting the time derivatives to zero. From Eqs. (5.10)-(5.12) this yields the equations

$$A_{0,x} = -A_0 A_s^2 \cos^2 \phi, \quad (5.16)$$

$$A_{s,x} = -A_0^2 A_s \cos^2 \phi. \quad (5.17)$$

Combining Eqs. (5.12) and (5.15) yields $\tan \phi = -\Delta$. The amplitudes must be positive so from (5.12) it can be concluded that

$$\cos \phi = \frac{1}{\sqrt{1 + \Delta^2}}, \quad \sin \phi = \frac{-\Delta}{\sqrt{1 + \Delta^2}}. \quad (5.18)$$

Equations (5.16) and (5.17) can then be integrated to yield

$$A_0^2 = \frac{A^2(1-R)}{1 - R \exp(-2(1-R)A^2\Gamma x)}, \quad (5.19)$$

$$A_s^2 = \frac{A^2 R(1-R)}{\exp(2(1-R)A^2\Gamma x) - R}, \quad (5.20)$$

$$A_a = \Gamma^{1/2} A_0 A_s, \quad \Gamma = (1 + \Delta^2)^{-1}, \quad (5.21)$$

subject to

$$A_s(x=L) = \epsilon. \quad (5.22)$$

The reflectivity R is determined by the boundary condition at $x=L$. Its value must be obtained numerically.

Plugging in for A_a and $\sin \phi$ in Eqs. (5.14) and (5.15) yields

$$\phi_{0,x} = \frac{\Delta}{1 + \Delta^2} A_s^2, \quad (5.23)$$

$$\phi_{s,x} = -\frac{\Delta}{1 + \Delta^2} A_0^2. \quad (5.24)$$

Using Eqs. (5.19) and (5.20), the phases Eqs (5.23) and (5.24) can be integrated to yield

$$\phi_0 = \frac{\Delta}{2} \ln \left[\frac{1 - R \exp(-2A^2(1-R)\Gamma x)}{1 - R} \right], \quad (5.25)$$

$$\phi_s = -\frac{\Delta}{2} \ln \left[\frac{\exp(2A^2(1-R)\Gamma x) - R}{\exp(2A^2(1-R)\Gamma L) - R} \right], \quad (5.26)$$

where the B.C.

$$\phi_0(x=0) = 0, \quad \phi_s(x=L) = 0, \quad (5.27)$$

have been applied. The phases are fixed by the boundary conditions and increase as they travel towards the opposite end. The pump phase has an upper bound of $\phi_0(L) \leq -(\Delta/2) \ln(1-R)$ while the Stokes phase is unbounded for large A .

The spatial profile of the fixed state for the envelope moduli for parameters $A = 1.6$, $\Delta = 0$, $L = 40$, $\epsilon = 0.0025$ is shown in Fig. 5-3. In this particular example the reflectivity R for the Stokes wave is close to unity. The Stokes wave has a definite decay length in space given by

$$l_s \simeq (1 + \Delta^2)/(2(1-R)A^2). \quad (5.28)$$

For distances beyond $x \simeq l_s$ the Stokes wave has negligible amplitude and the pump passes through unaffected. Thus l_s gives an effective interaction length. Although the system box may be larger, the dynamics take place in the interaction region $0 < x < l_s$.

The stability of the fixed state can be examined by plugging $E_l = A_l \exp(i\phi_l) + \delta E_l$ into Eqs. (5.4)-(5.6), where δE_l are small perturbations. If the perturbations are assumed to have a time dependence of $\exp(st)$, the linearized equations form an inhomogeneous fourth order boundary value problem for the real and imaginary parts of δE_0 and δE_s . These equations must be solved numerically. This has not yet been done. For no temporal dephasing ($\Delta = 0$), Blaha *et al.* (1988) showed that this

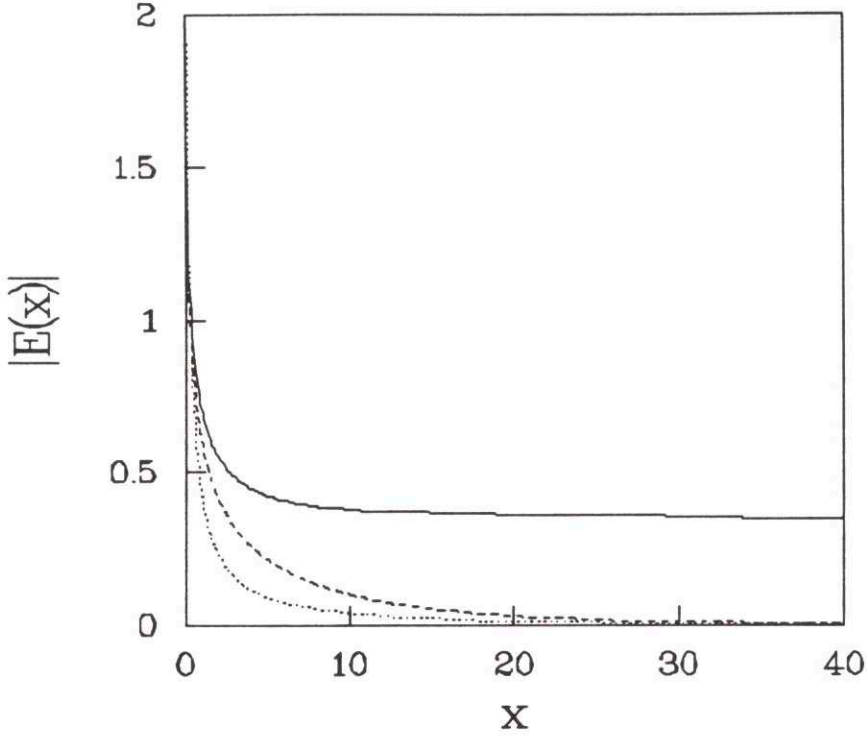


Figure 5-3: Fixed State spatial profiles of the pump (solid line), Stokes wave (dashed line) and acoustic wave (dotted line) for the parameters $\Delta = 0.$, $A = 1.6$, $L = 20$, $\epsilon = 0.0025$.

fourth order system reduces to two second order equations, one each for the real and imaginary parts. These second order equations can then each be transformed into Legendre equations and the time evolution of perturbations can be found in terms of associated Legendre functions. They showed that the fixed state is unstable in a semi-infinite medium. Applying boundary conditions for a finite medium to their solutions, the fixed state can be shown to always be stable.

Numerically it was found that the fixed state Hopf bifurcates to a periodic state along a 'L' shaped curve in the parameter plane (see Fig. 5-2). Although an analytic condition for the stability of the fixed state cannot be found, this particular shape can be deduced. Consider a nonzero value of A . The fixed state is stable for $\Delta = 0$. The only difference in the fixed state between $\Delta = 0$ and $\Delta \neq 0$ is the 'phase twist' given in Eqs. (5.25) and (5.26). I postulate that the criterion for stability is determined by the amount of 'phase twisting'. For example when $\phi_s(x = 0)$ exceeds a critical

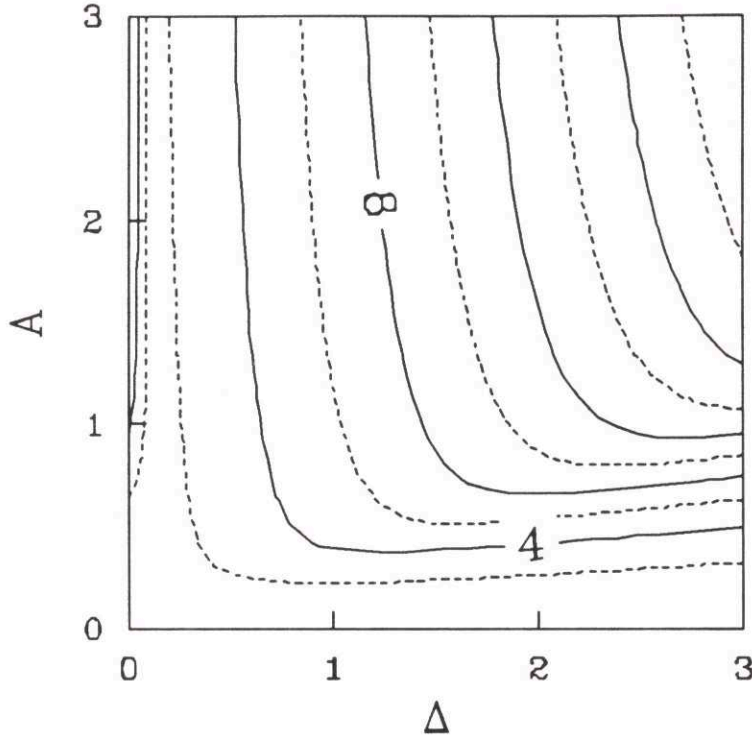


Figure 5-4: Contour plot of $\phi_s(x=0)$ in the Δ - A plane for $L = 40$, $\epsilon = 0.0025$.

threshold, the fixed state becomes unstable. A contour portrait of $\phi_s(x=0)$ in the Δ - A plane for $L = 40$ and $\epsilon = 0.0025$ is shown in Fig. 5-4.

Notice that the $\phi_s(x=0) \simeq 5$ contour matches very closely to the numerically determined stability boundary in Fig. 5-2. The bifurcation seems to be a codimension one supercritical Hopf bifurcation (Guckenheimer and Holmes, 1986).

From Eq. (5.26) it appears that the phase $\phi_s(0)$ depends on A^2 and L in the same way. This is not entirely true because the reflection coefficient depends nontrivially on the parameters. However it has a relatively weak dependence and numerical simulations do show that the bifurcation point responds similarly to A^2 and L . In the parameter plane, L was set large enough so that all the bifurcations were included.

5.2.2 Periodic Orbits

When the stability line is crossed in parameter space the fixed state Hopf bifurcates to a periodic state. Points in the parameter plane will be denoted by the ordered

pair (Δ, A) . An example of the spatial profile of a periodic state at $(1, 1)$ is shown in Fig. 5-5. The three profiles have the form of the fixed state profiles shown in Fig. 5-3 but now with modulations. In this and the following spatial profile figures, the pump is the solid line, the Stokes wave is the dashed line and the acoustic wave is the dotted line. The pump consists of a periodic pattern that propagates across the box. The interaction between the waves is confined to a small region given roughly by the decay length of the Stokes wave Eq. (5.28). Figure 5-6 shows the output time series for the pump and Stokes wave. They are periodic. The power spectrum of the pump is shown in Fig. 5-7 and shows the frequency is very near Δ . The power spectra of the other two waves are similar. The phase portrait of E_s vs. E_a is shown in Fig. 5-8 (a). A closed curve is seen confirming periodic behaviour. The phase portrait strobed at the dephasing rate $\Delta = 1$ is shown in Fig. 5-8 (b). In this case the frequency is locked to the dephasing rate. There are 38 discrete points indicating the frequency is $\omega = (37/38)\Delta$. In all cases the frequency will be near Δ but not necessarily locked to it. Periodic states can also be composed of interesting shapes. Figure 5-9 shows the spatial profile of the state $(0.8, 1.6)$. The pump is composed of a modulated periodic pattern. The phase portrait is shown in Fig. 5-10. It is a closed figure but no longer convex.

One small section of the periodic regime, indicated by a line of x's in Fig. 5-2, has a phase coexistence between a periodic state and a quasi-periodic state. Figure 5-11 shows the output time series $E_0(x = L, t)$ for the pump at $(1.1, 1)$ for two different initial conditions. In Fig. 5-11 (a) a periodic pattern is observed, however in (b) a completely different quasi-periodic orbit appears. Figure 5-12 shows the phase portraits for the corresponding time series. In (a) there is a closed oval, but in (b) one sees a double looped figure that does not close. The two different runs were continued for very long times to test their robustness. However even after many hundreds of thousands of periods, the quasi-periodic state did not fall into the periodic attractor. It is unknown what the basin of attraction is for each phase. This coexistence regime was discovered by chance. It is uncertain whether more regimes exist in the periodic regime. In many of the runs made in the periodic regime, the relaxation times were

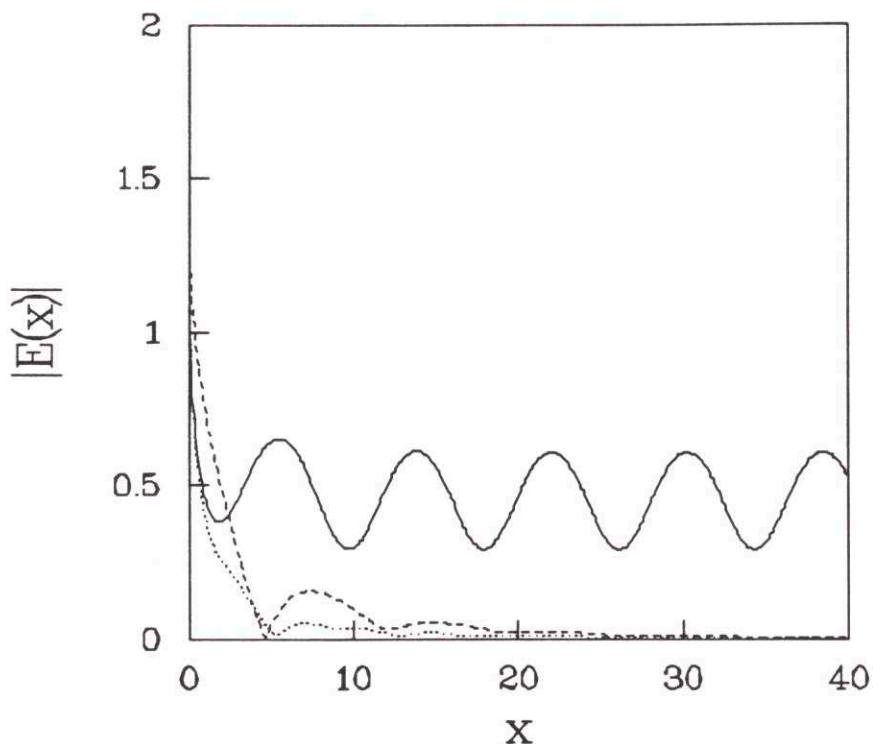


Figure 5-5: Spatial profile of the amplitudes at a fixed time at (1,1).

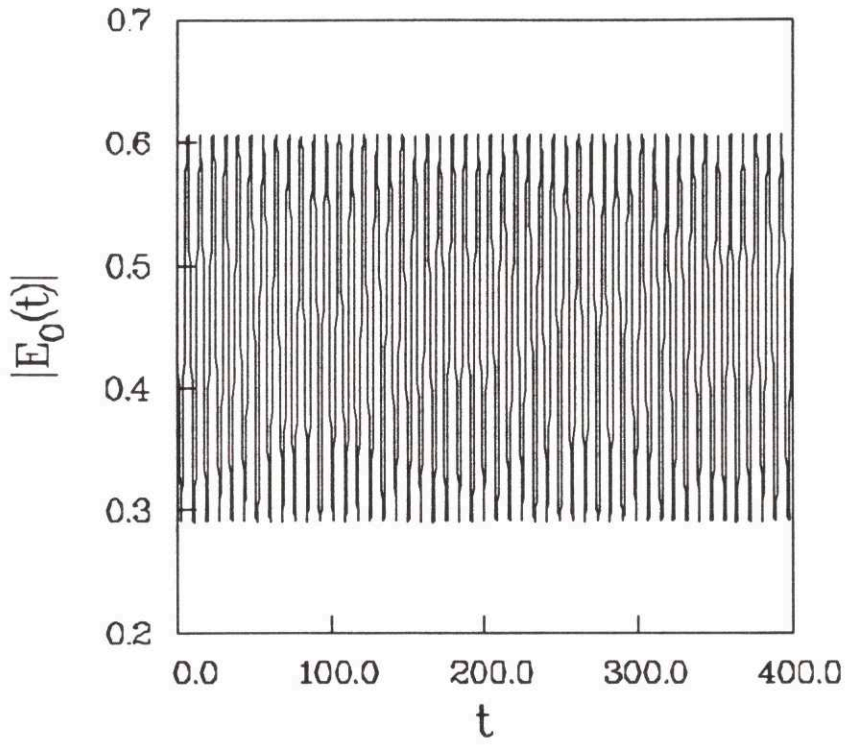
extremely long. Often it was difficult to distinguish between periodic and nonperiodic states because the transients were so long lived.

5.2.3 Quasi-periodicity and Chaos

The periodic state can make a transition to a quasi-periodic state. As the bifurcation boundary to quasi-periodicity is approached, a second frequency corresponding to the round trip transit time across the box begins to make an appearance. Its decay time becomes longer and longer as the boundary is approached until finally it becomes stable. Very long computation times were required to resolve the boundary.

Figure 5-13 shows the time series for the quasi-periodic orbit at (1, 2) for the pump and the Stokes wave. The two frequencies are readily observed. A spatial profile is shown in Fig. 5-14. The pump is composed of periodic 'dimpled' structures. The Stokes and acoustic waves are modulated. The slow frequency is barely perceptible in the pump. The phase portrait in Fig. 5-15 shows an attractor that has a width and

(a)



(b)

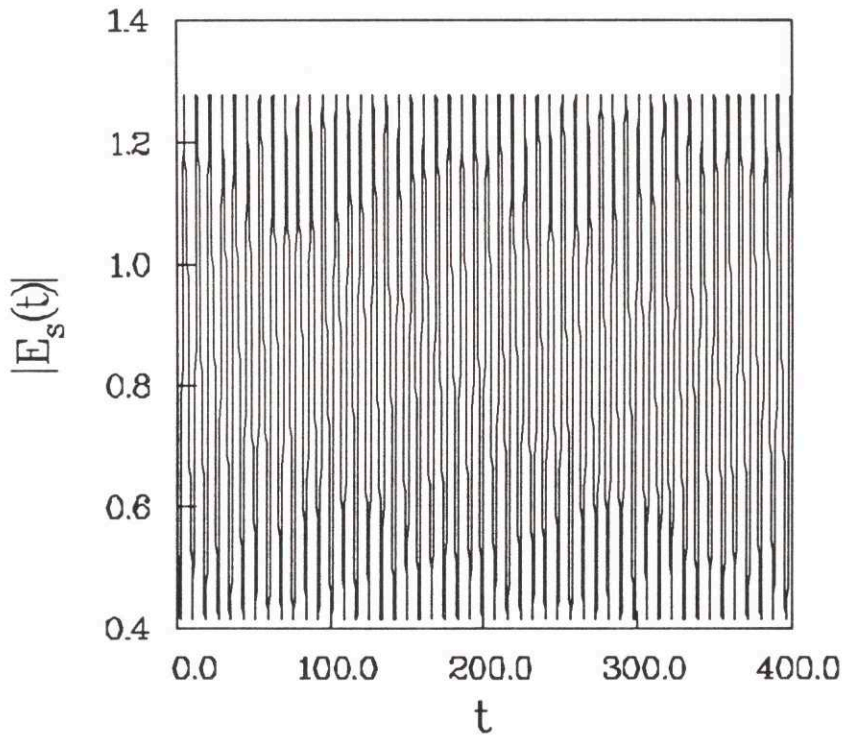


Figure 5-6: Time series for (a) pump and (b) Stokes wave at (1,1).

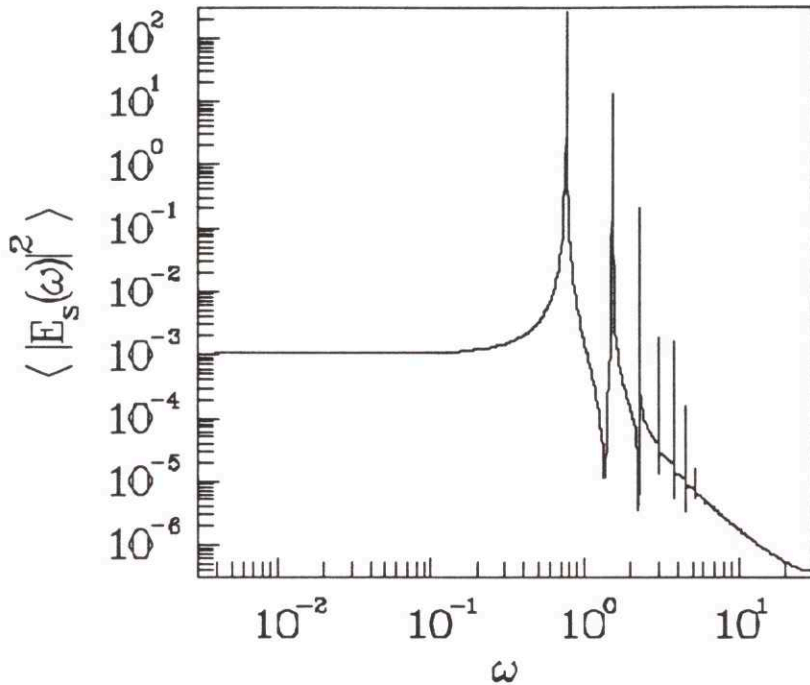


Figure 5-7: Power spectrum of pump at (1,1).

is clearly nonperiodic. The power spectrum for the pump is in Fig. 5-16. The other waves have similar power spectra. There are many peaks in the spectrum confirming quasi-periodic behaviour. The peak at $\omega \simeq 1$ is the fast frequency from the periodic orbit. The broader peak near $\omega \simeq 0.07$ corresponds to a time scale of twice the transit time across the box.

The quasi-periodic state makes a subcritical bifurcation to chaos. At the boundary between the two phases there is a region of hysteresis. This region is very narrow. For instance at (1,2) there is another attractor. The phase portrait in Fig. 5-17 shows that the orbit has a double loop structure like that for the quasi-periodic phase at (1.1,1) in Fig. 5-8 (b). The orbit alternates between one loop and the other. Figure 5-18 shows the time series for the pump and Stokes wave. They resemble time series for intermittency. However a measurement of how the laminar periods scale with the unfolding parameter was not made to verify this. The time-only equations were observed to exhibit Type I intermittency (Meunier *et al.*, 1982). The power

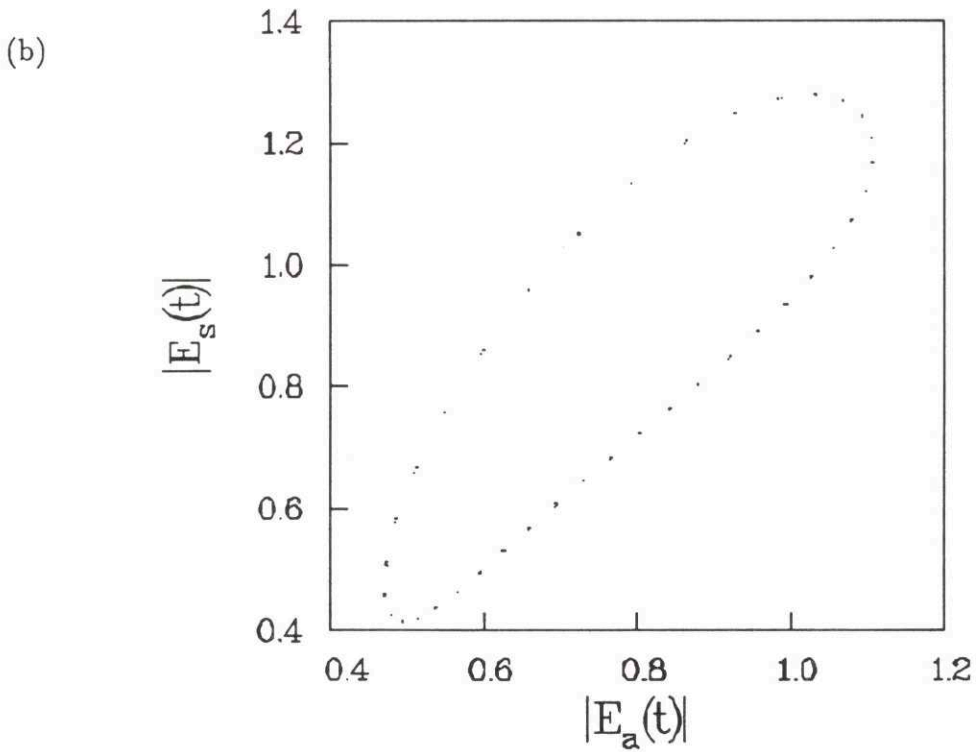
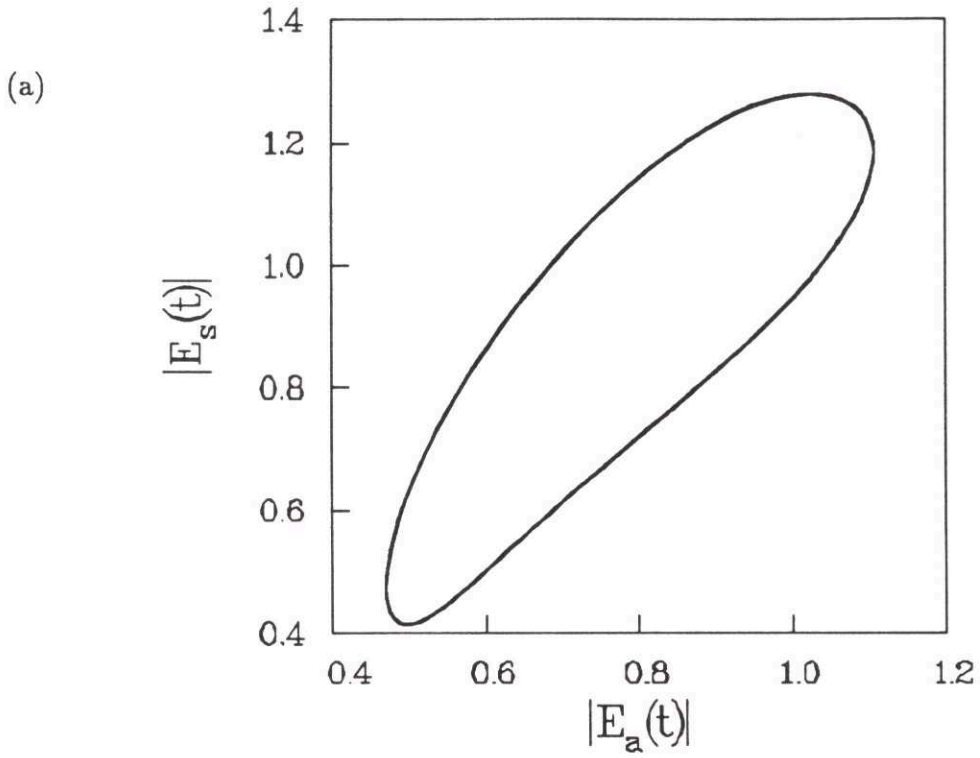


Figure 5-8: (a) Phase portrait E_s vs. E_a at (1,1); (b) strobed at $t_n = 2\pi/\Delta$.

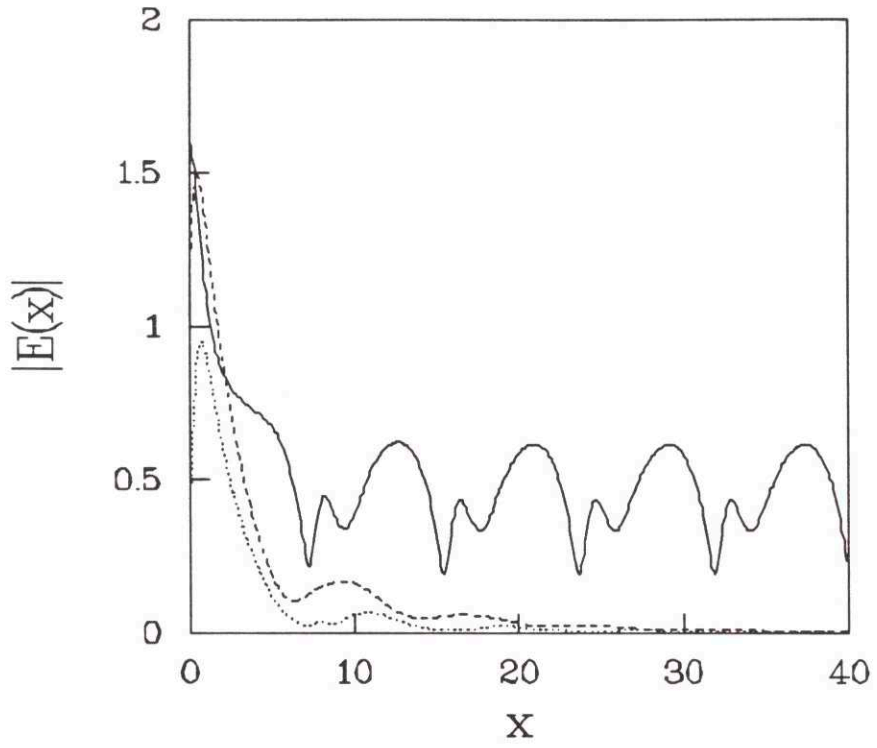


Figure 5-9: Spatial profile of the amplitudes at (0.8,1.6).

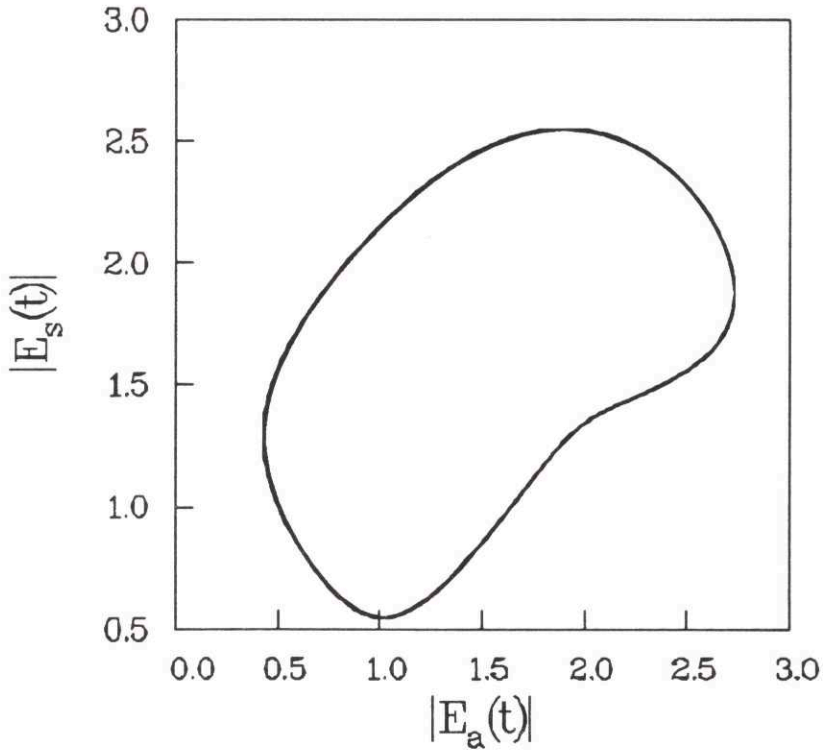


Figure 5-10: Phase portrait at (0.8,1.6).

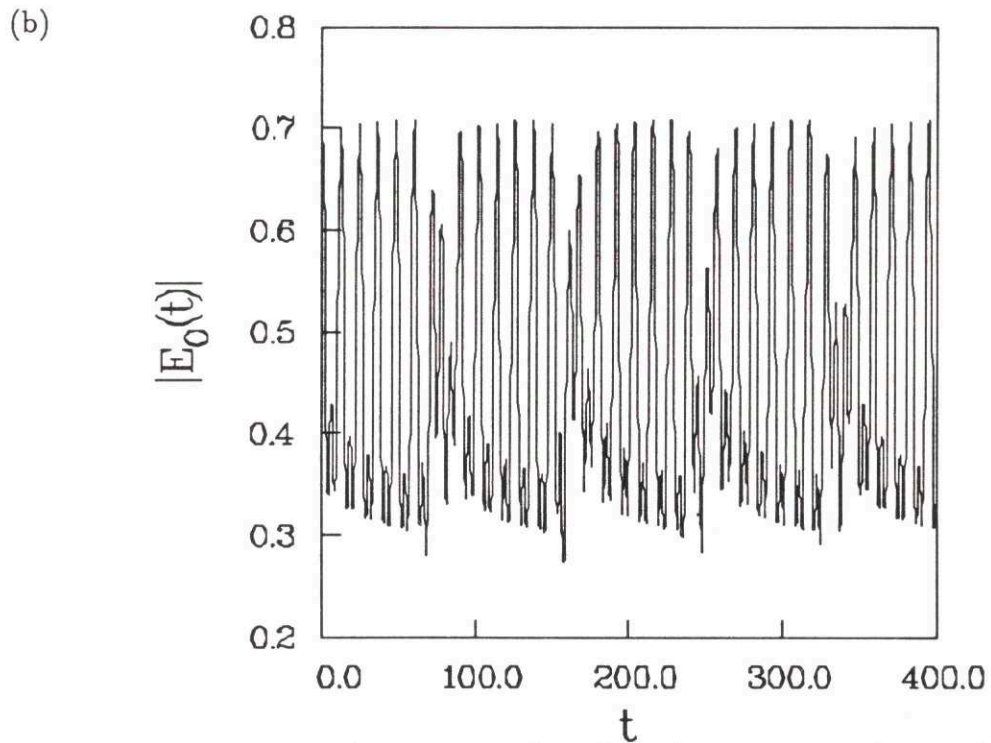
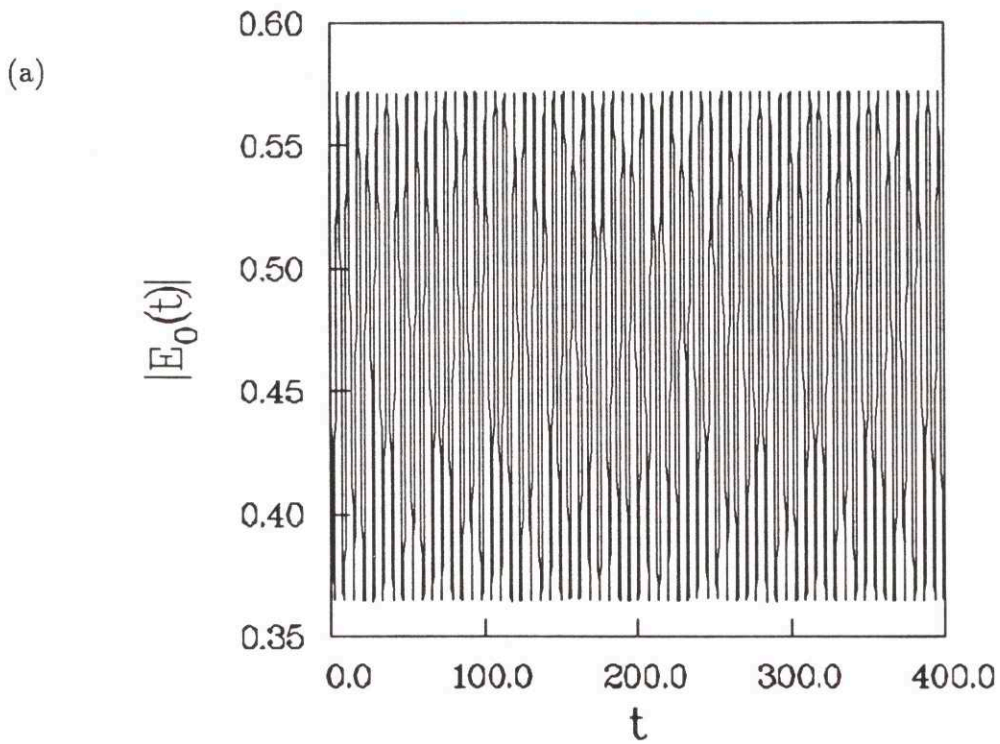


Figure 5-11: Time series for pump at (1.1,1) with coexisting phases: (a) periodic orbit, (b) quasi-periodic orbit.

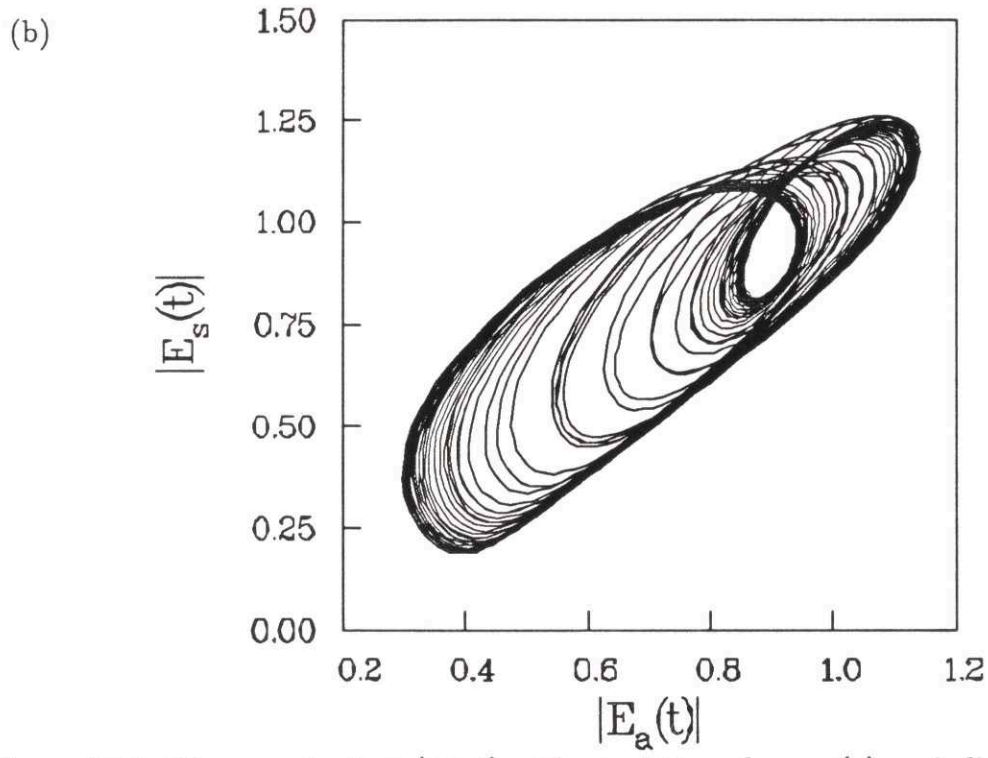
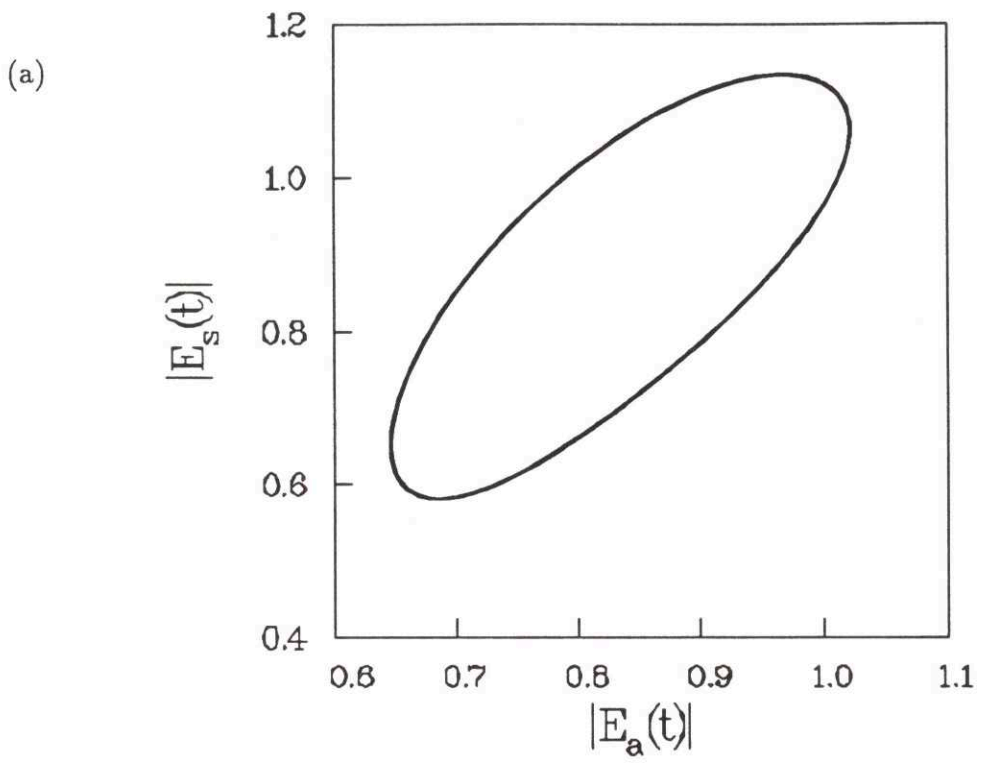
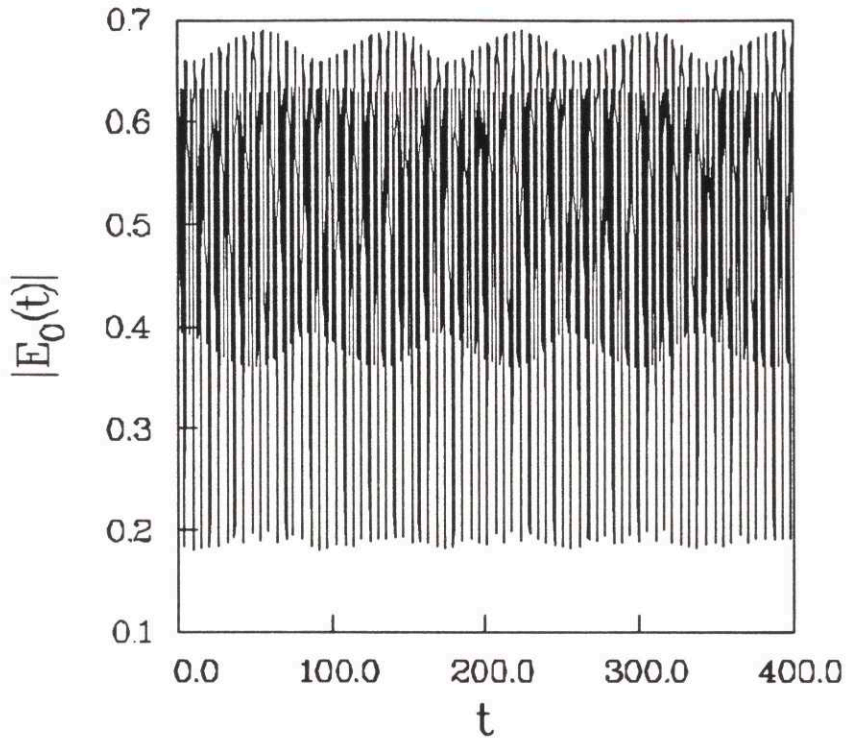


Figure 5-12: Phase portrait at (1.1,1) with coexisting phases: (a) periodic orbit, (b) quasi-periodic orbit.

(a)



(b)

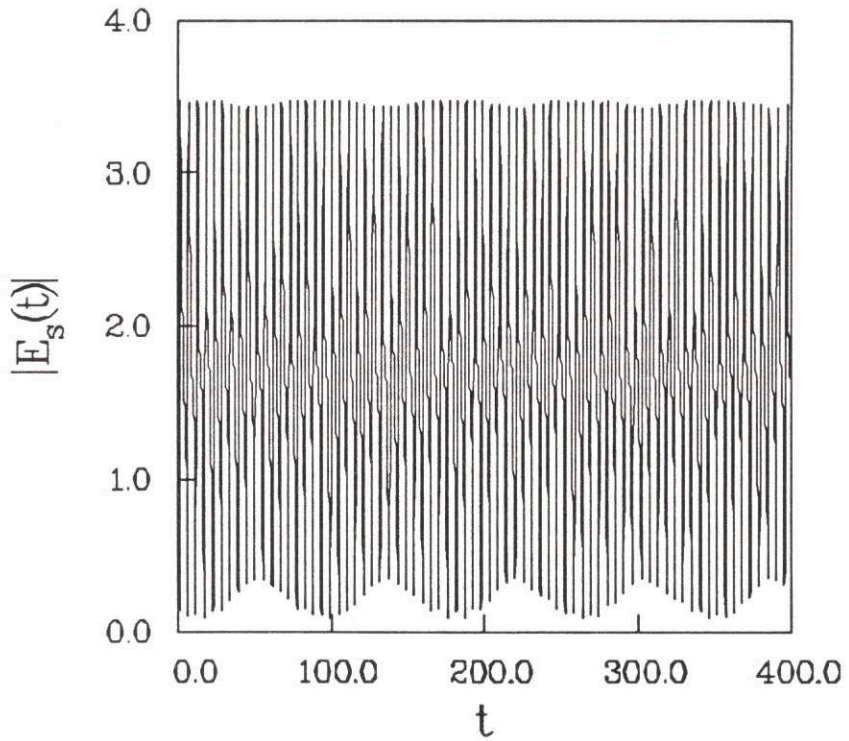


Figure 5-13: Time series at (1,2) of (a) pump and (b) Stokes wave.

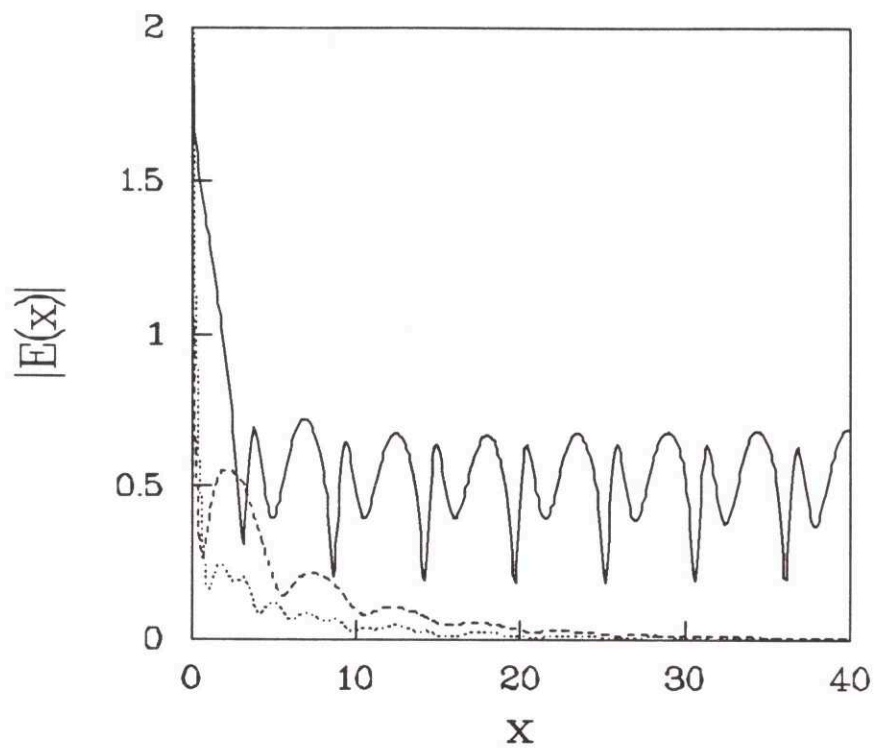


Figure 5-14: Spatial profile at (1,2).

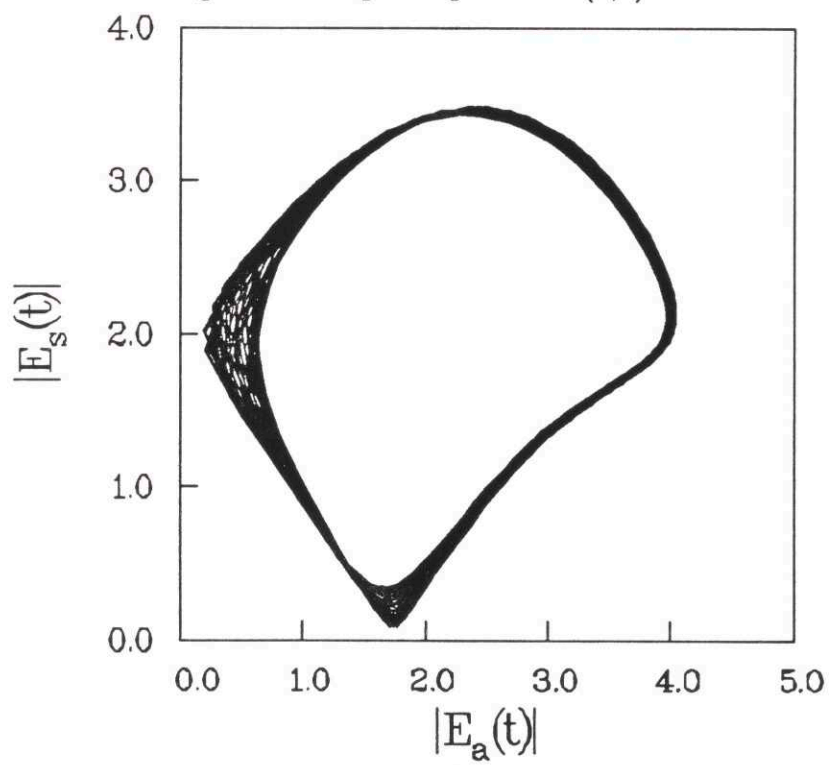


Figure 5-15: Phase portrait at (1,2).

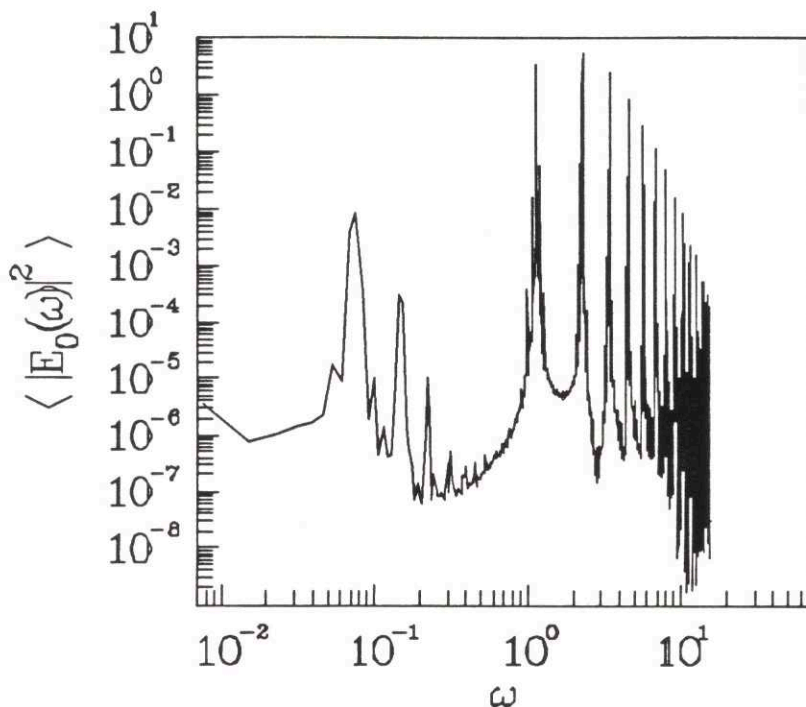


Figure 5-16: Power spectrum of the pump at (1,2).

spectrum in Fig. 5-19 for the pump shows broad band behaviour indicative of chaos. A measurement of the largest Lyapunov exponent λ was made by linearizing about a fiducial orbit (see Wolf *et al.* (1985)). It was found to be very small but positive ($\lambda \simeq 0.001$).

Plunging deeper into the chaotic regime at (1.1,2.6) the orbits become more aperiodic. Figure 5-20 shows the time series for the pump and Stokes wave. The laminar regions are reduced in size from those in Fig. 5-18. The general structure of the time series looks different. The phase portrait in Fig. 5-21 shows that a third loop has just begun to form. The power spectrum for the pump in Fig. 5-22 is broad band. The remnant of the periodicity still exists as indicated by a broad peak near $\omega \simeq 1$. The largest Lyapunov exponent has increased to around $\lambda \simeq 0.002$.

Finally, well into the chaotic region at (1,5), the time series of the pump is clearly chaotic in Fig. 5-23. The phase portrait in Fig. 5-24 has no real structure. The power spectrum in Fig. 5-25 flattens out below $\omega \simeq 1$ defining a coherence time. The spatial

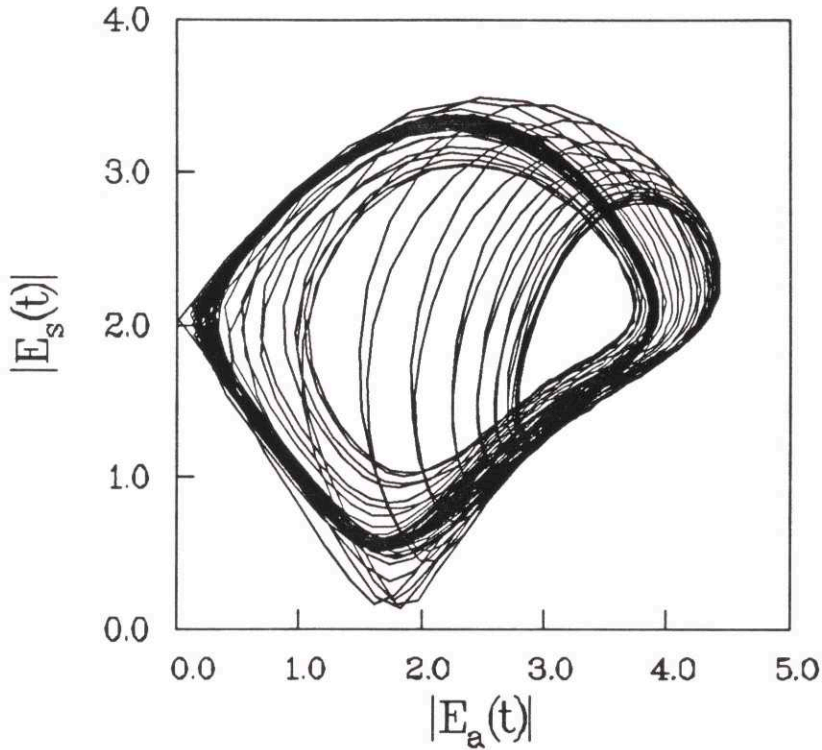


Figure 5-17: Phase portrait of chaotic orbit at (1,2)

profile is in Fig. 5-26. The waves appear chaotic yet the interaction length where the Stokes wave has substantial amplitude remains small. From the plot it appears that the coherence length of the pump structures is on the order of the decay length of the Stokes wave. Thus the resulting chaos is low dimensional.

5.3 Conclusions

Given that temporal dephasing is present in SBS, a sequence of transitions from steady state to chaos is possible. For the chaotic regime to occur, the reflectivity must be high and the medium must be larger than the decay length (growth length) for the Stokes wave. This appears to be the simplest SBS model thus far that has chaotic solutions. Gaeta and Boyd (1991) have strong evidence that the aperiodicity observed thus far in experiments with optical fibers is due to amplification of noise. This is not to say that chaotic SBS due to dephasing may not exist in other experiments. For high reflectivity in a large medium the effect of the noise need not be as great (Gaeta,

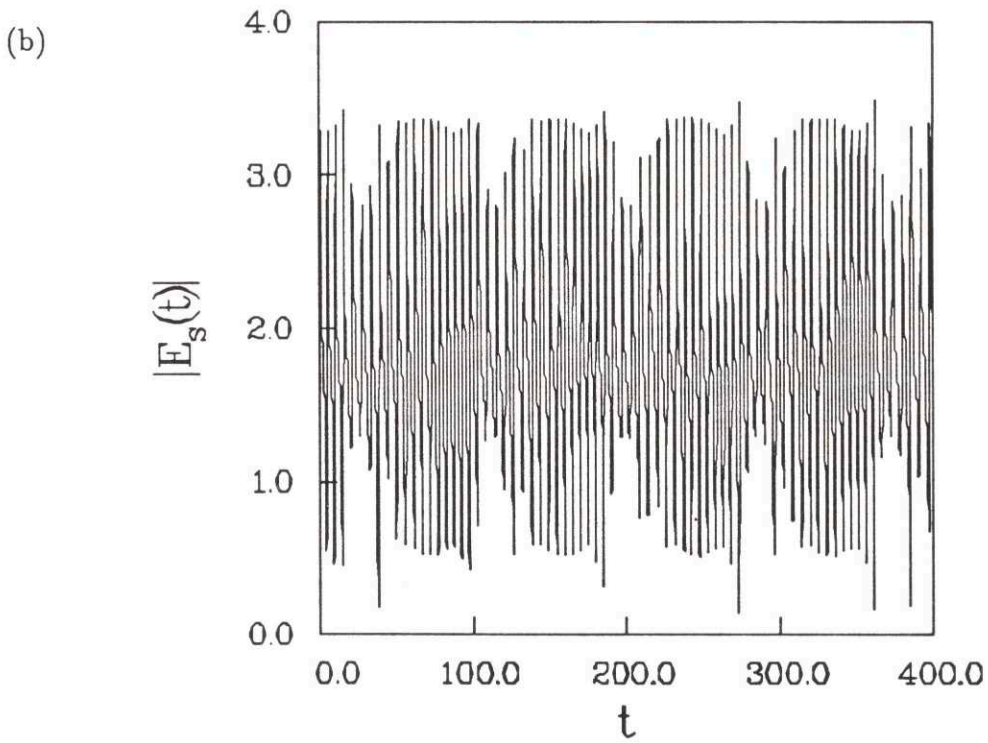
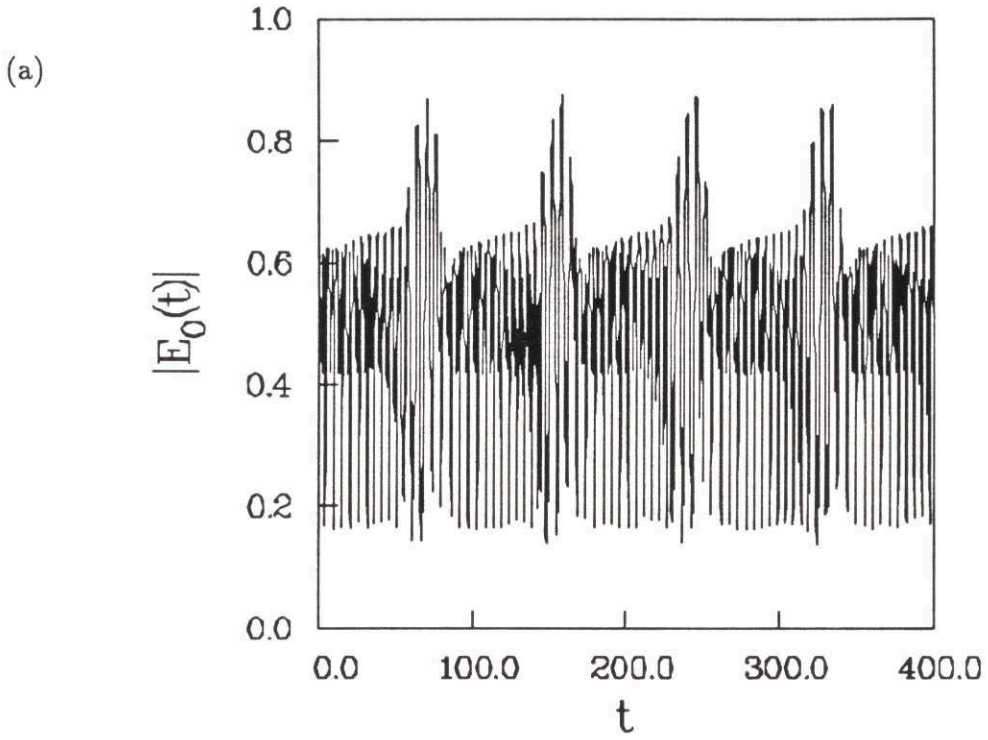


Figure 5-18: Time series for the chaotic orbit at (1,2) for (a) pump and (b) Stokes wave.

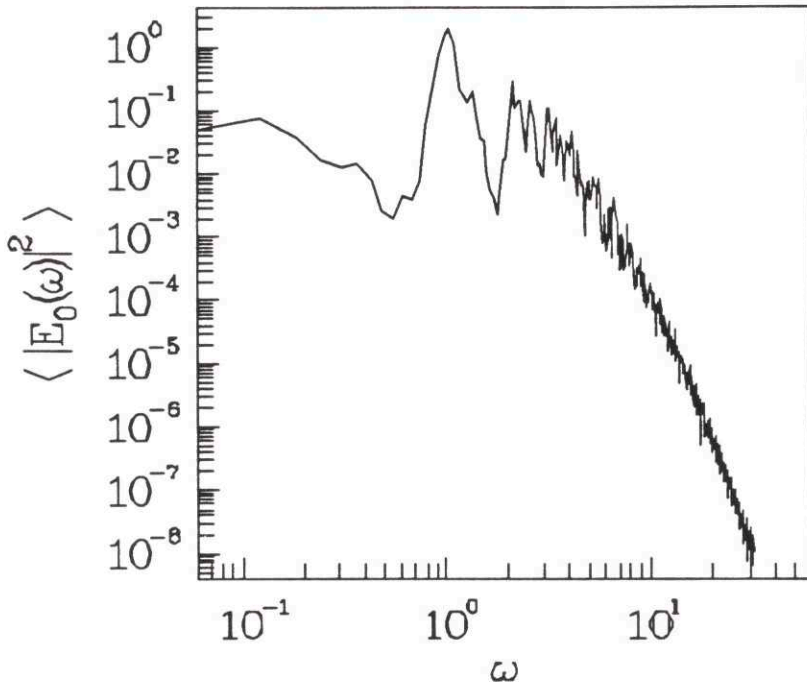
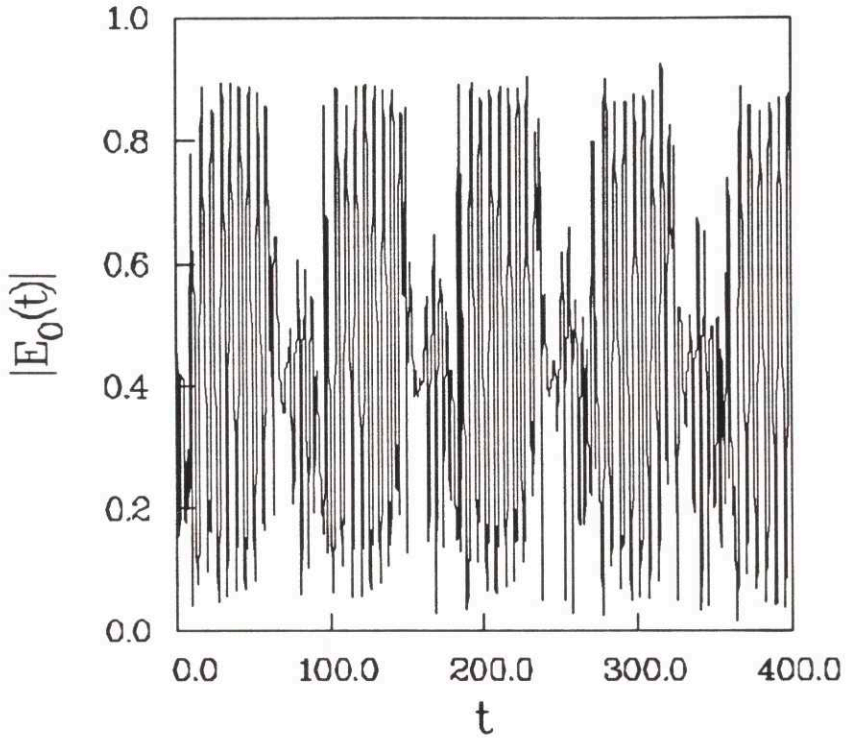


Figure 5-19: Power spectrum for the chaotic orbit (1,2) of the pump.

1991). Future experiments using a second laser at very low powers to seed the Stokes wave may be employed to reduce the effects of noise. The temperature of the optical fiber could also be lowered. The frequencies could be scanned to search for acoustic modes that would lead to dephased SBS. The power of the lasers and length of the fiber could then be varied to search for chaotic behaviour.

As the equations stand, the results are very difficult to interpret. Even the linear stability analysis is difficult. However the phase twist hypothesis (Fig. 5-4) seems to work. This fact along with the existence of a relatively well defined bifurcation sequence to chaos is an indication that there may be a reduced ODE description for the dynamics. This has been accomplished with other systems (mostly fluid convection) with a variety of methods (Malkus and Veronis, 1958; Lorenz, 1963; Guckenheimer and Knobloch, 1983; Coulet and Spiegel, 1983; Rucklidge, 1991). A typical method is a Galerkin truncation procedure. The Lorenz (1963) equations for instance are a set of third order ODE's for Rayleigh-Bénard convection derived this way. However

(a)



(b)

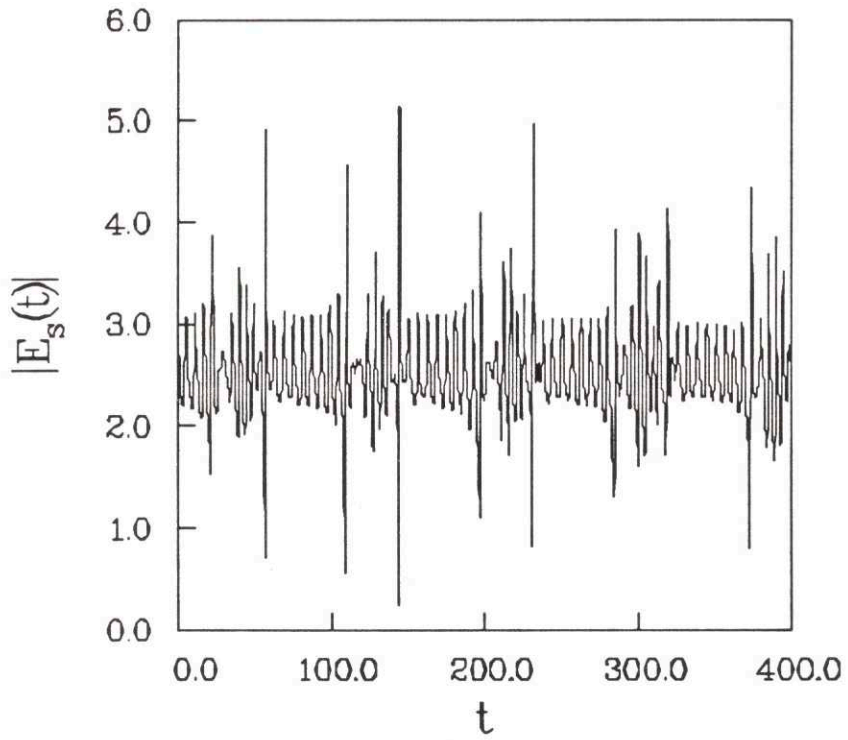


Figure 5-20: Time series at (1.1,2.6) for (a) pump and (b) Stokes wave.

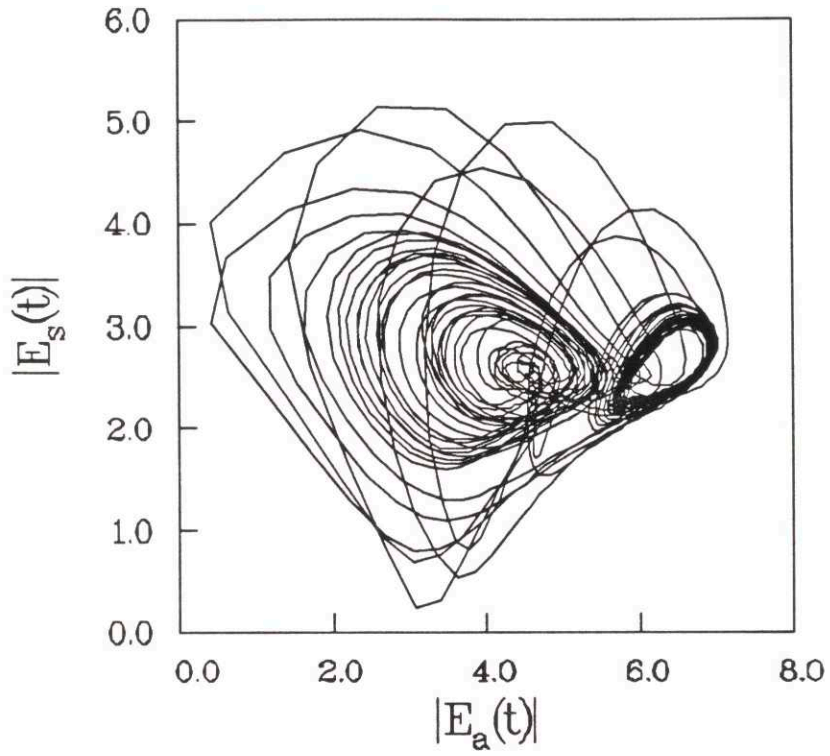


Figure 5-21: Phase portrait at (1.1,2.6).

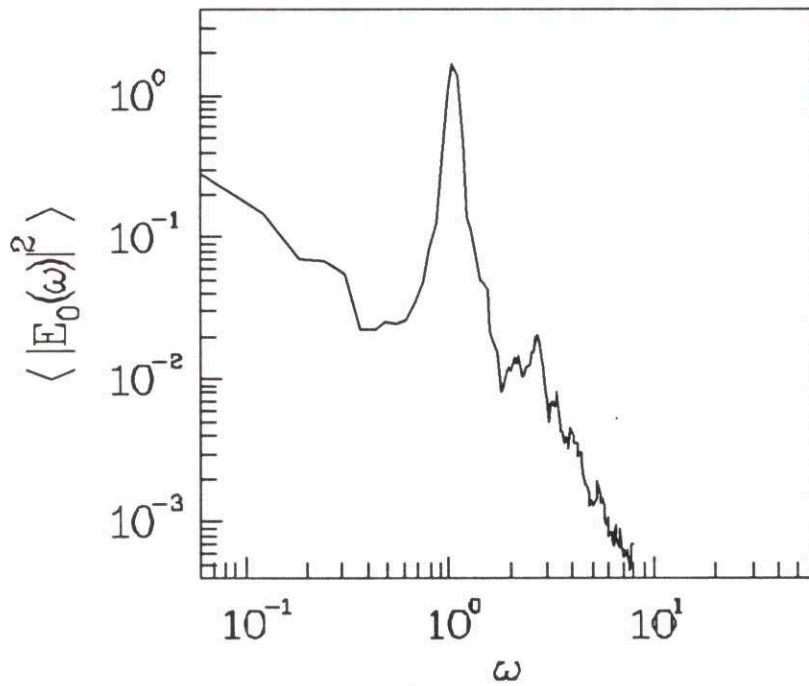


Figure 5-22: Power spectrum of the pump at (1.1,2.6).

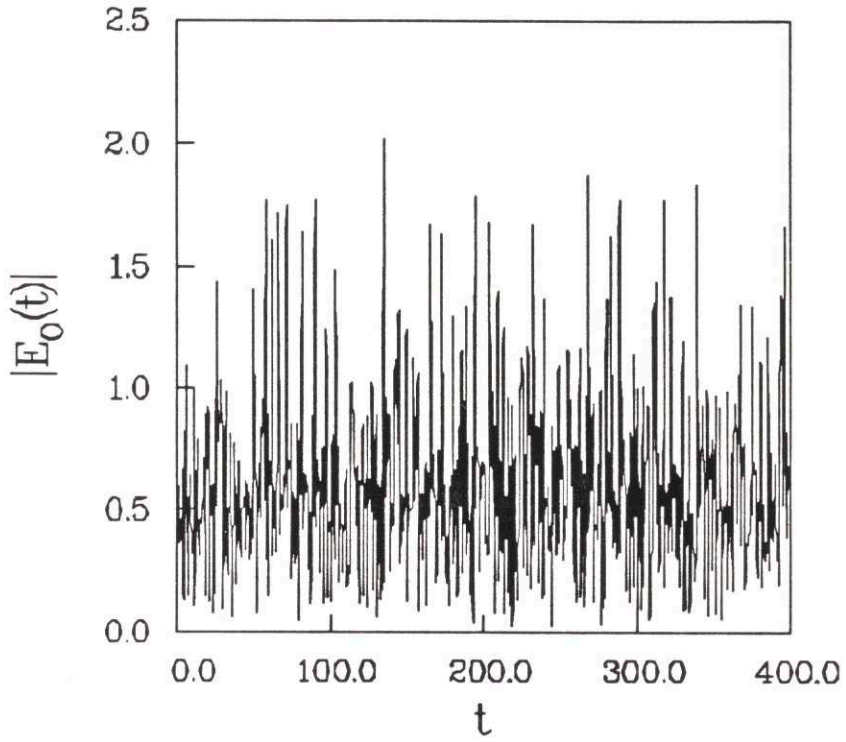


Figure 5-23: Time series of pump at (1,5).

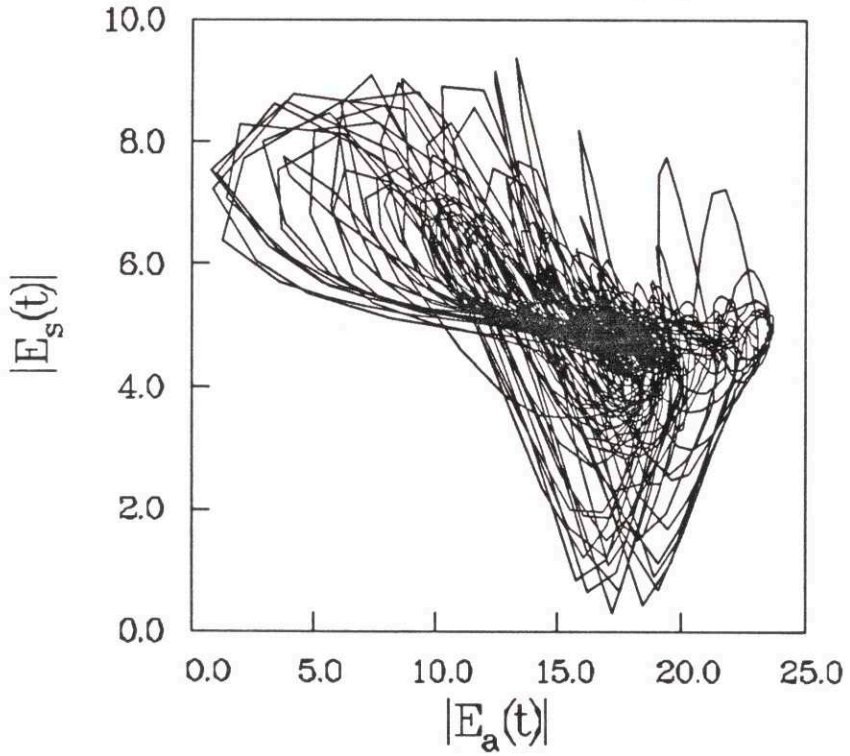


Figure 5-24: Phase Portrait at (1,5).

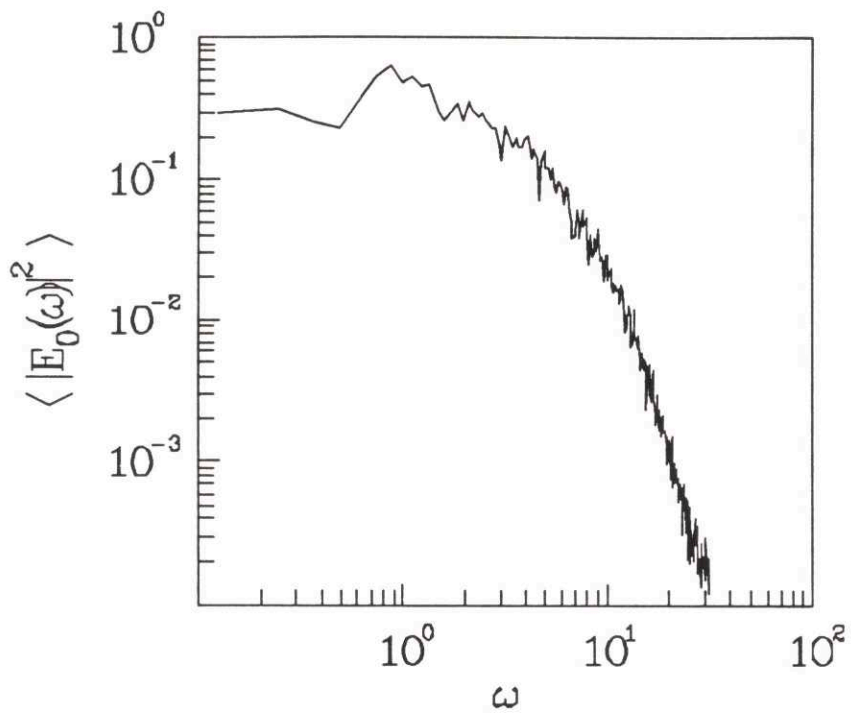


Figure 5-25: Power spectrum of the pump at (1,5).

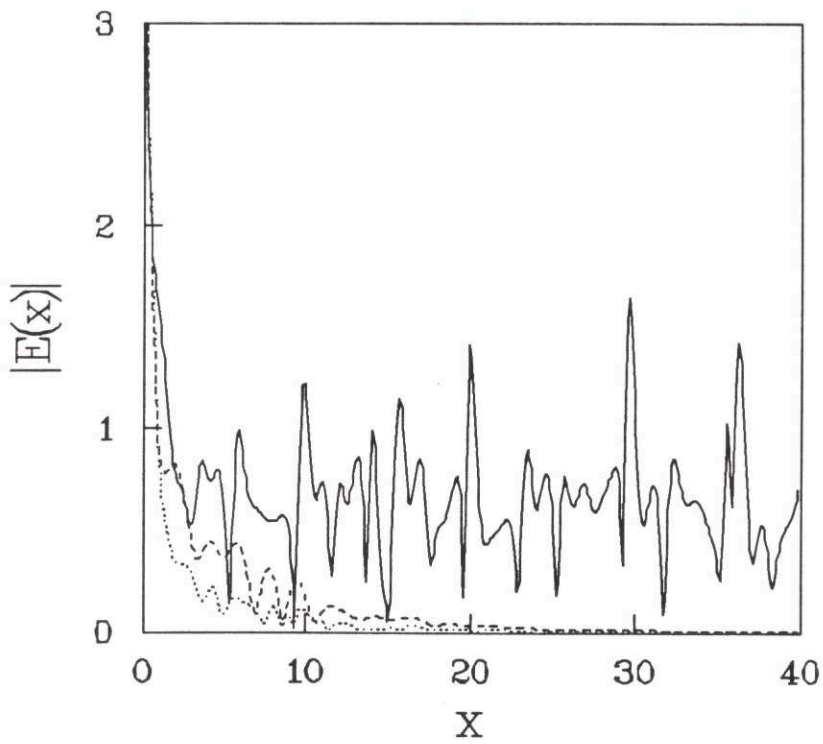


Figure 5-26: Spatial profile at (1,5).

it has been shown that the chaotic solutions of the Lorenz equations do not actually appear when more modes are kept (Curry *et al.* 1984) or when the full PDE's are simulated (Moore and Weiss, 1973). Care must be taken that the reduced equations are asymptotically exact descriptions (Rucklidge, 1991). The difficulty of the model considered here is that the boundary conditions impose an inhomogeneous fixed state. The linear equations must be solved numerically to obtain the eigenvalues. Simple expansions in a harmonic series do not satisfy the boundary conditions. Thus, some nontrivial mode expansion is likely to be required. Hopefully, in the future this can be done and the bifurcation diagram can be unravelled.

Chapter 6

Conclusions

In this dissertation I have considered three models of the nonintegrable three wave interaction. The intent was to study their spatiotemporal dynamic behaviour and in particular spatiotemporal chaos. Two of the models exhibited STC. Both involve the nonlinear saturation of a linearly unstable high-frequency wave by coupling to two damped low-frequency waves. They were distinguished by the relative order of the group velocities. The third model, applicable to stimulated Brillouin scattering in a finite medium exhibited low dimensional chaos. In the models that had STC, the correlation function was measured and showed definite length and time scales. The chaos arose from the interaction of these coherent structures. The conservative 3WI is integrable by IST. The existence of analytical nonlinear solutions was paramount to elucidating the dynamics. By means of perturbation expansions around the IST solutions, and guidance from the numerical results, it was possible to provide approximate analytical expressions for the essential scales of the dynamics.

Hohenberg and Shraiman (1989) have presented an exposition of STC using the Kuramoto-Sivashinsky (KS) equation as a paradigm. In that case a well defined correlation length exists, and the manifested chaos arises from the interaction of the coherent structures. Hohenberg and Shraiman (1989) addressed the issue of whether a statistical description borrowed from linear response theory is appropriate for describing STC. One postulate is that the Fourier transformed field fluctuations obey a Gaussian distribution. It appears that this is observed in the KS equation. Gaus-

sian distributions have been observed experimentally as well (Ciliberto and Caponeri, 1990; Arecchi et al., 1990). Other work on spatiotemporal chaos (see Goldstein *et al.*, 1991) have concentrated on the transition of regular spatial patterns to chaotic spatial states. Perturbed integrable systems such as the nonlinear Schrödinger and sine Gordon equations have also been investigated and will be reviewed by McLaughlin (1992). Chaotic Rayleigh-Bénard convection in one and two dimensions have also been studied intensively (see Greenside *et al.*, 1988; Ciliberto and Caponeri, 1990) along with other systems cited in Chapter 1. The body of work on STC continues to grow.

In this dissertation, I have shown that STC is exhibited by the simplest nonlinear interaction of three waves when the highest frequency wave is linearly unstable and the other two waves are linearly damped. The STC is associated with the slowly-varying spacetime amplitudes of these waves. I have characterized STC in the nonintegrable 3WI and found that it to be a very rich system. As shown in Section 2.1, the 3WI is a set of amplitude equations akin to the nonlinear Schrödinger and Ginzburg-Landau equations (see Newell, 1988). A study of the 3WI could have been approached from various directions. I chose to look at the large system dynamics and try to understand the length and time scales that arise in STC. However, important questions remain unresolved and could be the subject of future work. Most of the statistical issues addressed by Hohenberg and Shraiman (1989) have not been dealt with in this dissertation. That would constitute the next phase in the study of the 3WI. The precise mechanisms for STC are only understood at a rudimentary level. Studying smaller systems may shed some light onto that area. When the correlation length approaches the system size a transition to low dimensional dynamics would presumably occur. This needs to be investigated. The existence of nonlinear solutions to perturb around made it possible to estimate for the nearly integrable regime the average saturation amplitudes. In other systems without nonlinear solutions to perturb around this would be more difficult. For example, this has not been done in the KS equation.

There are other topics to study that follow naturally from this work that were mentioned in the conclusions of each chapter. In addition, other general issues remain.

Given that the 3WI is the lowest order nonlinear, nondispersive effect of a generalized amplitude expansion the effect of the terms ignored in the equations I studied comes into question. If the saturated amplitudes are fairly large, the self-modal interaction may become significant. On longer time scales the dispersion that was ignored could also play a role. The Ginzburg-Landau equation that ignores three wave coupling has a whole host of interesting behaviour. A combination of the the two systems awaits investigation.

The model of stimulated Brillouin scattering (SBS) in a finite medium presented in Chapter 5, is the simplest model that exhibits chaos for the given boundary conditions. Nonstationary SBS remains a subject of active research. This effect could be very important to optical fiber communication. The results of recent experiments may be due to amplified noise (Gaeta and Boyd, 1991), yet this is not to discount the possibility of chaos in future experiments. I have demonstrated that a small amount of frequency dephasing is all that is necessary for nonstationary and chaotic behaviour. The dynamics are fairly complicated but low dimensional and it maybe possible to have a reduced ODE description that would be very useful in untangling the behaviour. This may require novel mathematical techniques because the boundary conditions impose an inhomogeneous fixed state. Defects and inhomogeneity in the fiber may also produce interesting spatiotemporal effects.

This dissertation is not an end but rather a beginning. It introduces the 3WI as a paradigm for STC. On a grander level, it is part of an effort to understand nonlinear, nonintegrable behaviour in general. Perhaps, by comprehending simple systems such as the 3WI a step closer to unlocking some of nature's secrets has been made.

Appendix A

The Zakharov-Manakov Scattering Problem

In this appendix, the IST equations for the 3WI will be stated to introduce terminology and notation to be used in the text. All of what is presented in this section follows Kaup (1976a) and Kaup *et al.* (1979).

For conservative couplings the magnitude of the coupling coefficient can be scaled away by a simple transformation $Q_l = |\theta_l| a_l$. The conservative 3WI Eqs. (2.11)-(2.13) then take the form

$$Q_{1t} + c_1 Q_{1x} = \gamma_1 Q_2^* Q_3^*, \quad (\text{A.1})$$

$$Q_{2t} + c_2 Q_{2x} = \gamma_2 Q_1^* Q_3^*, \quad (\text{A.2})$$

$$Q_{3t} + c_3 Q_{3x} = \gamma_3 Q_1^* Q_2^*, \quad (\text{A.3})$$

where $Q_l(x, t)$ are the slowly varying amplitudes, c_i are the corresponding group velocities satisfying

$$c_1 < c_2 < c_3, \quad (\text{A.4})$$

and γ_i are the phases of the coupling coefficients given by

$$\gamma_i = \text{sign}(w_i \times \omega_i), \quad (\text{A.5})$$

where w_i is the energy of the i th wave, and ω are the resonant frequencies, whose

relative signs are determined from

$$\omega_1 + \omega_2 + \omega_3 = 0. \quad (\text{A.6})$$

The appropriate scattering problem for the 3WI is the Zakharov-Manakov (ZM) scattering problem (Zakharov and Manakov, 1973; Kaup, 1976a) given by

$$-iv_{1x} + V_{12}v_2 + V_{13}v_3 = -c_1\zeta v_1, \quad (\text{A.7})$$

$$-iv_{2x} + V_{21}v_1 + V_{23}v_3 = -c_2\zeta v_2, \quad (\text{A.8})$$

$$-iv_{3x} + V_{31}v_1 + V_{32}v_2 = -c_3\zeta v_3, \quad (\text{A.9})$$

where V_{ij} are the potentials and are given by

$$V_{23} = \frac{-iQ_1}{\sqrt{(c_2 - c_1)(c_3 - c_1)}}, \quad V_{32} = -\gamma_3\gamma_2V_{23}^*, \quad (\text{A.10})$$

$$V_{31} = \frac{-iQ_2}{\sqrt{(c_2 - c_1)(c_3 - c_2)}}, \quad V_{13} = \gamma_1\gamma_3V_{31}^*, \quad (\text{A.11})$$

$$V_{12} = \frac{-iQ_3}{\sqrt{(c_3 - c_1)(c_3 - c_2)}}, \quad V_{21} = -\gamma_1\gamma_2V_{12}^*. \quad (\text{A.12})$$

For $V_{ij} \rightarrow 0$ sufficiently rapidly as $|x| \rightarrow \infty$ and for real ζ , two sets of linearly independent eigenfunctions of Eqs. (A.7)-(A.9), $\Phi^{(n)}$ and $\Psi^{(n)}$ can be defined with the following boundary conditions

$$\Phi_j^{(n)} \sim \delta_j^n e^{-ic_j\zeta x} \quad \text{as } x \rightarrow -\infty, \quad (\text{A.13})$$

$$\Psi_j^{(n)} \sim \delta_j^n e^{-ic_j\zeta x} \quad \text{as } x \rightarrow \infty, \quad (\text{A.14})$$

where $n = 1, 2, 3$ denotes the n th eigenfunction and $j = 1, 2, 3$ denotes the j th component. These two sets are then 'connected' through the relation

$$\Phi^{(m)} = \sum_{n=1}^3 [a_{mn}](\zeta) \Psi^{(n)}, \quad (\text{A.15})$$

defining the scattering matrix

$$S(\zeta) = [a_{mn}(\zeta)], \quad (\text{A.16})$$

the elements of which are referred to as scattering data.

The potentials Q_1, Q_2, Q_3 have been mapped into the scattering data S . In the linear limit of Eqs (A.1)-(A.3) for infinitesimal potentials the diagonal elements of S are unity and the off-diagonal elements are the Fourier transforms of these potentials. For the nonlinear situation such a simple relation no longer exists between the potentials and the scattering data. However given S the potentials can be reconstructed uniquely. The time dependence of S is exactly the same as the linear limit and is given by

$$a_{mn}(\zeta, t) = a_{mn}(\zeta, 0) \exp \left[i\zeta t c_1 c_2 c_3 \left(\frac{1}{c_m} - \frac{1}{c_n} \right) \right]. \quad (\text{A.17})$$

Given any initial condition going to zero sufficiently fast for $|x| \rightarrow \infty$, the scattering data $S(\zeta, 0)$ are obtained, evolved in time with (A.17), then inverse transformed to obtain the time evolved potentials.

The actual inverse scattering procedure for the ZM scattering problem is very involved and detailed in (Kaup, 1976a). However for most purposes a simplification is possible. Whenever the three envelopes are separated, the scattering data for the ZM problem can be given in terms of the simpler second order Zakharov-Shabat scattering problem (Zakharov and Shabat, 1973). Consider Eqs. (A.7)-(A.9) in a region of space where Q_1 and Q_2 are zero, but Q_3 is nonzero. Then by Eqs. (A.10)-(A.12), the only nonzero potentials in this region are V_{12} and V_{21} . The ZM system decouples into a trivial equation for v_3 and a second scattering problem for v_1 and v_2 which can be transformed into the ZS problem (see Appendix B) by appropriate rescaling. Similarly this applies for the region where Q_1 and Q_2 are nonzero. For each envelope,

$$q^{(1)} = \frac{-\gamma_2 \gamma_3 Q_1^*}{\sqrt{(c_2 - c_1)(c_3 - c_1)}}, r^{(1)} = \gamma_2 \gamma_3 q^{(1)*}, \quad (\text{A.18})$$

$$\lambda^{(1)} = \zeta(c_3 - c_2)/2, \quad (\text{A.19})$$

$$q^{(2)} = \frac{-Q_2}{\sqrt{(c_2 - c_1)(c_3 - c_2)}}, r^{(2)} = -\gamma_1 \gamma_3 q^{(2)*}, \quad (\text{A.20})$$

$$\lambda^{(2)} = \zeta(c_3 - c_1)/2, \quad (\text{A.21})$$

$$q^{(3)} = \frac{-\gamma_1 \gamma_2 Q_3^*}{\sqrt{(c_3 - c_1)(c_3 - c_2)}}, r^{(3)} = \gamma_1 \gamma_2 q^{(3)*}, \quad (\text{A.22})$$

$$\lambda^{(3)} = \zeta(c_2 - c_1)/2, \quad (\text{A.23})$$

where $q^{(n)}$, $r^{(n)}$ and $\lambda^{(n)}$ are the corresponding ZS potentials and eigenvalue for the n th envelope. If the three envelopes are separated than the scattering matrix S can be factored in terms of the scattering matrices of the three ZS eigenvalue problems. For instance if at some time the envelopes have negligible overlap and are arranged with the i th envelope to the right of the j th which is to the right of the k th then S may be factored as

$$S = S^{(i)}S^{(j)}S^{(k)}, \quad (i, j, k = 1, 2, \text{ or } 3), \quad (\text{A.24})$$

For situations where the three envelopes are initially well separated and again at a later time after interacting, the ZM problem need never be used. The final ZS scattering data can be expressed directly in terms of the initial ZS scattering data.

If at $t = 0$ the envelopes are ordered (3,2,1) from left to right then

$$S = S_0^{(3)}S_0^{(2)}S_0^{(1)}, \quad (\text{A.25})$$

where the zero subscript denotes initial value. Since the time evolution of the scattering data is given by Eq. (A.17) this determines S for all times. If the envelopes separate as $t \rightarrow \infty$ then

$$S = S_f^{(1)}S_f^{(2)}S_f^{(3)}. \quad (\text{A.26})$$

Setting the expressions for S equal gives

$$\frac{b_f^{(3)}}{a_f^{(3)}} = \frac{a_0^{(1)}b_0^{(3)} + a_0^{(3)}b_0^{(2)}\bar{b}_0^{(1)}}{a_0^{(2)}a_0^{(3)}}, \quad (\text{A.27})$$

$$\frac{b_f^{(2)}}{a_f^{(2)}} = \frac{a_f^{(3)}}{a_0^{(2)}a_0^{(3)}}[a_0^{(3)}b_0^{(2)}\bar{a}_0^{(1)} - b_0^{(1)}b_0^{(3)}], \quad (\text{A.28})$$

$$\frac{b_f^{(1)}}{a_f^{(1)}} = \frac{a_f^{(2)}}{a_0^{(1)}a_0^{(2)}}[\bar{a}_f^{(3)}a_0^{(2)}b_0^{(1)} + \bar{b}_f^{(3)}b_0^{(2)}]. \quad (\text{A.29})$$

Equations (A.27)-(A.29) contain all the information about the exchange of solitons and radiation density. The bound-state eigenvalues are given by the poles of $b(\lambda)/a(\lambda)$ (zeros of $a(\lambda)$) for λ in the upper half plane. From Eq. (A.27) it is seen that zeros $a_0^{(2)}$ and $a_0^{(3)}$ become zeros of $a_f^{(3)}$. It then follows from Eq. (A.28) that $a_f^{(2)}$ has no zeros. Also from Eq. (A.29) zeros of $a_0^{(1)}$ and $a_0^{(2)}$ become zeros of $a_f^{(1)}$. Thus solitons

are never lost from the slow and fast envelopes. The middle envelope always loses its solitons, giving solitons to both the slow and fast envelopes. In the stimulated backscatter case, the middle envelope can never contain solitons (see Appendix B), so this exchange will never occur.

Appendix B

The Zakharov-Shabat Scattering Problem

A complete discussion of the Zakharov-Shabat scattering problem is given in Ablowitz *et al.* (1974), as well as the many texts mentioned in Chap 3. The ZS equation is

$$v_{1x} + i\lambda v_1 = qv_2, \quad (\text{B.1})$$

$$v_{2x} - i\lambda v_2 = rv_1, \quad (\text{B.2})$$

where

$$v = \begin{bmatrix} v_1 \\ v_2 \end{bmatrix}, \quad (\text{B.3})$$

is the eigenvector, λ is the eigenvalue, and q and r are the potentials. The potentials are assumed to vanish rapidly as $|x| \rightarrow \infty$ and satisfy the condition

$$\int_{-\infty}^{\infty} [|q| + |r|] dx < \infty. \quad (\text{B.4})$$

With this in mind, define eigenfunctions $\phi, \bar{\phi}$, with the following boundary conditions

$$\phi \rightarrow \begin{bmatrix} 1 \\ 0 \end{bmatrix} e^{-i\lambda x} \text{ as } x \rightarrow -\infty, \quad \phi \rightarrow \begin{bmatrix} a(\lambda)e^{-i\lambda x} \\ b(\lambda)e^{+i\lambda x} \end{bmatrix} \text{ as } x \rightarrow +\infty, \quad (\text{B.5})$$

and

$$\bar{\phi} \rightarrow \begin{bmatrix} 0 \\ -1 \end{bmatrix} e^{-i\lambda x} \text{ as } x \rightarrow -\infty, \quad \bar{\phi} \rightarrow \begin{bmatrix} \bar{b}(\lambda)e^{-i\lambda x} \\ -\bar{a}(\lambda)e^{+i\lambda x} \end{bmatrix} \text{ as } x \rightarrow +\infty. \quad (\text{B.6})$$

The scattering matrix is usually defined as

$$S = \begin{pmatrix} a & b \\ \bar{b} & -\bar{a} \end{pmatrix}. \quad (\text{B.7})$$

For the continuous part of the eigenvalue spectrum the important quantity is the ‘reflection coefficient’

$$\rho(\lambda) = \frac{b(\lambda)}{a(\lambda)}. \quad (\text{B.8})$$

The soliton part of the spectrum is determined by the zeros of $a(\lambda)$ in the upper half λ -plane. These correspond to discrete eigenvalues (bound states). The zeros are designated by $\{\lambda_k\}_{k=1}^N$, where N is finite. At an eigenvalue

$$\phi(\lambda_k, x) \rightarrow \begin{bmatrix} 0 \\ b_k e^{i\lambda_k x} \end{bmatrix} \text{ as } x \rightarrow \infty, \quad (\text{B.9})$$

and when $b(\lambda)$ can be analytically continued into the upper half λ -plane,

$$b_k = b(\lambda_k). \quad (\text{B.10})$$

Define also the residue at the eigenvalue

$$D_k = -i \frac{b_k}{a'_k}, \quad (\text{B.11})$$

where

$$a'_k = \left. \frac{\partial a(\lambda)}{\partial \lambda} \right|_{\lambda=\lambda_k}. \quad (\text{B.12})$$

The pair $[\lambda_k, D_k]$ corresponds to one soliton, where the imaginary part of λ_k determines the amplitude and width, the real part of λ_k determines the spatial phase modulation, and D_k determines its initial position and phase.

For the 3WI, only cases where

$$r = \pm q^*, \quad (\text{B.13})$$

are involved. For this situation

$$\bar{a}(\lambda) = [a(\lambda^*)]^*, \quad (\text{B.14})$$

$$\bar{b}(\lambda) = \mp [b(\lambda^*)]^*. \quad (\text{B.15})$$

For $q = +r$ and Eq. (B.4) the ZS problem is self-adjoint and so the eigenvalues are real and no bound states can occur. For $q = -r$ bound states and hence solitons can occur. Whenever q is real the spectrum is further restricted. Eqs. (B.14) and (B.15) imply

$$a(-\lambda^*) = a^*(\lambda), \quad (\text{B.16})$$

$$b(-\lambda^*) = b^*(\lambda). \quad (\text{B.17})$$

When q is a square pulse, analytic solutions can be given for a and b . Take $q = Q$ when $l_- < x < l_+$, and zero elsewhere. For $r = \pm q^*$, Eqs. (B.1) and (B.2) can be solved exactly to yield

$$a(\lambda) = \frac{1}{2} \exp(i\lambda L) \left[\left(1 - \frac{\lambda}{\Delta}\right) \exp(i\lambda L) + \left(1 + \frac{\lambda}{\Delta}\right) \exp(-i\Delta L) \right], \quad (\text{B.18})$$

$$b(\lambda) = \mp \frac{Q}{2i\Delta} [\exp(i\Delta L) - \exp(-i\Delta L)] \exp[-i\lambda(l_+ + l_-)], \quad (\text{B.19})$$

where $L = l_+ - l_-$ and $\Delta = [\lambda^2 + Q^2]^{1/2}$.

Appendix C

Numerical Methods

The numerical method is based on the one used by Reiman and Bers (1975) to integrate the conservative 3WI. Each envelope is transformed to its characteristic frame by substituting $b_i(\mathbf{x}, t) = a_i(\mathbf{x} + \mathbf{v}_i t, t)$. The SDI and LDI simulations used the same code. Recall that the relevant equations were already transformed to the frame of the high frequency waves. Each wave was put on a grid that moved along the characteristics. The grid spacing $\mathbf{x}_p - \mathbf{x}_{p-1} = h$ was fixed and chosen so as to resolve the smallest dynamical structures that may arise. The diffusion term in the high frequency wave Eq. (3.1) was finite differenced by a five point scheme. The resulting equations were then

$$\begin{aligned} b_{i,t}(\mathbf{x}_l, t) &= -b_j(\mathbf{x}_m - \mathbf{v}_j t, t) b_k(\mathbf{x}_n - \mathbf{v}_k t, t) + \gamma_i b_i(\mathbf{x}_l, t), \\ &+ \frac{D}{12h^2} [(-b_i(\mathbf{x}_{l+2}, t) + 16b_i(\mathbf{x}_{l+1}, t) \\ &- 30b_i(\mathbf{x}_l, t) + 16b_i(\mathbf{x}_{l-1}, t) - b_i(\mathbf{x}_{l-2}, t))], \end{aligned} \quad (\text{C.1})$$

$$b_{j,t}(\mathbf{x}_m, t) = b_i(\mathbf{x}_l + \mathbf{v}_j t, t) b_k^*(\mathbf{x}_n + (\mathbf{v}_j - \mathbf{v}_k)t, t) - b_j(\mathbf{x}_m, t), \quad (\text{C.2})$$

$$b_{k,t}(\mathbf{x}_n, t) = b_i(\mathbf{x}_l + \mathbf{v}_k t, t) b_j^*(\mathbf{x}_m + (\mathbf{v}_k - \mathbf{v}_j)t, t) - b_k(\mathbf{x}_n, t). \quad (\text{C.3})$$

In the SDI case $\mathbf{v}_k = -\mathbf{v}_j = 1$; in the LDI case $\mathbf{v}_k = -2$, $\mathbf{v}_j = -1$. The \mathbf{x} coordinates of the nonlinear terms on the right hand sides often will not fall on the grid. A four point polynomial interpolation formula was used to calculate the amplitudes on the grid points. The time evolution was calculated using the IMSL, ODE solver DVERK,

which employs the Runge-Kutta-Verner fifth and sixth order method. All calculations were performed on a CRAY 2 at the National Energy Research Supercomputing Center. This numerical method is very stable.

At specified time intervals the entire grid would be recorded. The integrated energy was also calculated using Simpson's rule and recorded. They were then used with the conservation equations (3.2.3) where the derivatives were evaluated with a simple two point difference method to check for accuracy. The grids were made periodic. To simplify the computations only real envelopes were evolved. It can be shown that for real initial conditions the envelopes remain real for all time (Kaup, Reiman and Bers, 1979). Comparisons between complex and real initial conditions did not show any noticeable behaviour in the dynamics.

The correlation function was computed from the recorded spacetime data. The discrete correlation function was calculated and averaged over several time parcels with

$$S_l(x_m, t_n) = \frac{1}{NM} \sum_{i=1}^{M-1} \sum_{j=1}^{N-1} a(x_{m+i}, t_{n+j})a(x_i, t_j), \quad (\text{C.4})$$

where M is the number of grid points and N is the number of time slices for the correlation function. This double sum is evaluated for each grid point and for all of the time slices in the simulation. In a typical run, the simulation run was twenty to thirty times longer than the correlation function time corresponding to N . The correlation function was Fourier transformed along the x and t axes to obtain the spectra.

The SBS simulation used a similar code. However complex envelopes were required. Again each wave was transformed to its characteristic and placed on its own grid. The boundary conditions were different. The pump wave had a left boundary condition and the Stokes had a right boundary condition. In the characteristic frame this implied the boundary conditions were propagating.

Bibliography

- [1] M. J. Ablowitz, D. J. Kaup, A. C. Newell and H. Segur, 1974, *Stud. Appl. Math.* **53**, 249.
- [2] M. J. Ablowitz and H. Segur, 1981, *Solitons and the Inverse Scattering Transform* (SIAM, Philadelphia).
- [3] G. Ahlers and R. P. Behringer, 1978, *Prog. Theor. Phys., Suppl.* **64**, 186.
- [4] S. A. Akhmanov and R. V. Khokhlov, 1972, *Problems of Nonlinear Optics* (Gordon and Breach, New York).
- [5] F. T. Arecchi, G. Giacomelli, P. L. Ramazza, and S. Residori, 1990, *Phys. Rev. Lett.* **65**, 2531.
- [6] V. I. Arnol'd and A. Avez, 1968, *Ergodic Problems of Classical Mechanics* (Benjamin, New York).
- [7] I. Bar-Joseph, A. A. Friesem, E. Lichtman, and R.G. Waarts, 1985, *J. Opt. Soc. Am. B* **2**, 1606.
- [8] D. J. Benney, 1962, *J. Fluid Mech.*, **14**, 577.
- [9] D. J. Benney and A. C. Newell, 1967, *J. Math. Phys.* **46**, 133.
- [10] P. Bergé, 1979 in *Dynamical Critical Phenomena and Related Topics, Lecture Notes in Physics 104*, edited by C. P. Enz (Springer-Verlag, Heidelberg) p. 288.
- [11] P. Bergé, Y. Pomeau, C. Vidal, 1984, *Order within Chaos* (Hermann, Paris).

- [12] A. Bers, 1975 in *Plasma Physics-Les Houches 1972*, edited by C. De Witt and J. Peyraud (Gordon and Breach, New York).
- [13] A. Bers, 1983 in *Handbook of Plasma Physics*, edited by M. N. Rosenbluth and R. Z. Sagdeev (North Holland, Amsterdam), Vol . 1, Chap. 3.2.
- [14] A. Bers and A. Reiman, 1975, in *Proceedings of the Seventh Conference on Numerical Simulation of Plasmas*, Courant Institute, N.Y.U., June 1975, p. 192.
- [15] A. Bers, D. J. Kaup and A. H. Reiman, 1976, *Phys. Rev. Lett.* **37**, 182.
- [16] A. R. Bishop and P. S. Lomdahl, 1986, *Physica* **18D** , 54.
- [17] R. Blaha, E. W. Laedke, A. M. Rubenchik, and K. H. Spatschek, 1988, *Europhys. Lett.* **7**, 237.
- [18] N. Bloembergen, 1965, *Nonlinear Optics* (Benjamin, New York).
- [19] J. Botineau, C. Leycuras, C. Montes, and E Picholle, 1989, *J. Opt. Soc. Am. B* **6**, 300.
- [20] G. Bonnaud, D. Pesme, and R. Pellat, 1990, *Phys. Fluids B* **2**, 1618.
- [21] M. N. Bussac, 1982, *Phys. Rev. Lett.* **49**, 1939.
- [22] D. K. Campbell, 1987, *Nonlinear Science – From Paradigms to Practicalities* in Los Alamos Science, No. 15, Special Issue on Stanislaw Ulam, edited by Necia Grant Cooper.
- [23] S. Ciliberto and M. Caponeri, 1990, *Phys. Rev. Lett.* **64**, 2775.
- [24] H. Chaté and P. Manneville, 1987, *Phys. Rev. Lett.* **58**, 112.
- [25] C. C. Chow, A. Bers and A. K. Ram, 1991a, in *Research Trends in Physics: Chaotic Dynamics and Transport in Fluids and Plasmas* edited by I. Prigogine, *et al.*, to be published by AIP, 1992.
- [26] C. C. Chow, A. Bers and A. K. Ram, 1991b, submitted to *Phys. Rev. Lett.*

- [27] B. Coppi, M. N. Rosenbluth, and R. N. Sudan, 1969, *Ann. Phys. (N.Y.)* **55**, 207.
- [28] J. Coste and C. Montes, 1986, *Phys. Rev. A* **34**, 3940.
- [29] D. Cotter, 1983, *J. Opt. Commun.* **4**, 10.
- [30] D. Cotter, 1987, *Opt. Quantum Electron.* **19**, 1.
- [31] P. H. Coullet and E. A. Spiegel, 1983, *SIAM J. Appl. Math.* **43**, 776.
- [32] P. Coullet, C. Elphick, and D. Repaux, 1987, *Phys. Rev. Lett.* **58**, 431.
- [33] P. Coullet and G. Iooss, 1990, *Phys. Rev. Lett.* **64**, 866.
- [34] J. H. Curry, J. R. Herring, J. Loncarie and S. A. Orzag, 1984, *J. Fluid Mech.* **146**, 1.
- [35] R. C. Davidson, 1972, *Methods in Nonlinear Plasma Theory* (Academic, New York).
- [36] R. L. Devaney, 1989, *An Introduction to Chaotic Dynamical Systems* (Addison-Wesley, Reading, Massachusetts).
- [37] R. K. Dodd, J. C. Eilbeck, J. D. Gibbon, H. C. Morris, 1982, *Solitons and Nonlinear Wave Equations* (Academic Press, New York).
- [38] R. P. Drake and S. H. Batha, 1991, *Phys. Fluids B* **3**, 2936.
- [39] P. G. Drazin and R. S. Johnson, 1989, *Solitons: an introduction* (Cambridge University Press, New York).
- [40] D. F. DuBois, H. A. Rose, and D. Russell, 1991, *Phys. Rev. Lett.* **66**, 1970.
- [41] A. I. D'yachenko, V. E. Zakharov, A. N. Pushkarev, V. F. Shvets, and V. V. Yan'kov, 1989, *Zh. Eksp. Teor. Fiz.* **96**, 2026 [*Sov. Phys. JETP* **69**, 1144 (1989)].
- [42] W. Eckhaus and A. Van Harten, 1981, *The Inverse Scattering Transformation and the Theory of Solitons: an introduction* (North-Holland, New York).

- [43] A. B. Ezerskii, M. I. Rabinovich, V. P. Reutov, and I. M. Starobinets, 1986, Zh. Eksp. Teor. Fiz. **91**, 2070 [Sov. Phys. JETP **64**, 1228 (1986)].
- [44] D. Forster, 1975, *Hydrodynamic Fluctuations, Broken Symmetry and Correlation Functions* (Benjamin, New York).
- [45] A. L. Gaeta, 1991, Private Communication.
- [46] A. L. Gaeta, M. D. Skeldon, R. W. Boyd, P. Narum, 1989, J. Opt. Soc. Am. B **6**, 1709.
- [47] A. L. Gaeta and R. W. Boyd, 1991, Phys. Rev. A **44**, 3205.
- [48] G. Gamow, 1967, *One, Two, Three, Infinity* (Bantam Books, New York).
- [49] C. S. Gardner, J. M. Greene, M. D. Kruskal and R. M. Miura, 1967, Phys. Rev. Lett. **19**, 1095.
- [50] M. V. Goldman, 1986, Physica **18D**, 67.
- [51] R. E. Goldstein, G. H. Gunaratne, L. Gil, and P. Couillet, 1991, Phys. Rev. A **43**, 6700.
- [52] H. S. Greenside, M. C. Cross, and W. M. Coughran, Jr., 1988, Phys. Rev. Lett. **60**, 2269.
- [53] J. Guckenheimer and E. Knobloch, 1983, Geophys. Astrophys. Fluid Dynamics **23**, 247.
- [54] J. Guckenheimer and P. Holmes, 1986, *Nonlinear Oscillators, Dynamical Systems and Bifurcations of Vector Fields* (Springer-Verlag, New York).
- [55] R. G. Harrison, J. S. Uppal, A. Johnstone, and J. V. Moloney, 1990, Phys. Rev. Lett. **65**, 167.
- [56] J. A. Heikkinen and S. J. Karttunen, 1986, Phys. Fluids **29**, 1291.

- [57] J. R. Herring and R. H. Kraichnan, 1972, in *Statistical Models and Turbulence* edited by M. Rosenblatt and C. van Atta (Springer-Verlag, New York), p. 148.
- [58] P. C. Hohenberg and B. I. Shraiman, 1989, *Physica D* **37**, 109.
- [59] S. Hüller, P. Mulser, A. M. Rubenchik, 1991, to appear in *Phys. Fluids. B*.
- [60] J. Hyman, B. Nicolaenko and S. Zaleski, 1986, *Physica D* **23**, 265.
- [61] W. Kaiser and M. Maier, 1972, in *Laser Handbook, Vol 2*, edited by F. T. Arecchi, S. Dubois (North-Holland, Amsterdam).
- [62] D. J. Kaup, 1976a, *Stud. Appl. Math.* **55**, 9.
- [63] D. J. Kaup, 1976b, *SIAM J. Appl. Math.*, **31**, 121.
- [64] D. J. Kaup, 1980, *Physica* **1D**, 45.
- [65] D. J. Kaup, 1990, *Phys. Rev. A*, **42**, 5689.
- [66] D. J. Kaup and A. C. Newell, 1978, *Proc. R. Soc. Lond. A.* **361**, 413.
- [67] D. J. Kaup, A. Reiman and A. Bers, 1979, *Rev. Mod. Phys.* **51**, 915 (1979) and references therein.
- [68] Y. S. Kivshar and B. A. Malomed, 1989, *Rev. Mod. Phys.* **61**, 763.
- [69] R.H. Kraichnan and S. Chen, 1989, *Physica D* **37**, 160.
- [70] N. M. Kroll, 1963, *Proc. IEEE* **51**, 110.
- [71] M. Kruskal, 1991, Private Communication.
- [72] Y. Kuramoto and T. Tsuzuki, 1976, *Prog. Theor. Phys., Suppl.* **64**, 346.
- [73] L. D. Landau, 1944, *Dok. Akad. Nauk. SSSR* **44**, 339.
- [74] L. D. Landau and E. M. Lifshitz, 1980, *Statistical Physics* (Pergamon, New York).

- [75] P. D. Lax, 1968, *Comm. Pure Appl. Math.*, **21**, 467.
- [76] T. Y. Li and J. A. Yorke, 1975, *Amer. Math. Monthly* **82**, 985.
- [77] A. J. Lichtenberg and M. A. Lieberman, 1982, *Regular and Stochastic Motion* (Springer-Verlag, Berlin).
- [78] C. S. Liu, M. N. Rosenbluth, and R. B. White, 1974, *Phys. Fluids* **17**, 1211.
- [79] E. N. Lorenz, 1963, *J. Atmos. Sci.* **20**, 130.
- [80] W. V. R. Malkus and G. Veronis, 1958, *J. Fluid Mech.* **58**, 289.
- [81] B. Mandelbrot, 1983, *The Fractal Geometry of Nature* (W.H. Freeman and Co., New York).
- [82] P. Manneville, 1981, *Phys. Lett. A* **84**, 129.
- [83] P. C. Martin, 1968, *Measurements and Correlation Functions* (Gordon and Breach, New York).
- [84] L. McGoldrick, 1965, *J. Fluid Mech.* **21**, 305.
- [85] D. W. McLaughlin, 1992, to be published.
- [86] C. Meunier, M. Bussac and G. Laval, 1982, *Physica* **4D**, 236.
- [87] H. T. Moon and M. V. Goldman, 1984, *Phys. Rev. Lett.* **53**, 1921.
- [88] D. R. Moore and N. O. Weiss, 1973, *J. Fluid Mech.* **58**, 289.
- [89] P. Narum, A. L. Gaeta, M. D. Skeldon, and R. W. Boyd, 1988, *J. Opt. Soc. Am. B* **5**, 623.
- [90] A. C. Newell, 1988, in *Propagation in Systems Far from Equilibrium*, edited by J. E. Wesfreid, H. R. Brand, P. Manneville, G. Albinet, and N. Boccara (Springer, Berlin), p. 122, and references therein.
- [91] E. A. Overman II, D. W. McLaughlin and A. R. Bishop, 1986 *Physica* **19D**, 1.

- [92] O. M. Phillips, 1960, *J. Fluid Mech.* **9**, 193.
- [93] H. Poincaré, 1952, *Science and Method* (Dover, New York).
- [94] Y. Pomeau, A. Pumir and P. Pelcé, 1984, *J. Stat. Phys.* **37**, 39.
- [95] A. Pumir, 1985, *J. Phys. (Paris)* **46**, 511.
- [96] C. J. Randall and J. R. Albritton, 1984, *Phys. Rev. Lett.*, **52**, 1887.
- [97] A. H. Reiman, 1977, Ph.D. Thesis, Department of Physics, Princeton University.
- [98] A. Reiman, 1979, *Rev. Mod. Phys.* **51**, 311.
- [99] A. Reiman and A. Bers, 1975, in *Proceedings of the Seventh Conference on Numerical Simulation of Plasmas*, Courant Institute, N.Y.U., June 1975, p. 188.
- [100] A. H. Reiman, A. Bers, and D. J. Kaup, 1977, *Phys. Rev. Lett.* **39**, 245.
- [101] A. M. Rubenchik, 1991, Private Communication.
- [102] A. M. Rucklidge, 1991, *to appear in J. Fluid Mech.*
- [103] D. Ruelle and F. Takens, 1971, *Commun. Math. Phys.* **20**, 167.
- [104] J. S. Russell, 1838, in *Report of the 7th Meeting of British Association for the Advancement of Science, Liverpool*, p. 417.
- [105] R. Z. Sagdeev and A. A. Galeev, 1969, *Nonlinear Plasma Theory* (Benjamin, New York).
- [106] A. N. Šarkovskii, 1964, *Ukr. Math. Z.* **16**, 61. 0
- [107] K. Sauer and K. Baumgärtel, 1984, *Phys. Rev. Lett.*, **52** 1001.
- [108] G. S. Schuster, 1984, *Deterministic Chaos: An Introduction* (Physik-Verlag, Weinheim, FRG).
- [109] B. I. Shraiman, 1986, *Phys. Rev. Lett.* **57** 325.

- [110] L. Sirovich, 1989, *Physica D* **37**, 126.
- [111] G. I. Sivashinsky, 1983, *Ann. Rev. Fluid Mech.* **15**, 170.
- [112] H. Tennekes and J. L. Lumley, *A First Course in Turbulence* (M.I.T. Press, Cambridge, MA).
- [113] C. Vidal, A. Pagola, J. M. Bodet, P. Hanusse, and E. Bastardie, 1986, *J. Phys. (Paris)* **47**, 1999.
- [114] S. Y. Vyshkind and M.I. Rabinovich, 1976, *Zh. Eksp. Teor. Fiz* **71**, 557 [*Sov. Phys. - JETP* **44**, 292 (1976)].
- [115] J. Wersinger, J. Finn, and E. Ott, *Phys. Fluids*, 1980, **23**, 1142.
- [116] A. Wolf, J. B. Swift, H. L. Swinney, and J. A. Vastano, 1985, *Physica* **16D**, 285.
- [117] V. Yakhot, 1983, *Phys. Rev. A* **24**, 642.
- [118] N. J. Zabusky and M. D. Kruskal, 1965, *Phys. Rev. Lett.* **15**, 240.
- [119] V. E. Zakharov and A. B. Shabat, 1971, *Zh. Eksp. Teor. Fiz.* **61**, 118 [*Sov. Phys. - JETP* **34**, 62 (1971)].
- [120] V. E. Zakharov and S. V. Manakov, 1973, *Zh. Eksp. Teor. Fiz. Pis'ma Red.* **18**, 413 [*Sov. Phys.-JETP Lett.* **18**, 243 (1973)].
- [121] V. E. Zakharov and S. V. Manakov, 1975, *Zh. Eksp. Teor. Fiz.* **69**, 1654 [*Sov. Phys. - JETP* **42**, 842 (1976)].
- [122] V. E. Zakharov, A. N. Pushkarev, V. F. Shvets, and V. V. Yan'kov, 1988, *Pis'ma Zh. Eksp. Fiz.* **48**, 79 [*JETP Lett.* **48**, 83 (1988)].
- [123] S. Zaleski, 1989, *Physica D* **34**, 427.
- [124] G. M. Zaslavsky, 1985, *Chaos in Dynamical Systems* (Harwood Academic, New York).